Sum Frequency Generation Vibration Spectroscopy Investigation of Buried Polymer and Organic Interfaces

by

Arthur Alexander McClelland

A dissertation submitted in partial fulfillment
of the requirements for the degree of
Doctor of Philosophy
(Applied Physics)
in The University of Michigan
2009

Doctoral Committee:

Associate Professor Zhan Chen, Chair
Associate Professor Joerg Lahann
Professor David C. Martin
Associate Professor Adam J. Matzger
Professor Roseanne J. Sension

DEDICATION

To Lisa

ACKNOWLEDGEMENTS

There are really too many people, who have helped me in too many ways even to begin to write a comprehensive acknowledgements page. I apologize to anyone that I have forgotten.

First, I need to thank Dr. Chen for providing me with the opportunity to do research in his lab. Dr. Lahann was a very patient collaborator for the research discussed in Chapter 2. Dr. Matzger provided many helpful and insightful conversations during our collaborations on the research discussed in Chapter 3 and Chapter 5. Also thanks to Dr. Sension and Dr. Martin for serving on my committee.

I also need especially to thank my student collaborators. Dr. Hsien Yeh Chen prepared the functionalized PPX samples presented in Chapter 2. Seokhoon Ahn worked closely with me on the 2D crystals on graphite presented in chapter 3. Dr. Adam Grzesiak and Vilmali Lopez-Mejias worked closely with me on the acetaminophen polymer induced heteronucleation project presented in Chapter 5.

I would like to thank the entire Chen research group, which is really too large at this point to list individually. I would like particularly to thank Anne Vazquez, Cornelius Kristalyn, and Andy Boughton for always being ready to answer my questions about chemistry and being willing to discuss my SFG results.

I would like to thank that Applied Physics program for support, both financial and moral. I need to acknowledge my applied physics officemates for the first three years

who suffered through JD Jackson with me: Dr. Brenton Knuffman, Dr. Kevin Haworth, Eric Kim, Eric Harding, and Malavika Chandra.

I also need to thank my parents and grandparents who instilled an inquiring mind in me at a young age. They are the reason that I became a scientist.

Finally, I need to acknowledge the laser gods who smiled on me just enough over the many years here to complete this work.

TABLE OF CONTENTS

LIST OF FIGURES

List of Tables

CHAPTER 1 : BACKGROUND AND INTRODUCTION

1.1 Motivation

Surfaces and interfaces are important in many areas of science and technology, ranging from chemistry and physics to electronics and biology. They are the point of interaction for materials with the world. A material's surface/interfacial properties can be very different from its bulk properties. A material's surface properties can also change depending on the environment with which the material is in contact. A better understanding of surfaces and interfaces is of increasing importance to the development of nanoscience and nanotechnology. For example, various devices such as nanofluidic devices,[1-4] Micro-Electro-Mechanical Systems (MEMS),[5-9] sensors,[10-12] medical implants,[13-15] and of electronics[16-21] continue to shrink towards the nanoscale.

Many interfaces are hard to probe because they are actually buried, but most conventional surface science techniques are unable to probe buried interfaces *in situ*. By virtue of being an all-optical technique Sum Frequency Generation (SFG), vibrational spectroscopy can probe buried interfaces as long as they are accessible by light. For example, biomedical implants work in the aqueous environment of the human body. The acceptance or rejection of a biomedical implant depends on the molecular interactions between the implant surface and the body, which are mediated by the surface chemistry and structure of the implant in an aqueous environment.[22] Therefore it is necessary to investigate the surface chemistry and structure in aqueous environment *in situ*, which can

be quite different from those in vacuum. The surface chemistry for a potential biomedical implant polymer is examined in Chapter 2. SFG can provide molecular level information about the surface chemistry and structure in an aqueous environment *in situ* in real time.

1.2 Sum Frequency Generation (SFG) Vibrational Spectroscopy

Sum Frequency Generation Vibrational Spectroscopy (SFG) is a second order nonlinear optical technique that is intrinsically surface specific for centrosymmetric media.[23,24] It has been demonstrated to have sub monolayer sensitivity.[25] SFG provides a vibrational spectrum similar to those collected using Fourier Transform Infrared (FTIR) or Raman spectroscopic techniques, but the spectrum that SFG provides is specifically from the functional groups at the surface or interface. The major advantages of the SFG technique include superb surface specificity, the ability to measure the orientation of surface functional groups or molecules, and the capability to probe buried interfaces. It does not require a vacuum, as opposed to many other surface science techniques like X-Ray Photon Spectroscopy (XPS), Scanning Electron Microscopy, etc. This allows for *in situ* probing of surface properties at buried interfaces including aqueous environments. SFG has been applied to a wide range of systems including polymers,[26-31] proteins,[32,33] peptides,[34-38] DNA,[39] self assembled monolayers,[40-42] lung surfactants,[43-46] and metal surfaces.[41,47,48]

1.3 Mathematical Background of SFG

The following discussion of the physical origins of SFG closely follows the presentation of Colin Bain.[49] To a first approximation, the electron distribution in the

molecule responds harmonically to the electric field of incident light. The dipole moment μ of the molecule can be described as:

$$\mu = \mu^0 + \alpha E \qquad \textbf{Eq. 1}$$

Where μ^0 is the static dipole moment, α is the polarizability, and E is the electric field of the incident light. Since the induced dipole is not necessarily in the same direction as E, α is a (3x3) tensor.

In condensed phases the dipole moment per unit volume, or polarization P, can be written as.

$$P = P^{(0)} + \varepsilon_0 \chi^{(1)} E \qquad \textbf{Eq. 2}$$

Since few materials have a static polarization and certainly none of the materials studied here have a static polarization, $P^{(0)}$ will be set to 0.

For a simple molecular material, the susceptibility depends on the number of molecules per unit volume, N, multiplied by the molecular polarizability average over all the orientations of the molecules in the material.

$$\chi^{(1)} = \frac{N < \alpha >}{\varepsilon_0} \qquad \textbf{Eq. 3}$$

The linear properties of isotropic materials are characterized by the complex refractive index.

$$n = \sqrt{1 + \chi^{(1)}} \qquad \textbf{Eq. 4}$$

The real part determines the speed of light in the medium.

$$v = \frac{c}{\Re[n]} \qquad \textbf{Eq. 5}$$

The imaginary part determines the absorption coefficient, which unfortunately, is conventionally also denoted α,

$$\alpha = \frac{4\pi}{\lambda_0} \Im[n] \qquad \textbf{Eq. 6}$$

In intense light, such as a focused pulsed laser beam, the electric field is high enough that the electrons are no longer able to respond harmonically and higher order terms must be included in the expression for the dipole moment. The Taylor expansion of μ goes as Eq 7.

$$\mu = \mu^0 + \alpha E + \beta : EE + \gamma \vdots EEE + \ldots \qquad \textbf{Eq. 7}$$

The terms β and γ are known as the first and second hyperpolarizabilities, where

$$\beta : EE \text{ denotes } \sum_{j,k} \beta_{ijk} E_j E_k \qquad \textbf{Eq. 8}$$

The polarization of the material under irradiation can now be written as a Taylor expansion as in Eq. 9.

$$P = P^{(1)} + P^{(2)} + P^{(3)} + \ldots = \varepsilon_0 \chi^{(1)} E + \varepsilon_0 \chi^{(2)} : EE + \varepsilon_0 \chi^{(3)} \vdots EEE \ldots \qquad \textbf{Eq. 9}$$

where $\chi^{(2)}$ is a third rank tensor known as the second order nonlinear susceptibility. $\chi^{(3)}$ is a forth-rank tensor known as the third order nonlinear susceptibility. Since SFG is a second order nonlinear optical process, when we study SFG, we usually stop the Taylor expansion after the $\chi^{(2)}$ term.

If we describe the electric field as a cosine wave for a single laser beam, we have:

$$E(r,t) = E(r)\cos(\omega t) \qquad \textbf{Eq. 10}$$

If we then substitute in and look at just the second order term, we have:

$$P^{(2)} = \varepsilon_0 \chi^{(2)} : EE = \varepsilon_0 \chi^{(2)} E(r) E(r) \cos^2(\omega t) \qquad \textbf{Eq. 11}$$

Rearranging the double angle trigonometric identity

$$\begin{aligned} &\cos(2A) = 2\cos^2(A) - 1 \\ &\Rightarrow \cos^2(A) = \frac{1}{2}\cos(2A) + \frac{1}{2} \end{aligned} \qquad \textbf{Eq. 12}$$

and substituting the trigonometric identity back in we now have:

$$P^{(2)} = \frac{1}{2}\varepsilon_0 \chi^{(2)} E(r) E(r)(1 + \cos(2\omega t)) \qquad \textbf{Eq. 13}$$

As can be seen, light at 2ω can be generated and this process is known as second harmonic generation.

If two input laser beams at different frequencies interact at the sample, the polarization can be written as

$$P^{(2)} = \varepsilon_0 \chi^{(2)} : E_1(r) E_2(r) \cos(\omega_1 t) \cos(\omega_2 t) \qquad \textbf{Eq. 14}$$

Using the trigonometric identity

$$2\cos(A)\cos(B) = \cos(A-B) + \cos(A+B) \qquad \textbf{Eq. 15}$$

the polarization can be written as

$$P^{(2)} = \varepsilon_0 \chi^{(2)} : E_1(r) E_2(r) \frac{1}{2}[\cos(\omega_1 - \omega_2) + \cos(\omega_1 + \omega_2)] \qquad \textbf{Eq. 16}$$

As can be seen, light at the difference of the two input laser frequencies, ω_1-ω_2, can be generated. This process is known as difference frequency generation (DFG). Light at the sum of the two input laser beam frequencies, ω_1+ω_2, can also be generated. This process is known as sum frequency generation (SFG), which is the process that was used in this thesis to probe the surface chemistry at buried interfaces.

In the experiments described in this thesis, the two laser beams that are used are a visible beam at 532.1 nm, and an infrared beam that is tunable from 3 to 10μm. SFG and DFG are coherent phenomena, so the direction of emission is determined by the conservation of momentum parallel to the surface.

$$k_{sum} \sin(\theta_{sum}) = k_1 \sin(\theta_1) + k_2 \sin(\theta_2) \qquad \textbf{Eq. 17}$$

Where k is the wave number

$$k = \frac{2\pi}{\lambda} \qquad \textbf{Eq. 18}$$

The intensity of the emitted sum frequency light depends on the square of $P^{(2)}$, therefore it is proportional to $|\chi^{(2)}|^2$. The SFG second order nonlinear optical susceptibility $\chi^{(2)}$ is a macroscopic property of the sample media. It is the sum of all the molecular second

order hyperpolarizability $\beta^{(2)}$ or β for simplicity. An expression for β can be found by second order perturbation theory as an infinite sum over the quantum states of the system. This of course has a complicated general solution, but some physical insight can be gained into SFG if the simplifications of ω_{sum} and ω_{vis} are not in resonance with an electronic transition in the sample and the electric dipole approximation is assumed.

Near a vibrational transition, ω_0, in a molecule the hyperpolarizability, β, is given by

$$\beta_{lmn} = \frac{-1}{2\hbar}\sum_s \{\frac{< g \mid \mu_l \mid s >< s \mid \mu_m \mid v >}{\hbar(\omega_{sum} - \omega_{sg})} - \frac{< g \mid \mu_m \mid s >< s \mid \mu_l \mid v >}{\hbar(\omega_{vis} - \omega_{sg})}\} \otimes \{\frac{< v \mid \mu_n \mid g >}{\omega_{IR} - \omega_0 + i\Gamma}\}$$

Eq. 19

$\mid g >$ is the ground vibrational state

$\mid v >$ is the excited vibrational state

$\mid s >$ is any other state

Γ^{-1} is the relaxation time of the excited vibrational state

$\mu = er$ is the electric dipole operator

The first bracket is the Raman transition dipole moment. The second bracket is the infrared transition dipole moment. Therefore, a molecule is sum frequency active only if it is both infrared active AND Raman active.

For a molecule to be infrared active the electric dipole moment of the molecule must change as the atoms are displaced relative to each other. For example, homonuclear diatomic molecules are infrared inactive because their dipole moments remain zero during the stretching vibration.

Since an infrared absorption process is a one-photon process, the transition dipole moment can be deduced using first order perturbation. Assuming we can separate

vibrational motions from other motions of the molecules, the gross selection rule for infrared activity can be justified by considering the transition dipole moment as

$$< v_f \mid \hat{\mu} \mid v_i > \quad \textbf{Eq. 20}$$

where $\hat{\mu}$ is a dipole operator. Subscripts i and f are used to label the initial and final vibrational states for a vibrational transition.

Here we only discuss the one-dimensional case for simplicity. If we consider the dipole moment as arising from two partial charges $\pm$ δq separated by a distance R = Re + x, we can describe the displacement from equilibrium separation during a vibration, x, as

$$\hat{\mu} = \mu = R\delta q = \mathrm{Re}\,\delta q + \delta q = \mu_0 x + x\delta q \qquad \textbf{Eq. 21}$$

where μ_0 is the electric dipole moment when the nuclei are at their equilibrium separation. It follows that

$$< v_f \mid \hat{\mu} \mid v_i >= \mu_0 < v_f \mid v_i > + \delta q < v_f \mid x \mid v_i > \qquad \textbf{Eq. 22}$$

Since v_f and v_i are orthogonal states the term $<v_f|v_i>$ is zero. Thus

$$< v_f \mid \hat{\mu} \mid v_i >= \delta q < v_f \mid x \mid v_i > \qquad \textbf{Eq. 23}$$

$$\delta q = \frac{d\mu}{dx} \qquad \textbf{Eq. 24}$$

$$< v_f \mid \hat{\mu} \mid v_i >=< v_f \mid x \mid v_i > (\frac{d\mu}{dx}) \qquad \textbf{Eq. 25}$$

This shows that for the molecule to be infrared active the dipole moment must vary with displacement. A Raman scattering process is more complicated than an IR absorption process. A Raman scattering process involves two photons: one incident photon and one outing photon. Therefore, the Raman transition polarizability can be calculated by second order perturbation. After applying some assumptions, it can be written in a formula with a similar format as the IR transition dipole moment. The result shows that for a vibrational mode of a molecule to be vibrational Raman active the gross selection rule is that the polarizability should change as the molecule vibrates. Even though the

mathematical representation for a Raman tensor can be complicated, for an approximate picture, it can be regarded as the electron cloud around the nuclei in the molecule. For example, as a diatomic molecule swells and contracts during a vibration, the influence the atomic nuclei exert over the electron cloud varies, hence the molecular polarizability changes.

The ramifications of the gross selection rules of infrared activity and Raman activity for SFG are given here for the example system of a diatomic molecule. A diatomic molecule only has one vibrational mode: the stretching mode. This mode for a homonuclear diatomic molecule is Raman active, but infrared *in*active- hence it would be sum frequency inactive; while this mode for a heteronuclear diatomic molecule is infrared active and Raman active so it would be sum frequency active.

Returning to the expression Eq. 19 it should be noted that the $(\omega_{IR}-\omega_0)$ term in the denominator gives rise to a maximum in β, when the infrared frequency is in resonance with the molecular vibrational frequency. The damping term Γ determines the line width of the resonance peak.

As we discussed above, $\chi^{(2)}$ is a macroscopic property of a medium, which is the sum of hyperpolarizability β of all the molecules in the medium. From the expression of β, we know that $\chi^{(2)}$ is a polar tensor. This intrinsic symmetry of the $\chi^{(2)}$ tensor forbids SFG in centrosymmetric materials. Because $\chi^{(2)}$ is a polar tensor of rank three, it changes sign under the inversion operation.

$$\chi^{(2)}(r) = -\chi^{(2)}(-r) \qquad \textbf{Eq. 26}$$

A centrosymmetric material however is invariant under inversion so

$$\chi^{(2)}(r) = \chi^{(2)}(-r) \qquad \textbf{Eq. 27}$$

$$\Rightarrow \chi^{(2)}(-r) = -\chi^{(2)}(-r) = 0 \qquad \textbf{Eq. 28}$$

Hence, SFG under the electric dipole approximation does not occur in a centrosymmetric material. SFG can also occur by magnetic dipole or electric quadrupole mechanisms, but these mechanisms are usually much weaker than the electric dipole mechanisms.[33,50] At interfaces though, the centrosymmetric symmetry is broken, $\chi^{(2)}(r) \neq \chi^{(2)}(-r)$, and second order nonlinear optical phenomenon can occur.

This is the source of the surface specificity that is cited for second harmonic and sum frequency generation. Thus, using vibrational SFG is possible to differentiate the vibrational spectrum of the chemical functional groups that are at the surface from the vibrational spectrum of the same chemical functional groups in the bulk.

By varying the polarization, (orientation of the electric field of the light) used to excite the molecule, we can determine the molecular orientation. For example, intuitively, if the infrared electric field is oriented along the molecular vibrational axis, we will get a strong response, as opposed to if the electric field is oriented perpendicular to the molecular vibrational axis. When the infrared electric field is oriented transverse to the molecular vibrational axis, no response will be observed.

As discussed above, $\chi^{(2)}$ is a third rank tensor that has twenty-seven tensor components. For a particular vibrational mode, $\chi^{(2)}$ is the overall sum (or average) over hyperpolarizability of all the molecules (or functional groups) in the sample. If we want to use a mathematical formula to represent this relation, we have:

$$\chi_{ijk,q} = N_s \sum_{l,m,n} \langle (\hat{i} \cdot \hat{l})(\hat{j} \cdot \hat{m})(\hat{k} \cdot \hat{n}) \rangle \beta_{lmn,q} \qquad \textbf{Eq. 29}$$

We can also consider this relation as following: The SFG susceptibility tensor element χ_{ijk} (i, j, k = x, y, z) is related to the SFG molecular hyperpolarizability tensor

element β_{lmn} (l, m, n = a, b, c) by Euler angle projection where the signal is the sum of all the projections.

If all the molecules were randomly oriented, then the summed result, $\chi^{(2)}$, would be zero. If the molecules adopt some orientation order, such orientation information may be deduced by measuring different $\chi^{(2)}$ components if molecular hyperpolarizability is known.

Varied polarization combinations of the input and signal beams can be used to measure different tensor components in $\chi^{(2)}$, which will be further discussed at a later point. If the symmetry for a molecule or functional group under study for the vibrational mode q is known, the explicit expression between various $\chi^{(2)}$ tensor components and hyperpolarizability components would be known. More details will be given in the discussion of the orientation calculations in the later chapters. In general, for the systems that will be investigated in this thesis, only one orientation angle θ (the angle between the principle axis of a functional group and the surface normal) will be studied. $\chi^{(2)}$ tensor components are related to hyperpolarizability tensor components depending on this polar angle θ only through averages $<\cos\theta>$ and $<\cos^3\theta>$.

Different tensor components of $\chi^{(2)}$ are sampled by different laser polarizations. In general, P polarized light samples a combination of in plane and out of plane contributions, while S polarized light samples only in plane contributions. By convention, the polarization combinations are ordered signal, visible, and infrared. So the polarization combination SSP has S polarized SFG signal beam, S polarized visible beam and P polarized infrared beam. Figure 1-1 shows a cartoon of the direction of the electric field for P and S polarized light relative to a sample surface.

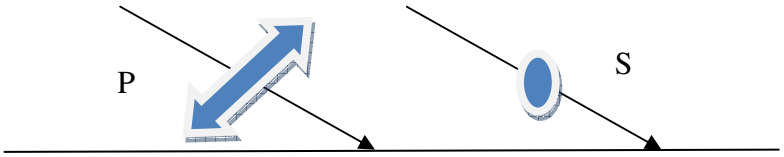

Figure 1-1 The electric field directions of P polarized light and S polarized light incident on a surface. S polarized light has an electric field that goes into the page

For a nonchiral surface that is isotropic in the x-y plane (like a spin-coated polymer), there are only four independent nonzero components of the 27 element tensor $\chi^{(2)}$

$$\begin{aligned} &\chi_{zzz} \\ &\chi_{xxz} = \chi_{yyz} \\ &\chi_{xzx} = \chi_{yzy} \\ &\chi_{zxx} = \chi_{zyy} \end{aligned} \qquad \textbf{Eq. 30}$$

For experiments that are conducted away from electronic resonances of the sample there is a further simplification known as the Kleinmann symmetry where

$$\chi_{xzx} = \chi_{zxx} \qquad \textbf{Eq. 31}$$

These different contributions can be probed by varying the polarization of the light. With s-polarized visible and infrared (E in the y direction) only χ_{zyy} contributes giving rise to p-polarized sum frequency emission. With s-polarized visible and p-polarized IR only χ_{yyz} contributes and gives rise to s-polarized sum frequency emission. With p-polarized visible and p polarized infrared all four components can contribute with their relative importance determined by the electric fields at the surface in the window geometry. The above discussion can be summarized using the following mathematical formulas:

$$\chi_{ppp} \propto \begin{vmatrix} -L_{xx}(\omega)L_{xx}(\omega_1)L_{zz}(\omega_2)\cos\beta\sin\beta_1\sin\beta_2\chi_{xxz} \\ -L_{xx}(\omega)L_{zz}(\omega_1)L_{xx}(\omega_2)\cos\beta\sin\beta_1\cos\beta_2\chi_{xzx} \\ +L_{zz}(\omega)L_{xx}(\omega_1)L_{xx}(\omega_2)\sin\beta\cos\beta_1\cos\beta_2\chi_{zxx} \\ +L_{zz}(\omega)L_{zz}(\omega_1)L_{zz}(\omega_2)\sin\beta\sin\beta_1\sin\beta_2\chi_{zzz} \end{vmatrix}$$

$$\chi_{ssp} \propto L_{yy}(\omega)L_{yy}(\omega_1)L_{zz}(\omega_2)\sin\beta_2\chi_{yyz}$$

$$I_{sps} \propto L_{yy}(\omega)L_{zz}(\omega_1)L_{yy}(\omega_2)\sin\beta_1\chi_{yzy} \qquad \textbf{Eq. 32}$$

In the prism geometry and the PPP polarization combination the χ_{zzz} component is an order of magnitude greater than any other component. When we adopt the near total reflection geometry, $L_{xx}(\omega)$ is close to zero. Therefore,

$$\chi_{ppp} \propto L_{zz}(\omega)L_{zz}(\omega_1)L_{zz}(\omega_2)\sin\beta\sin\beta_1\sin\beta_2\chi_{zzz} \qquad \textbf{Eq. 33}$$

Since SFG is a coherent process, it also carries information in the phase of the signal. Since inverting molecules changes the sign of $\chi^{(2)}$, it also changes the sign of $P^{(2)}$ and hence the phase of the emitted light by π, which can be measured by interference methods. The most common way this is implemented is by changing the substrate to something that has a nonresonant SFG signal. The nonresonant SFG will interfere either constructively or destructively with the resonant SFG signal of a sample providing relative orientation information about the molecules under investigation. If the phase of the nonresonant SFG signal can be calibrated using a reference sample of molecules with known orientation (thus known phase of the SFG signal), the absolute orientation of sample molecules can be deduced. None of the experiments reported here, used this interference technique.

1.3 SFG Instrumentation

In our SFG experimental setup, the sum frequency spectra are collected by overlapping a visible and a tunable infrared beam on a polymer surface, at incident angles of 60° and 54° (versus the surface normal), respectively. The visible beam at 532.1 nm is generated by frequency doubling the fundamental output pulses of 20 ps pulse width from an EKSPLA Nd:YAG laser. The infrared beam is tunable from 2.5 to 10μm, (1000 to 4000 cm^{-1}). It is generated from an EKSPLA optical parametric generation/amplification and difference frequency system based on LBO and $AgGaS_2$ crystals. Both beams are focused on the sample with diameters of approximately 0.5 mm. The sum frequency signal from the polymer surface is collected by a photomultiplier tube and processed with a gated integrator. Two photodiodes are used to monitor the input visible beam and infrared beam powers by collecting the back reflections of these two beams. These are used for normalization purposes to eliminate artifacts in the SFG signal from fluctuations in the infrared or visible beam intensities. Surface vibrational spectra are obtained by measuring the SFG signal as a function of the input infrared frequency. SFG spectra with different polarization combinations including ssp (s-polarized sum frequency output, s-polarized visible input, and p-polarized infrared input), ppp, pss, and sps can be collected to probe orientation of surface groups. Figure 1-2 shows a schematic of the SFG laser system in the Chen lab.

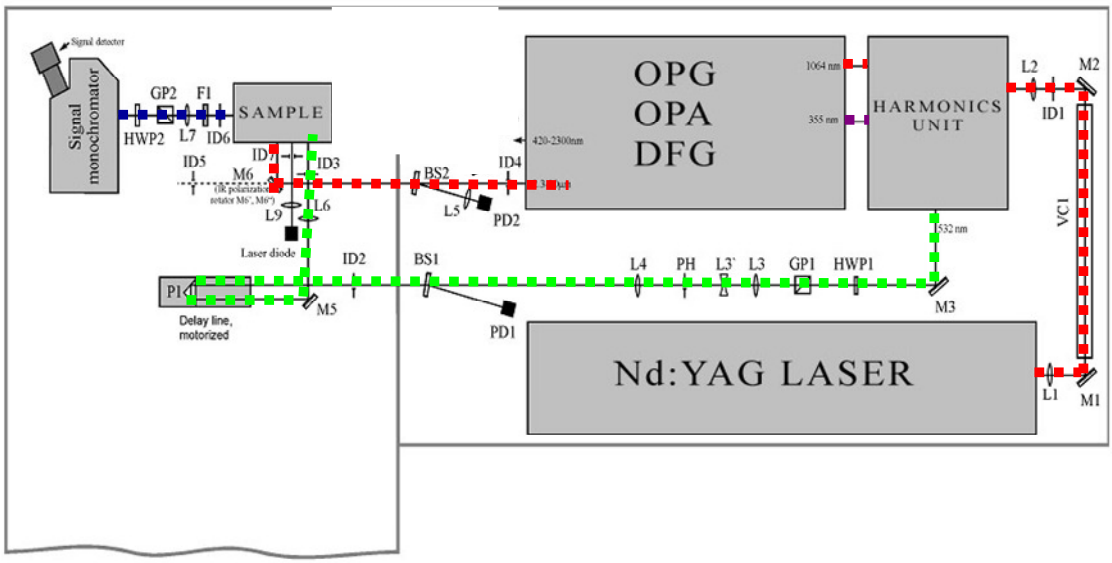

Figure 1-2 Schematic of single resonance SFG laser setup.

1.4 Sample Geometries

Two different sample geometries were used for the experiments reported here. In "window geometry", a fused silica or a CaF_2 substrate with parallel sides was used. (Figure 1-3) In "prism geometry", a right angle prism of either fused silica or a CaF_2 was

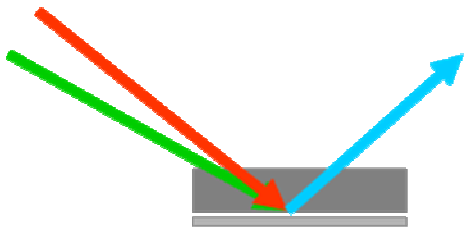

Figure 1-3 Schematic of window geometry.

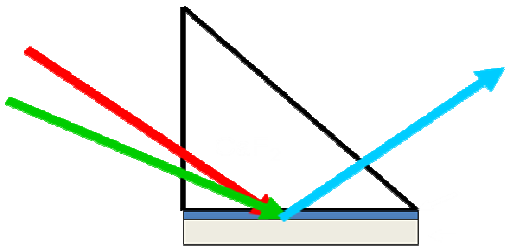

Figure 1-4 Schematic of prism geometry.

used. (Figure 1-4) In prism geometry, one of the right angles sides was coated with the sample under investigation. The prism geometry produced a stronger signal due to more favorable Fresnel coefficients. It has been shown that the polymer-substrate interface does not produce much SFG signal.[51] Thickness-dependent studies have shown that the bulk polymer does not contribute to the signal. If the bulk polymer contributed to the signal, then a thicker sample should give a stronger signal, which is not what is observed. Also surface specific changes such corona treating or contacting to water can show strong changes in the SFG spectrum. This clearly proves that the signal arises from the bottom free surface and not from the CaF_2 polymer interface. Experiments where the polymer was contacted to water or other liquids involved bringing the water up to contact the free polymer-air surface.

1.5 Overview of Presented Research

Buried interfaces, the juncture between two bulk media, are extremely important to understand and yet extremely difficult to probe. Until recently there has been no good nondestructive, *in situ,* analytical technique that can probe buried interfaces. SFG provides a powerful tool to probe molecular level structure and interactions at buried interfaces. This dissertation uses SFG to examine molecular level structure and interactions at a variety of buried interfaces. The research presented in this thesis applies SFG to aid in the understanding of a wide variety of problems and areas including polymer surface restructuring in water, polymer adhesion, two-dimensional organic crystals, and polymer induced heteronucleation of pharmaceuticals.

The goal of this research was to investigate chemical interactions at buried interfaces involving organic molecules or polymer materials using SFG vibrational spectroscopy. In Chapter 2, the SFG investigation of functionalized poly-p-xylylene (PPX) will be described. Polymer surface structures of PPX with different functionalities will be probed and compared. Surface restructures for these surfaces in varied chemical environments will be examined. Specifically, we will develop a molecular level understanding of the Solventless Adhesive Bonding (SAB) technique developed by the Lahann group using aldehyde and amine functionalized PPX.

In Chapter 3, the investigation of two dimensional crystallization of phthalate diester monolayers on graphite solid/liquid interface by combined scanning tunneling microscopy (STM) and SFG will be described. 2D crystals at the liquid/solid interface have attracted great attention because they may be used to build molecule-based devices such as sensors using well-patterned surface.[52] These 2D crystals have been investigated with the aid of STM offering direct information on local packing structure.[52] In general, the structural insight with atomic resolution based on the high-resolution STM images is complemented by computed models. Supplemented by computed models, STM can provide detailed structure of 2D crystals formed at the liquid/solid interface with atomic resolution. However, some structural information such as functional group orientations in such 2D crystals needs to be tested experimentally to ensure the accuracy of the deduced structures. Due to the limited sensitivity, many other experimental techniques such as Raman and infrared spectroscopy are not able to provide such structural information of 2D crystals. Here we show that SFG can measure average orientation of functional groups in such 2D crystals, or physisorbed monolayers, providing key

experimental data to aid in the modeling and interpretation of the STM images. The usefulness of combining these two techniques was demonstrated with a phthalate diester monolayer formed at the 1-phenyloctane/ highly oriented pyrolytic graphite (HOPG) interface. The spatial orientation of the ester C=O of the monolayer was successfully determined using SFG.

Chapter 4 will describe the investigation of a series of poly-n-methacrylates and the effect of side chain length on the C=O orientation. The effects of exposure to water on the C=O orientation were also investigated. Our group previously investigated the orientation of the terminal methyl group of a similar series of polymers.[53] However, the methyl groups are largely non-interacting groups though; while the carbonyl groups are well known hydrogen-bonding groups. Therefore the surface interactions of the polymers are more likely to be determined by the C=O orientation, which this research investigates. The C=O stretching spectra of the polymers in air and contacted to water were collected. . The SFG spectra of the polymers contacted to water showed that all the C=O groups were accessible to form hydrogen bonds with water.

In Chapter 5, the interface of the crystallized acetaminophen polymer interface was investigated. The Matzger group found that heteronucleating acetaminophen crystals on polymer surfaces led to previously inaccessible thermodynamically metastable polymorphs.[54-59] The mechanism however was unclear. The SFG study here provides insights to the interfacial interactions leading to polymer-induced heteronucleation. In this study, we investigated acetaminophen heteronucleation on two polymer surfaces, poly (methyl methacrylate) (PMMA) and poly (n-butyl methacrylate). It has been found that acetaminophen forms different polymorphs on these two polymer surfaces: on

PMMA it forms orthorhombic crystals while on PBMA it forms monoclinic crystals. SFG spectra were collected from polymer/acetaminophen solution interfaces to try to elucidate the crystal growth mechanism starting from the first adlayer. For comparison, saturated solutions of phenol and acetanilide were also studied. The C=O stretching peak of the polymer was observed to shift due to hydrogen bonding. The phenol induced a peak shift of around 30 cm^{-1}, while the acetaminophen and acetanilide induced peaks shifts of around 10 - 15 cm^{-1}. This implied that the NH group of the acetaminophen was hydrogen bonding to the C=O group in the polymers. The C=O groups in PMMA and PBMA were determined to have different orientations when hydrogen bonded to acetaminophen molecules, which lead to the different polymorph selection. These results are compared to the results obtained from the polymer/crystal interfaces deposited by solution and by subliming. The polymer/crystal interfaces deposited by solution showed evidence of hydrogen bonding, too, but the crystals deposited by subliming did not show evidence of hydrogen bonding. The sublimed samples only formed monoclinic crystals.

Chapter 6 will describe the designing and building of an SFG imaging system. A collinear beam scanning system using a cassegrain all reflective microscope objective was designed and built. Clearly extending the SFG technique to a heterogeneous surface would be of interest. An SFG image of microcontacted printed PMMA was obtained.

Chapter 7 will be a summary and conclusion chapter.

(1) Hibara, A.; Tsukahara, T.; Kitamori, T. *Journal of Chromatography A* **2009**, *1216*, 673-683.

(2) Kobryn, A. E.; Kovalenko, A. *Journal of Chemical Physics* **2008**, *129*.

(3) Schoch, R. B.; Han, J. Y.; Renaud, P. *Reviews of Modern Physics* **2008**, *80*, 839-883.

(4) Prakash, S.; Piruska, A.; Gatimu, E. N.; Bohn, P. W.; Sweedler, J. V.; Shannon, M. A. *Ieee Sensors Journal* **2008**, *8*, 441-450.

(5) Park, S. H.; Yang, D. Y.; Lee, K. S. *Laser & Photonics Reviews* **2009**, *3*, 1-11.

(6) Hill, C.; Amodeo, A.; Joseph, J. V.; Patel, H. R. H. *Expert Review of Anticancer Therapy* **2008**, *8*, 1891-1897.

(7) Bhushan, B. *Philosophical Transactions of the Royal Society a-Mathematical Physical and Engineering Sciences* **2008**, *366*, 1499-1537.

(8) Hierold, C.; Jungen, A.; Stampfer, C.; Helbling, T. *Sensors and Actuators a-Physical* **2007**, *136*, 51-61.

(9) Ko, W. H. *Sensors and Actuators a-Physical* **2007**, *136*, 62-67.

(10) Vichchulada, P.; Lipscomb, L. D.; Zhang, Q. H.; Lay, M. D. *Journal of Nanoscience and Nanotechnology* **2009**, *9*, 2189-2200.

(11) Monzon-Hernandez, D.; Luna-Moreno, D.; Martinez-Escobar, D. *Sensors and Actuators B-Chemical* **2009**, *136*, 562-566.

(12) Rajesh; Ahuja, T.; Kumar, D. *Sensors and Actuators B-Chemical* **2009**, *136*, 275-286.

(13) Onose, G.; Cturea, A. V.; Rizea, R. E.; Cbendreanu, C.; Angbelescu, A.; Haras, M.; Brehar, F.; Padure, L. *Journal of Optoelectronics and Advanced Materials* **2008**, *10*, 18-28.

(14) Pierstorff, E.; Ho, D. *Journal of Nanoscience and Nanotechnology* **2007**, *7*, 2949-2968.

(15) Kriparamanan, R.; Aswath, P.; Zhou, A.; Tang, L. P.; Nguyen, K. T. *Journal of Nanoscience and Nanotechnology* **2006**, *6*, 1905-1919.

(16) Zhu, H. W.; Wei, B. Q. *Journal of Materials Science & Technology* **2008**, *24*, 447-456.

(17) Vulillaume, D. *Comptes Rendus Physique* **2008**, *9*, 78-94.

(18) Yanushkevich, S. N. *Journal of Computational and Theoretical Nanoscience* **2007**, *4*, 384-407.

(19) Ray, A. K.; Huda, M. N. *Journal of Computational and Theoretical Nanoscience* **2006**, *3*, 315-341.

(20) Taniguchi, M.; Kawai, T. *Physica E-Low-Dimensional Systems & Nanostructures* **2006**, *33*, 1-12.

(21) Wang, L.; Fine, D.; Sharma, D.; Torsi, L.; Dodabalapur, A. *Analytical and Bioanalytical Chemistry* **2006**, *384*, 310-321.

(22) Sefton, M. V.; Stevenson, W. T. K. *Advances in Polymer Science* **1993**, *107*, 143-197.

(23) Shen, Y. R. *Nature* **1989**, *337*, 519-525.

(24) Shen, Y. R. *Surface Science* **1994**, *300*, 551-562.

(25) Stiopkin, I. V.; Jayathilake, H. D.; Bordenyuk, A. N.; Benderskii, A. V. *Journal of the American Chemical Society* **2008**, *130*, 2271-2275.

(26) Chen, C.; Wang, J.; Woodcock, S. E.; Chen, Z. *Langmuir* **2002**, *18*, 1302-1309.

(27) Chen, C. Y.; Clarke, M. L.; Wang, J.; Chen, Z. *Physical Chemistry Chemical Physics* **2005**, *7*, 2357-2363.

(28) Chen, C. Y.; Even, M. A.; Wang, J.; Chen, Z. *Macromolecules* **2002**, *35*, 9130-9135.

(29) Chen, C. Y.; Loch, C. L.; Wang, J.; Chen, Z. *Journal of Physical Chemistry B* **2003**, *107*, 10440-10445.

(30) Chen, C. Y.; Wang, J.; Chen, Z. *Langmuir* **2004**, *20*, 10186-10193.

(31) Chen, H. Y.; McClelland, A. A.; Chen, Z.; Lahann, J. *Analytical Chemistry* **2008**, *80*, 4119-4124.

(32) Chen, X. Y.; Boughton, A. P.; Tesmer, J. J. G.; Chen, Z. *Journal of the American Chemical Society* **2007**, *129*, 12658-+.

(33) Chen, X. Y.; Wang, J.; Paszti, Z.; Wang, F. L.; Schrauben, J. N.; Tarabara, V. V.; Schmaier, A. H.; Chen, Z. *Analytical and Bioanalytical Chemistry* **2007**, *388*, 65-72.

(34) Chen, X. Y.; Chen, Z. *Biochimica Et Biophysica Acta-Biomembranes* **2006**, *1758*, 1257-1273.

(35) Chen, X. Y.; Tang, H. Z.; Even, M. A.; Wang, J.; Tew, G. N.; Chen, Z. *Journal of the American Chemical Society* **2006**, *128*, 2711-2714.

(36) Chen, X. Y.; Wang, J.; Boughton, A. P.; Kristalyn, C. B.; Chen, Z. *Journal of the American Chemical Society* **2007**, *129*, 1420-1427.

(37) Chen, X. Y.; Wang, J.; Kristalyn, C. B.; Chen, Z. *Biophysical Journal* **2007**, *93*, 866-875.

(38) Chen, X. Y.; Wang, J.; Sniadecki, J. J.; Even, M. A.; Chen, Z. *Langmuir* **2005**, *21*, 2662-2664.

(39) Stokes, G. Y.; Gibbs-Davis, J. M.; Boman, F. C.; Stepp, B. R.; Condie, A. G.; Nguyen, S. T.; Geiger, F. M. *Journal of the American Chemical Society* **2007**, *129*, 7492-+.

(40) Cimatu, K.; Baldelli, S. *Journal of Physical Chemistry B* **2006**, *110*, 1807-1813.

(41) Cimatu, K.; Baldelli, S. *Journal of Physical Chemistry C* **2007**, *111*, 7137-7143.

(42) Cimatu, K.; Moore, H. J.; Barriet, D.; Chinwangso, P.; Lee, T. R.; Baldelli, S. *Journal of Physical Chemistry C* **2008**, *112*, 14529-14537.

(43) Ma, G.; Allen, H. C. *Langmuir* **2007**, *23*, 589-597.

(44) Ma, G.; Allen, H. C. *Photochemistry and Photobiology* **2006**, *82*, 1517-1529.

(45) Ma, G.; Allen, H. C. *Langmuir* **2006**, *22*, 11267-11274.

(46) Schurmann, K.; Lahann, J.; Niggemann, P.; Klosterhalfen, B.; Meyer, J.; Kulisch, A.; Klee, D.; Gunther, R. W.; Vorwerk, D. *Radiology* **2004**, *230*, 151-162.

(47) Bratlie, K. M.; Komvopoulos, K.; Somorjai, G. A. *Journal of Physical Chemistry C* **2008**, *112*, 11865-11868.

(48) Kliewer, C. J.; Bieri, M.; Somorjai, G. A. *Journal of Physical Chemistry C* **2008**, *112*, 11373-11378.

(49) Bain, C. D. *J. Chem. Soc. Faraday Trans.* **1995**, *91*, 1281-1296.

(50) Wei, X.; Hong, S. C.; Lvovsky, A. I.; Held, H.; Shen, Y. R. *Journal of Physical Chemistry B* **2000**, *104*, 3349-3354.

(51) Wang, J.; Chen, C. Y.; Buck, S. M.; Chen, Z. *Journal of Physical Chemistry B* **2001**, *105*, 12118-12125.

(52) Plass, K. E.; Engle, K. M.; Matzger, A. J. *Journal of the American Chemical Society* **2007**, *129*, 15211-15217.

(53) Clarke, M. L.; Chen, C. Y.; Wang, J.; Chen, Z. *Langmuir* **2006**, *22*, 8800-8806.

(54) Grzesiak, A. L.; Uribe, F. J.; Ockwig, N. W.; Yaghi, O. M.; Matzger, A. J. *Angewandte Chemie-International Edition* **2006**, *45*, 2553-2556.

(55) Grzesiak, A. L.; Matzger, A. J. *Journal of Pharmaceutical Sciences* **2007**, *96*, 2978-2986.

(56) Grzesiak, A. L.; Matzger, A. J. *Inorganic Chemistry* **2007**, *46*, 453-457.

(57) Grzesiak, A. L.; Matzger, A. J. *Crystal Growth & Design* **2008**, *8*, 347-350.

(58) Price, C. P.; Matzger, A. J. *Abstracts of Papers of the American Chemical Society* **2005**, *229*, 057-IEC.

(59) Price, C. P.; Grzesiak, A. L.; Matzger, A. J. *Journal of the American Chemical Society* **2005**, *127*, 5512-5517.

CHAPTER 2 : FUNCTIONALIZED POLY-P-XYLYENE

2.1 Introduction

Thin-film polymer coatings are currently being studied for many high-tech applications including biomaterials,[1-4] biosensors,[5,6] insulating layers in integrated circuits,[7,8] thin-film transistors,[9-13] light-emitting diodes,[14-18] optical systems,[19-21] microelectrical-mechanical systems (MEMS),[22-27] lasers,[28-31] waveguides,[32-38] and photodiodes.[39-44] In some applications (e.g., for protein and cell patterning or biosensing purposes), a polymer coating with a micro patterned surface structure is required.[24,45-47]

Poly (*p*-xylylenes) (PPX) belong to a group of special polymers that are under investigation for such thin-film applications.[48-69] For example, PPX has been examined for use as a coating for drug eluting vascular stents.[54] PPX coatings can have many favorable properties such as coating homogeneity, high mechanical stability, and low cost. However, PPX is relatively thrombogenic. In the Lahann group in the Department of Chemical Engineering at the University of Michigan a chemical vapor deposition (CVD) method to deposit functionalized PPX polymer coatings on a variety of substrates has been developed. The functionalization of PPX can be used to optimize the surface structures and surface properties of such coatings. Currently, various functional groups, such as hydrophilic ethylene glycol groups, hydrophobic fluorinated side chains, reactive aldehyde groups and amino groups, and aromatic phenyl groups, have been introduced into the PPX coatings.

SFG spectroscopy was used to examine the surface structures of these functionalized PPX polymers in different chemical environments, e.g., air and water. It was found that SFG is sensitive enough to differentiate between varied surface structures of different functionalized PPX. SFG was successfully used to probe PPX/water interfaces in situ, showing that the surface structure changes when the PPX coating is in an aqueous environment. Finally, SFG has been applied to investigate molecular interactions of an interface between two PPX polymers functionalize with different reaction groups (PPX-CHO and PPX-NH_2), providing molecular level understanding of polymer adhesion.

2.2 Sample Preparation

The sample preparation was done by Hsien Yeh Chen in the Lahann group. Functionalization of PPX materials was accomplished using the CVD method (Figure 2-1). The unfunctionalized PPX (Figure 2-2) was made by subliming paracyclophanes under vacuum between 90-100º C. The molecules then underwent pyrolysis at 700º C and converted into quinodimethanes. Spontaneous polymerization occurred when the molecules condensed on to a cooled and rotating substrate maintained at 15º C. By changing the functionalized group on the precursor paracyclophane various functionalized PPX copolymers shown in Figure 2-3 to Figure 2-8 were prepared. All this work was performed in a custom-made CVD polymerization system.[53] Throughout CVD polymerization, a constant argon flow of 20 sccm and a working pressure of 0.5 mbar were maintained. Films of ~100nm thickness were used for the SFG studies.

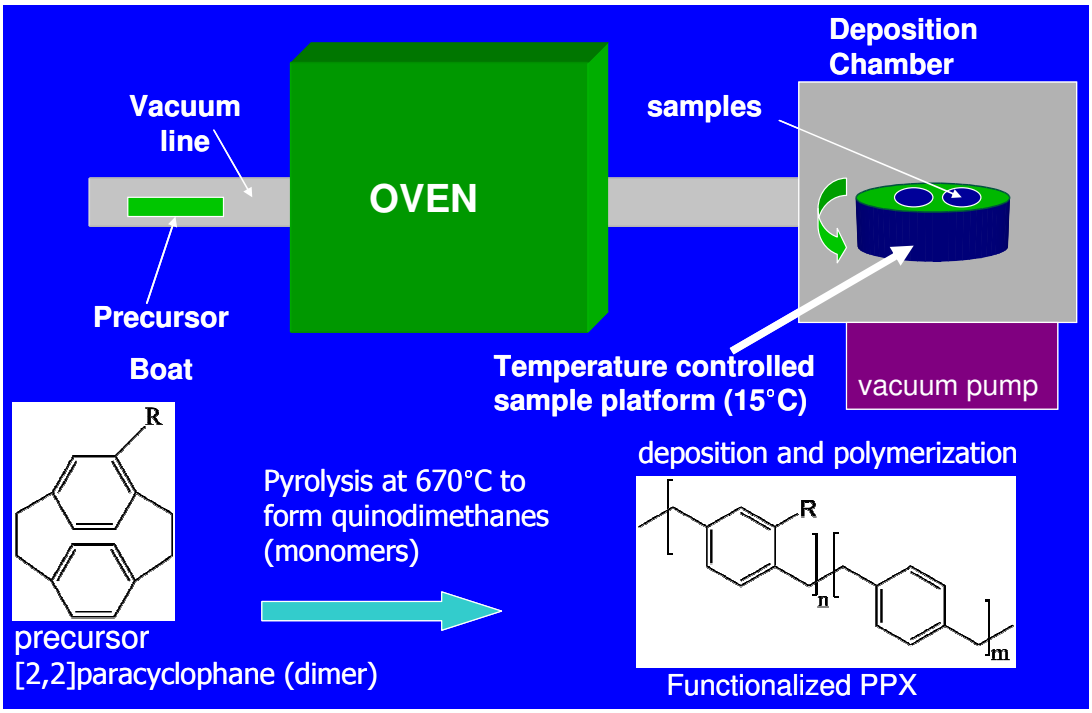

Figure 2-1 CVD setup in the Lahann group used to make functionalized PPX films.

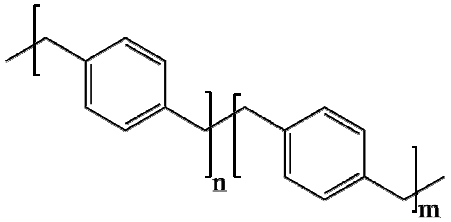

Figure 2-2 Unfunctionalized PPX structure

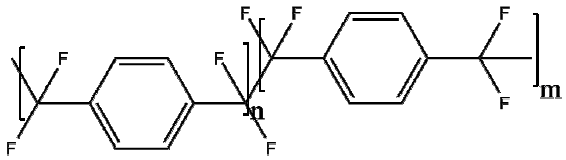

Figure 2-3 PPX-AF4 structure

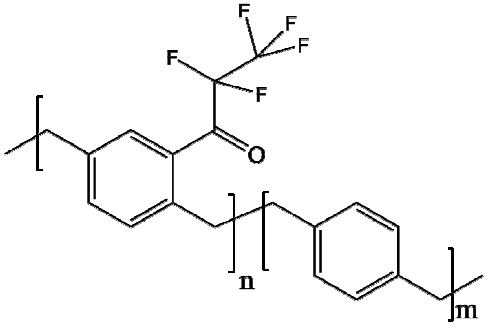

Figure 2-4 PPX-CO-C2F5 structure

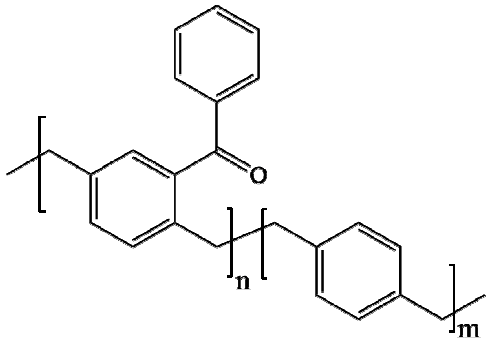

Figure 2-5 PPX-CO-Ph structure

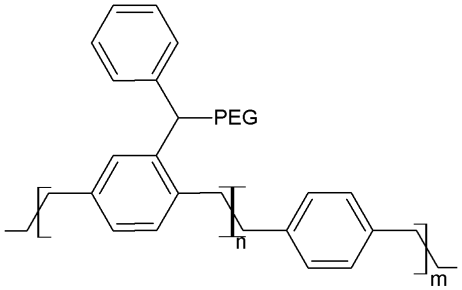

Figure 2-6 PPX-Ph-PEG structure

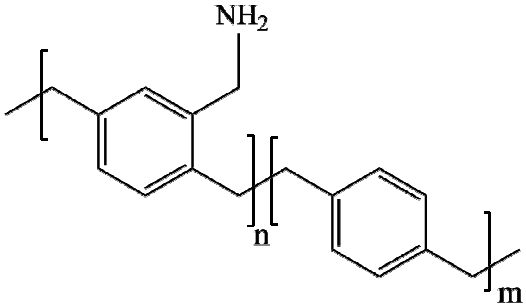

Figure 2-7 PPX-CH_2NH_2 structure

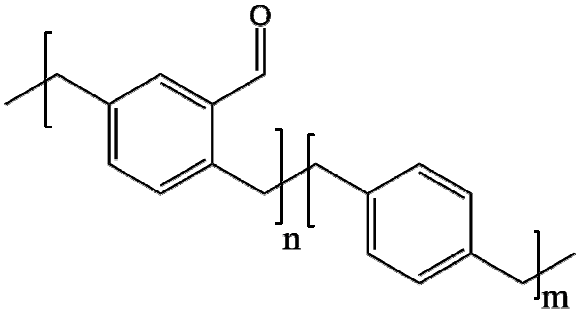

Figure 2-8 PPX-CHO structure

2.3 Verification that functionalization modifies the surface chemistry of PPX via SFG spectroscopy

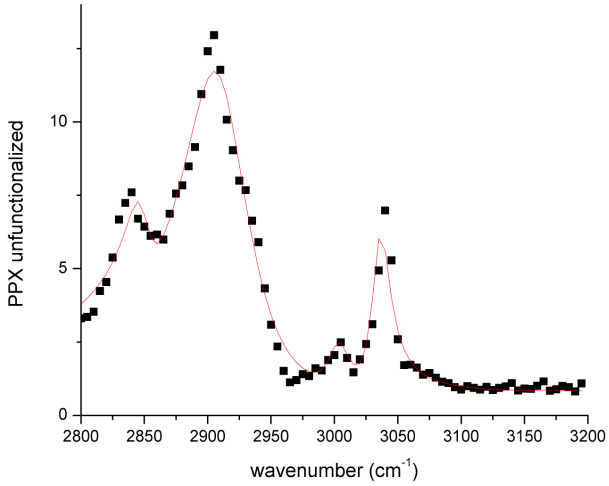

Figure 2-9 SSP SFG spectra of unfunctionalized PPX

Our first goal was to verify that the functionalization did indeed change the surface chemistry. To this end, SFG spectra were collected on the unfunctionalized PPX various functionalized PPX samples. Figure 2-9 clearly shows three peaks at 2845, 2910, and 3045 cm^{-1} in the ssp spectrum collected from the unfunctionalized PPX sample. These peaks can be assigned to the symmetric (2845 cm^{-1}) and asymmetric (2910 cm^{-1}) stretching of the CH_2 linkers and aromatic C-H stretching (3045 cm^{-1}) of the phenyl rings. In Figure 2-10 CH_2 and phenyl rings peaks are also observed from the PPX-Phenyl samples. The phenyl ring peaks are different (e.g., with a large peak width), perhaps due to the different chemical environments for the phenyl in the backbone and the phenyl ring in the side chain. Therefore, the overall signal has a wider peak. Figure 2-11 clearly shows that the SFG spectrum of PPX-CO-PEG is different from unfunctionalized PPX.

We believe the spectra difference indicates that the surface is predominately PEG groups. The spectrum agrees with previously published SFG spectra of PEG.[70] Figure 2-10 shows the CF_2 peaks from the fluorinated linkers, indicating functionalized fluorinated groups present on the surface. In conclusion, we clearly show that the functionalization of PPX does change the surface chemistry of the polymer film.

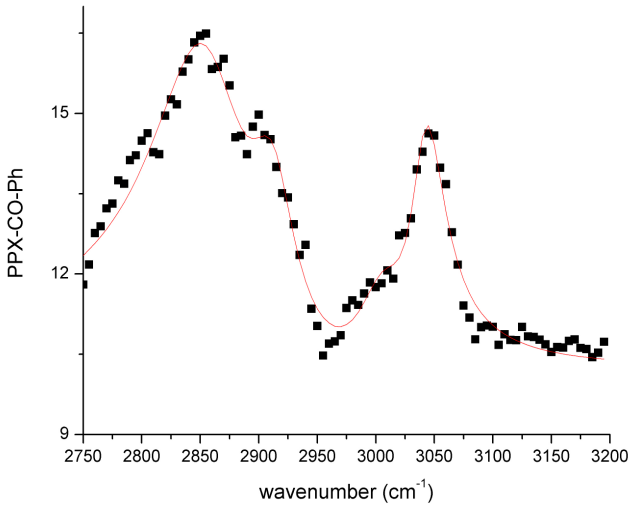

Figure 2-10 SSP SFG spectra of PPX-CO-Ph

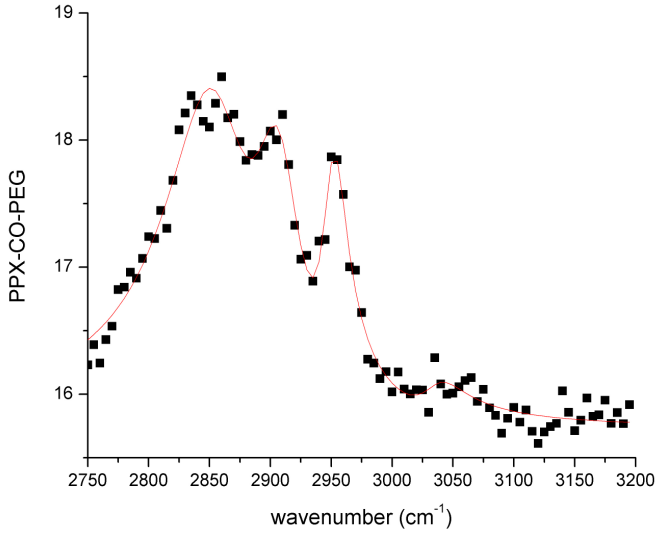

Figure 2-11 SSP SFG spectra of PPX-CO-PEG

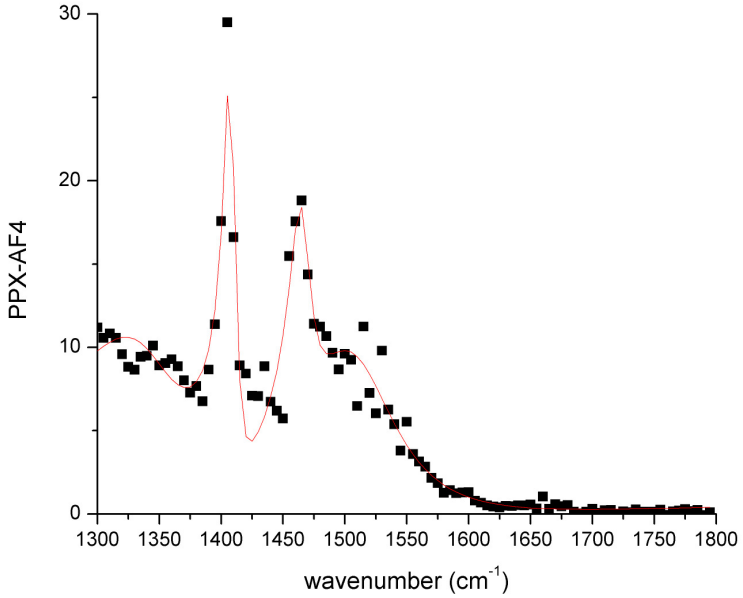

Figure 2-10 SSP SFG spectra of PPX-AF4 showing the F related peaks

2.4 PPX in contact with water

Knowledge about the surface structure of a polymer in an aqueous environment is important for a number of applications, such as biomedical implants, marine antifouling coatings, and biological molecule separation using polymer membranes. As mentioned in Chapter 1, many conventional surface sensitive techniques require high vacuum to operate, thus it is difficult to probe polymer/liquid interfaces. SFG has been applied to investigate polymer surfaces structures in aqueous environment. SFG studies indicate that some polymers reorient in an aqueous environment.[71,72] In this work we observe the reorientation of the phenyl rings in the functionalized PPX films in water.

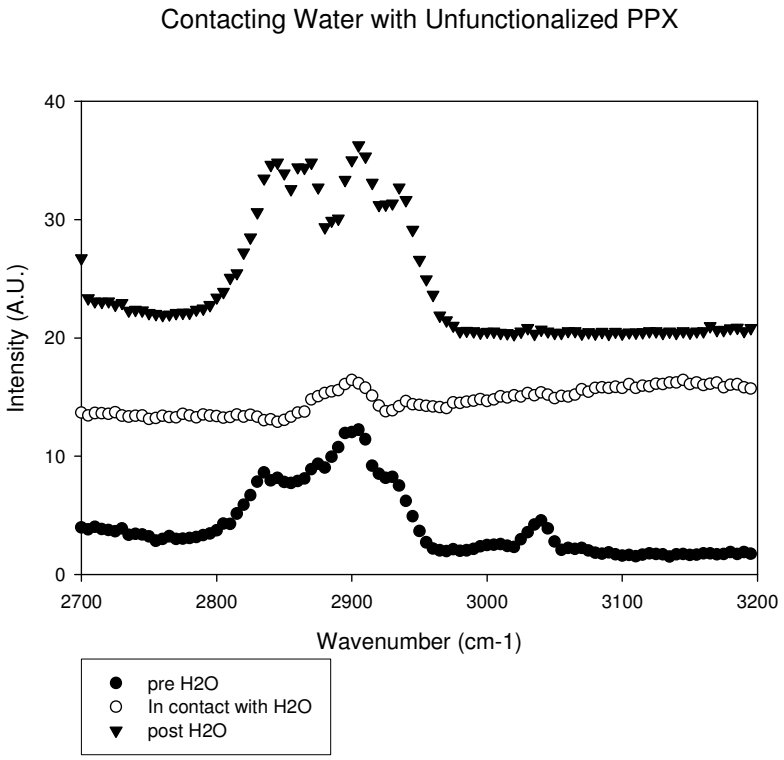

Figure 2-11 The effect of exposure of water to unfunctionalized PPX surfaces.

For polymer applications that are for an aqueous environment, it is important to understand the polymer surface chemistry *in situ*, as the surface structures of polymers in aqueous environments has been shown to be different in aqueous environments and air or vacuum environments. Therefore, prediction of the polymer surface structure in water based on the structure studied in air or vacuum may not be correct.

SFG spectra were collected from an unfunctionalized PPX surface in air, in water, and after removing the sample from water and exposing it to air again (Figure 2-11). Similar SFG studies have been performed on the phenyl functionalized PPX (PPX-CO-Ph, Figure 2-12). As can be seen from Figure 2-11 and Figure 2-12 the phenyl ring signal at 3050 cm^{-1} disappears during and after exposure to water. With the SSP polarization combination, this implies that the phenyl rings are standing up in the as deposited films and lie down after exposure to water. This might be due to the unfavorable interactions between the aromatic ring and water molecules. Such

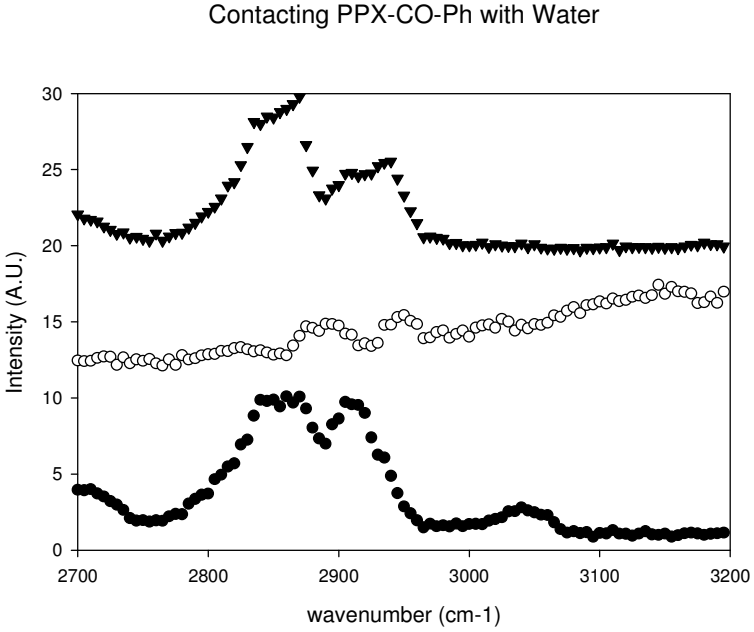

Figure 2-12 Effect of exposure to water of PPX-CO-Ph, solid circles – as deposited, open circles – contact to water, triangles – in air after contact to water

unfavorable interactions push aromatic rings to lie down on the surface to minimize the interactions. Changes in the surface structure induced by an aqueous environment have important effects on how biological molecules interact with polymer surfaces. For example, the surface reorientation of aromatic ring at the PPX surface in an aqueous environment may change its interactions with protein molecules. The interaction of

proteins with an implant has been shown to determine the acceptance or rejection of an implant.[71]

2.5 Solventless Adhesive Bonding (SAB) Introduction

SFG was also applied to investigate buried interface between two functionalized PPX polymers with different reactive groups. After annealing two such polymer materials, the two functional groups were found to react, resulting in strong adhesion at the interface to bond two polymers together. This Solventless Adhesive Bonding (SAB) method has been developed by the Lahann at the University of Michigan. Such a method can be used to bind any two materials together by chemical vapor deposition of the functionalized PPX on surface materials.

This SAB method is important for many applications, in biotechnology as well as related fields. As mentioned in Chapter 1, recent years have seen rapid progress in biotechnology and related fields towards progressively smaller devices with increasing biological complexity.[73-77] This has led to a need for novel materials and advanced micro-fluidic device fabrication processes, which can be precisely tailored towards specific applications. Device integration always comes with a series of challenges. One of the outstanding challenges in this field is effective bonding of independently designed sub-structures.[78,79] Poly(dimethylsiloxane) (PDMS) is a common and widely used material for low-cost, biotechnological applications, but it requires oxidative pretreatment, such as oxygen plasma[27,80-82] or UV/ozone[83] activation for bonding. Silanol groups are created after exposure to a highly oxidative environment. These silanol groups can result in strong intermolecular bonding,[82] but the oxidative activation effects tend to be temporary due to hydrophobic recovery,[84] meaning that the oxidation reaction must be conducted

immediately prior to bonding. Hydrophobic recovery of the PDMS may be slowed down by storage of the material in water or extraction of the low-molecular weight components.[78,83,85]Even so, these oxidative approaches remain limited to a small group of substrates, such as PDMS, silicon, or glass,(materials with Si atoms) impeding the use of these methods to produce new or novel materials with desirable properties. Progress in bonding technology has been limited by the lack of precision in the chemical reactions used for bonding, many of which require empirical process optimization to make feasible.

SAB process is an alternate strategy for chemical bonding, which relies on reactive polymer coatings with precisely engineered surface chemistries and is applicable to a wide range of materials, including (but not limited to) PDMS. Because SFG has the capability to probe buried interfaces in situ, the exact molecular mechanism of the SAB process can be elucidated using SFG. Because of the high degree of selectivity of the chemistry exploited for SAB, the process lends itself to simultaneous bonding and surface modification.

The interfacial bonding here was achieved through reactions between two complementary polymer coatings, one amine functionalized and one aldehyde functionalized. (Figure 2-13) These CVD-based polymer films were shown to form well-adherent coatings on a wide range of different substrate materials including polymers, glass, silicon, metals, or paper. The coated materials can be stored for an extended period prior to bonding without losing their bonding capability. Tensile stress experiments were performed on PDMS with various substrates, and the results compared favorably to current methods of bonding such as oxygen plasma and UV/ozone treatment.

SFG was used here to probe for the presence of amine and aldehyde groups on the surface after CVD polymerization, and their conversion during bonding.

2.5.1 SAB sample preparation

Here, poly(4-aminomethyl-*p*-xylylene-co-*p*-xylylene) and poly(4-formyl-*p*-xylylene-*co*-*p*-xylylene) are used to create reactive surfaces for adhesion. Details of how to prepare these two functionalized PPX materials have been presented in section 2.2 above.

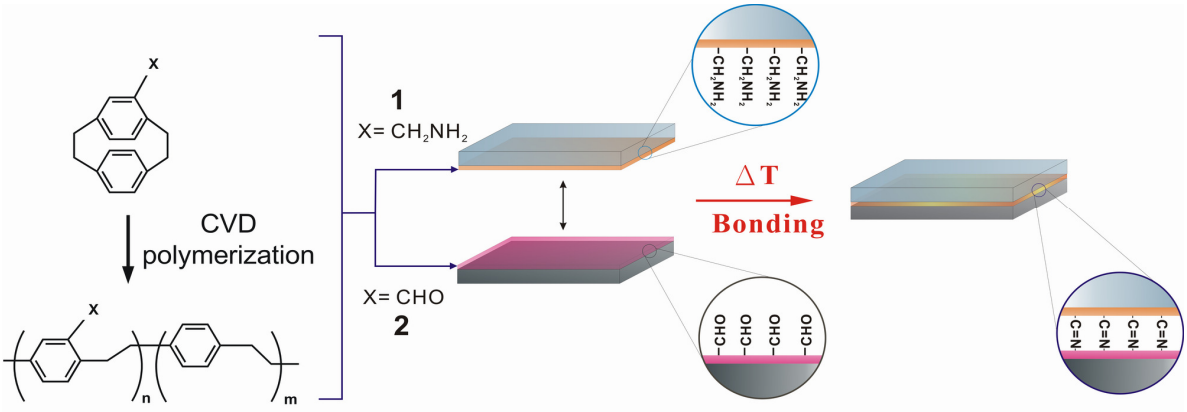

Figure 2-13 Schematic illustration of the solventless adhesive bonding (SAB) process. During SAB, formation of a strong adhesion layer is achieved by bonding of two complementary CVD reactive coatings 1 and 2.

2.5.2 Materials

PDMS samples were prepared by uniformly mixed PDMS prepolymer and curing agent (Sylgard 184, Dow Corning) at a ratio of 10:1 and were cured at 70 ºC for 1 hr.[13] Glass slides (Fisher), PTFE films (0.01 mm, Goodfellow), and stainless steel foils (AISI 316L - Fe/Cr18/Ni10/Mo3, annealed, 0.1 mm, Goodfellow) were used as received. Gold samples were prepared on silicon wafers (Silicon Valley Microelectronics, Inc.) by e-beam deposition, with 3 nm of titanium followed by 80 nm of gold.

2.5.3 Surface characterization method

The film thicknesses reported here were measured using a multi-wavelength rotating analyzer ellipsometer (M-44, J. A. Woollam) at an incident angle of 75°. The data were analyzed using WVASE32 software. Thickness measurements were recorded by fitting the ellipsometric psi and delta data with An = 1.65, Bn = 0.01 for polymer **1** and An = 1.76 and Bn = 0.01 for polymer **2** using a Cauchy model and software module integrated with the system. The ellipsometry measurements were performed by Hsien Yeh Chen.

The details of the SFG setup and experimental geometry were detailed in Chapter 1.[24-28] Window geometry was used for this system. SFG spectra were selectively detected from the buried polymer interface using SSP and PPP polarization combinations.

2.5.4 Bonding process and tensile stress test.

The tensile tests were performed by Hsien Yeh Chen. The SAB process was performed by first coating various substrates with polymer **1**(the amine functionalized surface) and **2** (the aldehyde functionalized surface). After the CVD coating process, the samples were brought into contact, and placed in oven at 140 ^{o}C for 3 hr. The resulting bonded samples were tensile tested and stored at room temperature (20 ^{o}C). The UV/ozone bonding control experiments were performed by using an UVO-cleaner (model 342, Jelight Co.) to treat the substrates for 30 min. The UV/ozone treated samples were then cured at 120 ^{o}C for 20 min. The oxygen plasma bonding control experiments were performed using a plasma etcher (SPI Plasma-Prep II, SPI Supplies/Structure Probe, Inc.).The plasma treatment was performed with a 10 W

energetic oxygen plasma under 200 - 300 mTorr pressure for 30 sec. The plasma-treated samples were then cured at 60 ^{o}C for 10 min or 120 ^{o}C for 10 min. All tensile stress tests were performed with a Bionix 100 mechanical tester (MTS, Co.) equipped with a 10N load sensor. The samples were prepared in a cross-section area of 10 mm x 10 mm, and the measurements were recorded at the displacement rate of 0.05 mm/min.

As can be seen in Table 1 the SAB method failed in the bulk PDMSs and not at the joint for PDMS-PDMS, PDMS-stainless steel, PDMS-silicon wafer, PDMS-glass, and PDMS-gold. SAB method for PDMS-PTFE also showed stronger adhesion than the conventional plasma or ozone methods.

The reactive coatings used here, poly(4-aminomethyl-*p*-xylylene-co-*p*-xylylene)[97,98] (**1**) and poly(4-formyl-*p*-xylylene-*co*-*p*-xylylene)[52] (**2**), were stable under dry conditions until contacted to the complimentary film at elevated temperatures. Prior to mechanical testing, the chemical structures of all polymer films were confirmed by X-ray photoelectron spectroscopy (XPS). Film thicknesses were in the range of 40 - 80 nm as measured by ellipsometry.

Method	Material	Bonding Strength (MPa)
SAB	PDMS – PTFE	1.21±0.35
	PDMS - PDMS	> 2.44±0.15[a]
	PDMS - Stainless Steel	> 2.44±0.15
	PDMS - Silicon Wafer	> 2.44±0.15
	PDMS – Glass	> 2.44±0.15
	PDMS – Gold	> 2.44±0.15
Physical contact	PDMS - PDMS	0.02±0.11
Heat (140 ^{o}C)		0.19±0.09
UV/Ozone		0.78±0.08
Oxygen Plasma (cured at 60 ^{o}C)		1.15±0.18
Oxygen Plasma (cured at 120 ^{o}C)		2.34±0.27

[a] Fracture strength of PDMS was 2.44±0.15 MPa compared to 2.24 MPa reported in *Polymer Data Handbook* (Mark, J. E., *Polymer data handbook*. Oxford University Press: New York, 1999).

Table 1 Comparison of tensile tests between SAB and traditional bonding methods

2.5.4 SFG studies of the SAB mechanism

To elucidate the underlying mechanism of the bonding process at the molecular level, we used sum frequency generation (SFG) spectroscopy. It was hypothesized that the adhesion in the SAB process was due to covalent binding *via* imine bonds formed between CHO and CH_2NH_2 groups of the two polymer coatings. If there is a chemical reaction that occurred at the buried interface, then the characteristic stretches of the amine and aldehyde groups should disappear.

The SFG spectra of the two polymer films deposited on CaF_2 windows were collected individually. (Figure 2-14 and Figure 2-15)

When a PDMS substrate coated with aldehyde functionalized polymer was contacted to a CaF_2 substrate coated with the amine functionalized polymer, the characteristic vibrational spectra related to the primary amino groups of amine functionalized polymer was still detected at 1635 cm^{-1} (NH_2 bending coupled with aromatic ring stretching, Figure 2-14) and 3325 cm^{-1} (N-H stretch, Figure 2-16). This proves that the disappearance of the SFG signal was not merely due to the change in optical constants when the two films were contacted.

The characteristic C=O stretch (Figure 2-15) of the aldehyde groups stemming from the aldehyde functionalized polymer was detected at 1725 cm^{-1}. The spectra of the aldehyde functionalized polymer after heating is also shown in Figure 2-15. The fact that the C=O signal is still there implies that any disappearance of the SFG signal was not due to surface reordering during the heat treatment.

Prior to exposure to sufficiently high temperatures, the complementary chemical groups continue to co-exist without detectable chemical conversion. Also heating the

samples individually does not cause the SFG signal to disappear. After the samples were contacted and heated to 140 ºC, however, both amines and aldehyde groups were simultaneously consumed as indicated by the disappearance of the SFG signals at 1635 cm^{-1} and 3325 cm^{-1} in one case, and 1725 cm^{-1} on the other. Again, these effects were not observed when the substrates were brought in contact without heating (Figure 2-14) or when one coating alone was heated (Figure 2-15), suggesting that the observed changes in the SFG spectra indeed correlate with the bonding event. Based on these experiments, we concluded that the strong bonding is due to the chemical reaction between amino and aldehyde groups, as opposed to mechanical interlock of the polymer chains. The implications are that we now understand the mechanism for the adhesion in this system and can work to further refine the SAB method for specific applications. In addition, we have shown that SFG can be used to probe the buried interfacial chemical reactions paving the way to future studies of surface chemical reaction sites.

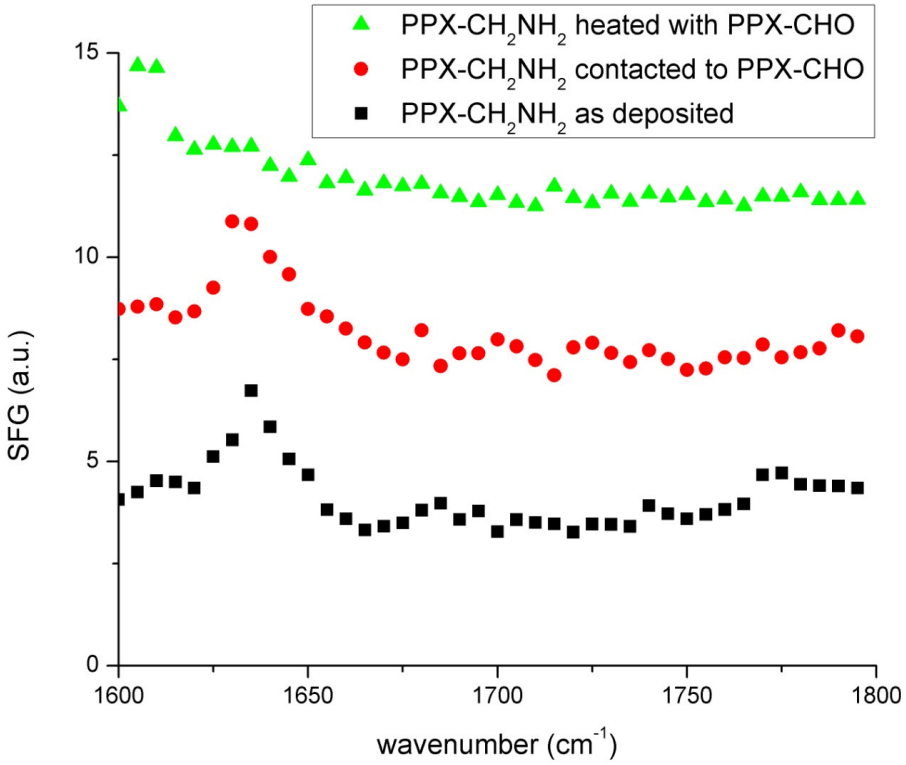

Figure 2-14 SFG spectra of PPX-CH_2NH_2 films

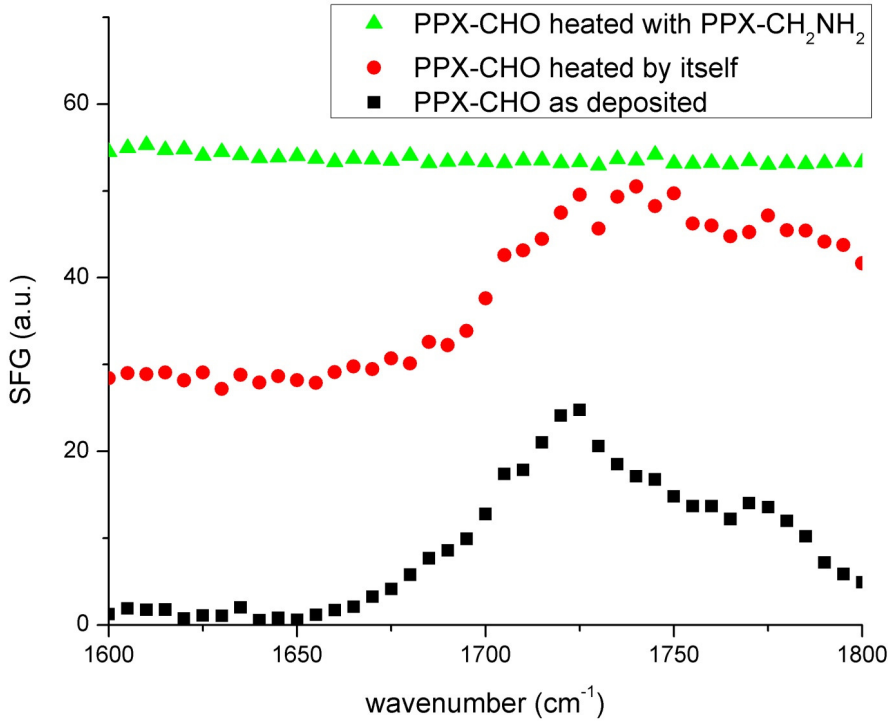

Figure 2-15 SFG spectra of PPX-CHO films

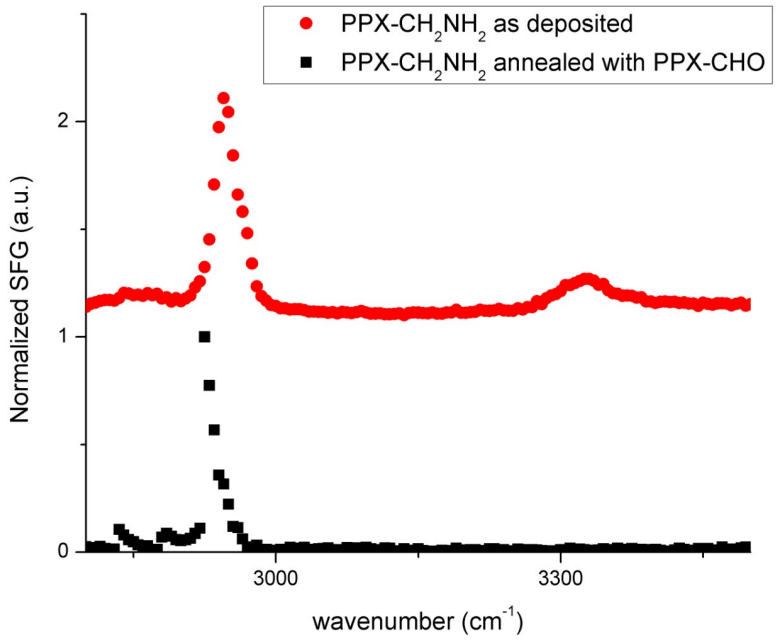

Figure 2-16 SFG spectra of PPX-CH_2-NH_2 in air and cured with PPX-CHO

2.6 Summary and Conclusions

We studied a variety of functionalized PPX thin films. With sum frequency vibrational spectroscopy we verified that the functionalization did indeed change the surface structure of the samples. We also verified that the PPX films underwent some irreversible reorientation when exposed to an aqueous environment. We then probed the mechanism behind the SAB process using an aldehyde functionalized PPX film and a amine functionalized film. It was found that there was strong evidence for a chemical reaction occurring between the aldehyde group and the amine group. This research shows that SFG is a powerful surface analytical technique that can provide molecular level surface structure and can selectively probe buried polymer interfaces in situ. This research also demonstrates the feasibility to develop SFG as a nondestructive tool to test polymer adhesion.

2.7 Acknowledgments for the PPX project

We thank Professor Shuichi Takayama and Yaokuang Chung, University of Michigan, for the assistance with oxygen plasma bonding. We thank Prof. Kotov, University of Michigan, for use of the ellipsometer. We gratefully acknowledge Dr. Shuji Ye for the *ab initio* calculations. Dr. Hsien Ye Chen prepared all the samples and performed the tension tests.

(1) Liu, T. Y.; Hu, S. H.; Liu, D. M.; Chen, S. Y.; Chen, I. W. *Nano Today* **2009**, *4*, 52-65.

(2) Srivastava, S.; Kotov, N. A. *Accounts of Chemical Research* **2008**, *41*, 1831-1841.

(3) Haynie, D. T.; Zhang, L.; Rudra, J. S.; Zhao, W. H.; Zhong, Y.; Palath, N. *Biomacromolecules* **2005**, *6*, 2895-2913.

(4) Chan, C. M.; Ko, T. M.; Hiraoka, H. *Surface Science Reports* **1996**, *24*, 3-54.

(5) Rusling, J. F.; Hvastkovs, E. G.; Schenkman, J. B. *Current Opinion in Drug Discovery & Development* **2007**, *10*, 67-73.

(6) Zheng, L. Z.; Yao, X.; Li, J. H. *Current Analytical Chemistry* **2006**, *2*, 279-296.

(7) Chiniwalla, P.; Manepalli, R.; Farnsworth, K.; Boatman, M.; Dusch, B.; Kohl, P.; Allen, S. A. B. *Low and High Dielectric Constant Materials: Materials Science, Processing, and Reliability Issues and Thin Film Materials for Advanced Packaging Technologies* **2000**, *99*, 135-142.

(8) Chiniwalla, P.; Manepalli, R.; Farnsworth, K.; Boatman, M.; Dusch, B.; Kohl, P.; Allen, S. A. B. *1999 International Conference on High Density Packaging and Mcms, Proceedings* **1999**, *3830*, 52-57.

(9) McCulloch, I.; Heeney, M.; Chabinyc, M. L.; DeLongchamp, D.; Kline, R. J.; Coelle, M.; Duffy, W.; Fischer, D.; Cundloch, D.; Hamadani, B.; Hamilton, R.; Richter, L.; Salleo, A.; Shkunov, M.; Sporrowe, D.; Tierney, S.; Zhong, W. *Advanced Materials* **2009**, *21*, 1091-1109.

(10) Lindner, E.; Gyurcsanyi, R. E. *Journal of Solid State Electrochemistry* **2009**, *13*, 51-68.

(11) de Boer, B.; Facchetti, A. *Polymer Reviews* **2008**, *48*, 423-431.

(12) Someya, T.; Pal, B.; Huang, J.; Katz, H. E. *Mrs Bulletin* **2008**, *33*, 690-696.

(13) Choi, M. C.; Kim, Y.; Ha, C. S. *Progress in Polymer Science* **2008**, *33*, 581-630.

(14) Lee, Y. S.; Lee, S. M.; Jung, S. K.; Lee, S. J.; Lee, S. H.; Hong, Y. H.; Kim, H. J.; Park, L. S. *Molecular Crystals and Liquid Crystals* **2009**, *498*, 203-213.

(15) Lee, Y. K.; Kwon, S. K.; Park, T. J.; Jeon, W. S.; Park, J. J.; Kim, S. Y.; Kwon, J. H.; Jang, J. *Molecular Crystals and Liquid Crystals* **2009**, *498*, 214-221.

(16) Coya, C.; de Andres, A.; Zaldo, C.; Alvarez, A. L.; Arredondo, B.; Gomez, R.; Segura, J. L.; Seoane, C. *Journal of Applied Physics* **2009**, *105*.

(17) Brondijk, J. J.; Li, X.; Akkerman, H. B.; Blom, P. W. M.; de Boer, B. *Applied Physics a-Materials Science & Processing* **2009**, *95*, 1-5.

(18) Tao, Y. F.; Ma, B. W.; Segalman, R. A. *Macromolecules* **2008**, *41*, 7152-7159.

(19) Eldada, L. *Review of Scientific Instruments* **2004**, *75*, 575-593.

(20) Samyn, C.; Verbiest, T.; Persoons, A. *Macromolecular Rapid Communications* **2000**, *21*, 1-15.

(21) Kaneto, K.; Kudo, K.; Ohmori, Y.; Onoda, M.; Iwamoto, M. *Ieice Transactions on Electronics* **1998**, *E81C*, 1009-1019.

(22) Liu, Y. F.; Zeng, J.; Wang, C. H. *Estc 2008: 2nd Electronics System-Integration Technology Conference, Vols 1 and 2, Proceedings* **2008**, 199-203.

(23) Fang, J.; Fu, J.; Ayazi, F. *Journal of Micromechanics and Microengineering* **2008**, *18*.

(24) Lee, C. Y.; Wu, G. W.; Hsieh, W. J. *Sensors and Actuators a-Physical* **2008**, *147*, 173-176.

(25) Zhou, F.; Arunasalam, P.; Murray, B.; Sammakia, B. *2008 11th Ieee Intersociety Conference on Thermal and Thermomechanical Phenomena in Electronic Systems, Vols 1-3* **2008**, 1063-1070.

(26) Bandorf, R.; Paulkowski, D. M.; Schiffmann, K. I.; Kuster, R. L. A. *Journal of Physics-Condensed Matter* **2008**, *20*.

(27) Niklaus, F.; Stemme, G.; Lu, J. Q.; Gutmann, R. J. *Journal of Applied Physics* **2006**, *99*.

(28) Uchida, S.; Martinez, A.; Song, Y. W.; Ishigure, T.; Yamashita, S. *2008 Conference on Lasers and Electro-Optics & Quantum Electronics and Laser Science Conference, Vols 1-9* **2008**, 1704-1705.

(29) Baumann, K.; Moll, N.; Stoferle, T.; Wahlbrink, T.; Bolten, J.; Mollenhauer, T.; Moormann, C.; Wang, B. L.; Scherf, U.; Mahrt, R. F. *Organic Optoelectronics and Photonics Iii* **2008**, *6999*, 99906-99906.

(30) Zhang, S. M.; Zhang, D. K.; Ma, D. G. *Chinese Physics Letters* **2008**, *25*, 1690-1692.

(31) Riedl, T.; Rabe, T.; Gorrn, P.; Wang, J.; Weimann, T.; Hinze, P.; Galbrecht, F.; Scherf, U.; Kowalsky, W. *Organic Light Emitting Materials and Devices Xi* **2007**, *6655*, V6550-V6550.

(32) Cheng, F. S.; Huang, P. Y.; Yang, S. Y. *International Polymer Processing* **2008**, *23*, 312-316.

(33) Massenot, S.; Grandidier, J.; Bouhelier, A.; des Francs, G. C.; Markey, L.; Weeber, J. C.; Dereux, A.; Renger, J.; Gonzalez, M. U.; Quidant, R. *Applied Physics Letters* **2007**, *91*.

(34) Begou, T.; Beche, B.; Goullet, A.; Landesman, J. P.; Granier, A.; Cardinaud, C.; Gaviot, E.; Camberlein, L.; Grossard, N.; Jezequel, G.; Zyss, J. *Optical Materials* **2007**, *30*, 657-661.

(35) Johnson, V. S.; Bowden, B.; Harrington, J. A. *Optical Fibers and Sensors for Medical Diagnostics and Treatment Applications VII* **2007**, *6433*, E4330-E4330.

(36) Ponnampalam, N.; DeCorby, R. G. *Optics Express* **2007**, *15*, 12595-12604.

(37) Voit, A.; Krekhov, A.; Kohler, W. *Physical Review E* **2007**, *76*.

(38) Seo, S. W.; Cho, S. Y.; Jokerst, N. M. *Optics Letters* **2007**, *32*, 548-550.

(39) Ng, T. N.; Wong, W. S.; Lujan, R. A.; Russo, B.; Chabinyc, M. L.; Sambandan, S.; Street, R. A. *Organic Field-Effect Transistors Vii and Organic Semiconductors in Sensors and Bioelectronics* **2008**, *7054*, M541-M541.

(40) Mikroyannidis, J. A.; Stylianakis, M. M.; Cheung, K. Y.; Fung, M. K.; Djurisic, A. B. *Synthetic Metals* **2009**, *159*, 142-147.

(41) Ng, T. N.; Wong, W. S.; Chabinyc, M. L.; Sambandan, S.; Street, R. A. *Applied Physics Letters* **2008**, *92*.

(42) Wang, X. H.; Levermore, P. A.; Hofmann, O.; deMello, J. C.; deMello, A. J.; Bradley, D. D. C. *Proceedings of the First Shenyang International Colloquium on Microfluidics* **2007**, 165-166.

(43) Arias, A. C. *Polymer Reviews* **2006**, *46*, 103-125.

(44) Moons, E. *Journal of Physics-Condensed Matter* **2002**, *14*, 12235-12260.

(45) Cai, G. B.; Guo, X. H.; Yu, S. H. *Progress in Chemistry* **2008**, *20*, 1001-1014.

(46) Embrechts, A.; Feng, C. L.; Mills, C. A.; Lee, M.; Bredebusch, I.; Schnekenburger, J.; Domschke, W.; Vancso, G. J.; Schonherr, H. *Langmuir* **2008**, *24*, 8841-8849.

(47) Mukherjee, R.; Sharma, A.; Patil, G.; Faruqui, D.; Pattader, P. S. G. *Bulletin of Materials Science* **2008**, *31*, 249-261.

(48) Chen, H. Y.; Lai, J. H.; Jiang, X. W.; Lahann, J. *Advanced Materials* **2008**, *20*, 3474-+.

(49) Elkasabi, Y.; Yoshida, M.; Nandivada, H.; Chen, H. Y.; Lahann, J. *Macromolecular Rapid Communications* **2008**, *29*, 855-870.

(50) Chen, H. Y.; McClelland, A. A.; Chen, Z.; Lahann, J. *Analytical Chemistry* **2008**, *80*, 4119-4124.

(51) Jiang, X. W.; Chen, H. Y.; Galvan, G.; Yoshida, M.; Lahann, J. *Advanced Functional Materials* **2008**, *18*, 27-35.

(52) Nandivada, H.; Chen, H. Y.; Lahann, J. *Macromolecular Rapid Communications* **2005**, *26*, 1794-1799.

(53) Chen, H. Y.; Lahann, J. *Analytical Chemistry* **2005**, *77*, 6909-6914.

(54) Schurmann, K.; Lahann, J.; Niggemann, P.; Klosterhalfen, B.; Meyer, J.; Kulisch, A.; Klee, D.; Gunther, R. W.; Vorwerk, D. *Radiology* **2004**, *230*, 151-162.

(55) Suh, K. Y.; Langer, R.; Lahann, J. *Applied Physics Letters* **2003**, *83*, 4250-4252.

(56) Schurmann, K.; Roos, A.; Meyer, J.; Ries, B.; Lahann, J.; Hermanns, B.; Kulisch, A.; Vorwerk, D.; Klee, D.; Gunther, R. W. *Rofo-Fortschritte Auf Dem Gebiet Der Rontgenstrahlen Und Der Bildgebenden Verfahren* **2003**, *175*, 262-270.

(57) Lahann, J.; Langer, R. *Macromolecules* **2002**, *35*, 4380-4386.

(58) Lahann, J.; Balcells, M.; Rodon, T.; Lee, J.; Choi, I. S.; Jensen, K. F.; Langer, R. *Langmuir* **2002**, *18*, 3632-3638.

(59) Lahann, J.; Choi, I. S.; Lee, J.; Jenson, K. F.; Langer, R. *Angewandte Chemie-International Edition* **2001**, *40*, 3166-+.

(60) Lahann, J.; Langer, R. *Macromolecular Rapid Communications* **2001**, *22*, 968-971.

(61) Lahann, J.; Hocker, H.; Langer, R. *Angewandte Chemie-International Edition* **2001**, *40*, 726-728.

(62) Lahann, J.; Klee, D.; Hocker, H. *Materialwissenschaft Und Werkstofftechnik* **1999**, *30*, 763-766.

(63) Lahann, J.; Klee, D.; Hocker, H. *Macromolecular Rapid Communications* **1998**, *19*, 441-444.

(64) Misurkin, I. A.; Titov, S. V.; Zhuravleva, T. S.; Klimenko, I. V.; Zav'yalov, S. A.; Grigor'ev, E. I.; Chvalun, S. N. *Russian Journal of Physical Chemistry A* **2009**, *83*, 450-456.

(65) Martin-Palma, R. J.; Demirel, M. C.; Wang, H.; Pantano, C. G. *Journal of Non-Crystalline Solids* **2009**, *355*, 208-212.

(66) Hopf, H. *Angewandte Chemie-International Edition* **2008**, *47*, 9808-9812.

(67) He, D. M.; Sun, W.; Schrader, T.; Ulbricht, M. *Journal of Materials Chemistry* **2009**, *19*, 253-260.

(68) Burnworth, M.; Knapton, D.; Rowan, S. J.; Weder, C. *Journal of Inorganic and Organometallic Polymers and Materials* **2007**, *17*, 91-103.

(69) Greiner, A.; Mang, S.; Schafer, O.; Simon, P. *Acta Polymerica* **1997**, *48*, 1-15.

(70) Chen, C. Y.; Even, M. A.; Wang, J.; Chen, Z. *Macromolecules* **2002**, *35*, 9130-9135.

(71) Clarke, M. L.; Chen, Z. *Langmuir* **2006**, *22*, 8627-8630.

(72) Clarke, M. L.; Chen, C. Y.; Wang, J.; Chen, Z. *Langmuir* **2006**, *22*, 8800-8806.

(73) Tian, J. D.; Gong, H.; Sheng, N. J.; Zhou, X. C.; Gulari, E.; Gao, X. L.; Church, G. *Nature* **2004**, *432*, 1050-1054.

(74) Pellois, J. P.; Zhou, X. C.; Srivannavit, O.; Zhou, T. C.; Gulari, E.; Gao, X. L. *Nature Biotechnology* **2002**, *20*, 922-926.

(75) Lucchetta, E. M.; Lee, J. H.; Fu, L. A.; Patel, N. H.; Ismagilov, R. F. *Nature* **2005**, *434*, 1134-1138.

(76) Petty, R. T.; Li, H. W.; Maduram, J. H.; Ismagilov, R.; Mrksich, M. *Journal of the American Chemical Society* **2007**, *129*, 8966-+.

(77) Fu, A. Y.; Spence, C.; Scherer, A.; Arnold, F. H.; Quake, S. R. *Nature Biotechnology* **1999**, *17*, 1109-1111.

(78) Chen, C. S.; Mrksich, M.; Huang, S.; Whitesides, G. M.; Ingber, D. E. *Science* **1997**, *276*, 1425-1428.

(79) Harrison, C.; Cabral, J.; Stafford, C. M.; Karim, A.; Amis, E. J. *Journal of Micromechanics and Microengineering* **2004**, *14*, 153-158.

(80) Duffy, D. C.; McDonald, J. C.; Schueller, O. J. A.; Whitesides, G. M. *Analytical Chemistry* **1998**, *70*, 4974-4984.

(81) McDonald, J. C.; Duffy, D. C.; Anderson, J. R.; Chiu, D. T.; Wu, H. K.; Schueller, O. J. A.; Whitesides, G. M. *Electrophoresis* **2000**, *21*, 27-40.

(82) Bhattacharya, S.; Datta, A.; Berg, J. M.; Gangopadhyay, S. *Journal of Microelectromechanical Systems* **2005**, *14*, 590-597.

(83) McDonald, J. C.; Whitesides, G. M. *Accounts of Chemical Research* **2002**, *35*, 491-499.

(84) Makamba, H.; Kim, J. H.; Lim, K.; Park, N.; Hahn, J. H. *Electrophoresis* **2003**, *24*, 3607-3619.

(85) Cygan, Z. T.; Cabral, J. T.; Beers, K. L.; Amis, E. J. *Langmuir* **2005**, *21*, 3629-3634.

(86) Quake, S. R.; Scherer, A. *Science* **2000**, *290*, 1536-1540.

(87) Janasek, D.; Franzke, J.; Manz, A. *Nature* **2006**, *442*, 374-380.

(88) Yoshida, M.; Langer, R.; Lendlein, A.; Lahann, J. *Polymer Reviews* **2006**, *46*, 347-375.

(89) Diaz, D. D.; Punna, S.; Holzer, P.; McPherson, A. K.; Sharpless, K. B.; Fokin, V. V.; Finn, M. G. *Journal of Polymer Science Part a-Polymer Chemistry* **2004**, *42*, 4392-4403.

(90) Kolb, H. C.; Finn, M. G.; Sharpless, K. B. *Angewandte Chemie-International Edition* **2001**, *40*, 2004-+.

(91) Lutz, J. F. *Angewandte Chemie-International Edition* **2007**, *46*, 1018-1025.

(92) Nandivada, H.; Jiang, X. W.; Lahann, J. *Advanced Materials* **2007**, *19*, 2197-2208.

(93) Lahann, J. *Chemical Engineering Communications* **2006**, *193*, 1457-1468.

(94) Nandivada, H.; Chen, H. Y.; Bondarenko, L.; Lahann, J. *Angewandte Chemie-International Edition* **2006**, *45*, 3360-3363.

(95) Suh, K. Y.; Langer, R.; Lahann, J. *Advanced Materials* **2004**, *16*, 1401-+.

(96) Lahann, J.; Balcells, M.; Lu, H.; Rodon, T.; Jensen, K. F.; Langer, R. *Analytical Chemistry* **2003**, *75*, 2117-2122.

(97) Elkasabi, Y.; Chen, H. Y.; Lahann, J. *Advanced Materials* **2006**, *18*, 1521-+.

(98) Chow, W. W. Y.; Lei, K. F.; Shi, G. Y.; Li, W. J.; Huang, Q. *Smart Materials & Structures* **2006**, *15*, S112-S116.

(99) Rozenberg, V. I.; Antonov, D. Y.; Sergeeva, E. V.; Vorontsov, E. V.; Starikova, Z. A.; Fedyanin, I. V.; Schulz, C.; Hopf, H. *European Journal of Organic Chemistry* **2003**, 2056-2061.

(100) Loch, C. L.; Ahn, D.; Chen, C. Y.; Wang, J.; Chen, Z. *Langmuir* **2004**, *20*, 5467-5473.

(101) Loch, C. L.; Ahn, D.; Chen, Z. *Journal of Physical Chemistry B* **2006**, *110*, 914-918.

(102) Chen, C. Y.; Loch, C. L.; Wang, J.; Chen, Z. *Journal of Physical Chemistry B* **2003**, *107*, 10440-10445.

(103) Wang, J.; Chen, C. Y.; Buck, S. M.; Chen, Z. *Journal of Physical Chemistry B* **2001**, *105*, 12118-12125.

CHAPTER 3 : TWO-DIMENSIONAL CRYSTALS OF ISOMERIC DIALKYL PHTHALATES TO COMPLEMENT SCANNING TUNNELING MICROSCOPY STUDIES

3.1 Introduction

Molecular thin films have attracted great attention to provide molecule-based devices such as sensors,[1-5] optoelectronic devices,[6-9] diodes,[10] and photovoltaic cells[11]. STM has been applied to study such 2D crystal structures with excellent spatial resolution.[12-19] Supplemented by computed models, STM can provide a detailed picture of the structure of 2D crystals formed at the liquid/solid interface with atomic resolution. However, some structural information (such as functional group orientations in these 2D crystals) needs to be tested experimentally to ensure the accuracy of the calculated structures. Due to the limited sensitivity, many other experimental techniques such as Raman and infrared spectroscopy have not been able to provide such structural information of 2D crystals. It will be shown in this chapter that Sum Frequency Generation Vibrational Spectroscopy (SFG) can measure average orientation of functional groups in such 2D crystals, or physisorbed monolayers, providing key experimental data to aid in the modeling and interpretation of the STM images. The usefulness of combining these two techniques is demonstrated here with a phthalate diester monolayer formed at the 1-phenyloctane/Highly Oriented Pyrolytic Graphite (HOPG) interface. The molecular formula for the phthalate diester studied here and the 1-phenyloctane solvent are displayed in Figure 3-1 and Figure 3-2 respectively. Recent

advances in laser systems have made it feasible to extend collection of SFG spectra to the C=O stretching frequency region (as shown in the previous chapter) and thus study the orientation of C=O groups using SFG.[20-25] Here the spatial orientation of the ester C=O of the monolayer was successfully determined using SFG.

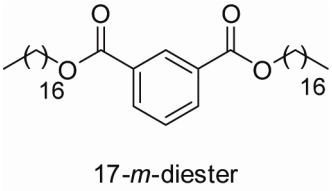

Figure 3-1 Structure of 17 metadiester

In general, computed models complement the structural insight with atomic resolution gained from the high-resolution STM images. Here, we demonstrate that the vibrational information from 2D crystals obtained using SFG can provide critical pieces of knowledge to understand the entire picture of the structure.

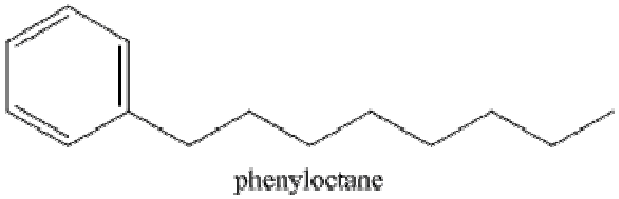

Figure 3-2 Structure of Phenyloctane

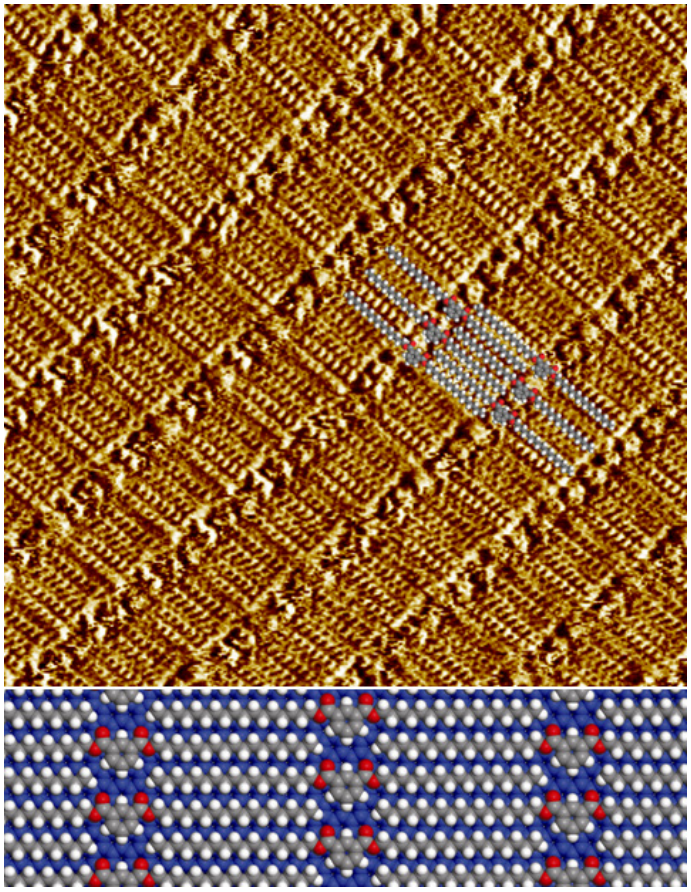

Figure 3-3 STM image (20×20 nm, 10.2 Hz, 800 mV, 300 pA) and computed model of the monolayer of 17-m-diester formed at the 1-phenyloctane/HOPG interface. The computed model is superimposed on STM image.

The diester molecule with long alkyl chains (Figure 3-1) was selected because long alkyl chains contribute to forming 2D crystals on HOPG. The C=O and C-H stretching are detectable at the interface by SFG if they have some ordering along the interface normal. The 2D arrangements on a graphite surface of 17-m-diester were reported previously.[15] According to energy minimization calculations the lowest energy packing, the column of benzene rings of 17-*m*-diester is aligned perpendicular to the alkyl chains and these alkyl chains are interdigitated to give a close packed structure in the

plane group *cm* (Figure 3-3). The modeling was done using Cerius2 version 4.2. Energy minimization was performed using a COMPASS force field.

3.2 Experimental Setup

In this work, SFG spectra were collected using the near-total internal reflection prism geometry previously described (Figure 3-4)[26] with the ssp and ppp polarization combinations. The ppp polarization combination in this prism geometry probes

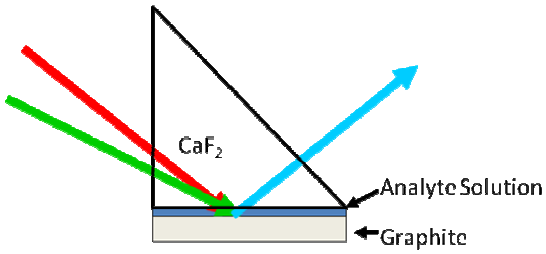

Figure 3-4 Sample geometry. The 17-metadiester in phenyloctane is sandwiched between a layer of HOPG and the CaF2 prism.

predominately the out of plane χ_{zzz} contribution, while the ssp polarization combination probes predominately the in plane χ_{yyz}. The spectra were then normalized by the intensities of the input IR and visible beams A CaF_2 prism instead of fused silica prism was used for these experiments because CaF2 prism is transparent to IR in the C=O stretching frequency region. Graphite sheets were thinned and separated with scotch tape. The thinned graphite was then mounted on a glass substrate. 1 μL of 0.1 mM 17-meta diester in phenyloctane was placed on the graphite and then contacted to the CaF_2 prism. The SFG spectra of the C=O stretch around 1720 cm^{-1} was collected in SSP and PPP polarization combinations (Figure 3-5). From these polarization combinations the orientation of the C=O group was calculated.

In control experiments, where the graphite surface was substituted with a glass microscope slide, no C=O signal was detected. This confirms that the signal arises from

ordering at the graphite surface, and not anywhere else in this experimental geometry. Monolayers that were isotopically labeled with deuterium were also examined, eliminating any possibility of the C=O signal being from oxidized graphite.

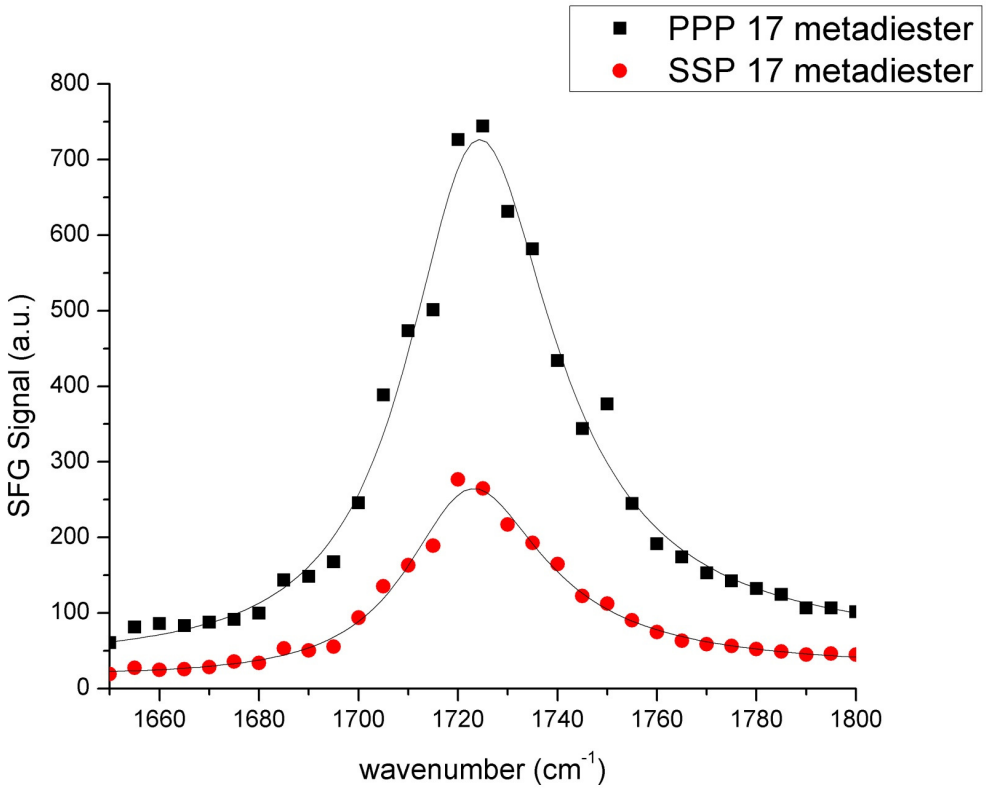

Figure 3-5 SFG spectra of 17 meta-diester monolayer on HOPG

3.3 Results and Discussion

As we discussed in Chapter 1, for a particular vibrational mode, components of SFG nonlinear susceptibility are related to molecular hyperpolarizability through average orientations of the functional groups. Therefore if hyperpolarizability for a vibrational mode is known, we should be able to deduce the orientation of the functional group by

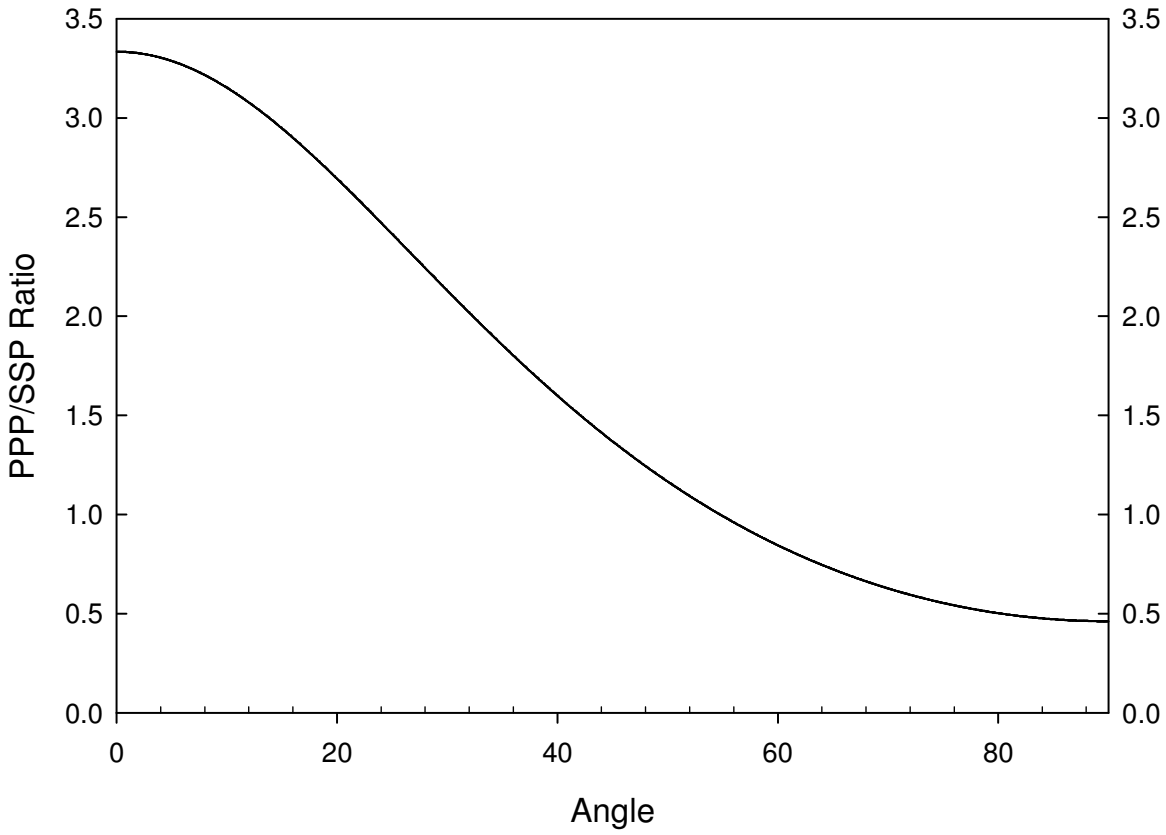

Figure 3-6 C=O Orientation curve

measuring different components of the SFG susceptibility with SFG spectra collected using different polarization combinations. Here we want to study the orientation of C=O groups. For a C=O group, there is only one vibrational mode, the stretching mode. The hyperpolarizability of the C=O stretching mode can be deduced by the IR transition moment and Raman polarizability of the mode.[25] Since C=O group has a $C_{\infty v}$ group, it is feasible to deduce the relation between the SFG susceptibility and hyperpolarizability, which was done in the literature.[25] For the $C_{\infty v}$ group we have three nonzero hyperpolarizabilities as shown in Eq. 34 and written in the molecular coordinates where c is along the C=O axis and the ab plane is perpendicular to the C=O axis.

$$\beta_{aac} = \beta_{bbc}; \beta_{ccc} \qquad \textbf{Eq. 34}$$

To determine orientation of the C=O bond, we need to know the relative values of the nonzero $\beta^{(2)}$'s which can be estimated directly from the Raman depolarization ratio since in this case there are only two independent hyperpolarizabilities and they have equal transition dipole moments μ_c. It follows then that

$$r = \frac{\beta_{aac}}{\beta_{ccc}} = \frac{\alpha_{aa}}{\alpha_{cc}} \qquad \textbf{Eq. 35}$$

The parameter r is related to the Raman depolarization ratio ρ as follows

$$\rho = \frac{3}{4}\left[1 + \frac{5}{4}\left(\frac{2r+1}{r-1}\right)^2\right]^{-1} \qquad \textbf{Eq. 36}$$

The Raman depolarization ratio ρ is reported as 0.1 in the literature.[27,28] Two values of r satisfy equation 3, r = 0.3 and r = 12. The r = 12 is regarded as unphysical since the change in polarizability along the C=O bond should be higher than across the C=O bond. So the value of r = 0.3 is used for these calculations. The expressions for the relevant $\chi^{(2)}$ components are as follows:

$$\chi_{zzz} = \frac{N}{\varepsilon_0} < \beta_{zzz} > = \frac{N}{\varepsilon_0} \beta_{ccc} \left[r < Cos\theta > + (1 - r) < Cos^3\theta > \right]$$
$$\chi_{yyz} = \frac{N}{\varepsilon_0} < \beta_{yyz} > = \frac{1}{2} \frac{N}{\varepsilon_0} \beta_{ccc} [(r + 1) < Cos\theta > + (r - 1) < Cos^3\theta >] \qquad \textbf{Eq. 37}$$

Where N is the number of oscillators, θ is the angle between the C=O axis and the surface normal. In the prism sample geometry, the PPP polarization combination is dominated by the χ_{zzz} component. The χ_{zzz} component is an order of magnitude greater than any other χ component. The χ_{yyz} component contributes to the signal in the SSP polarization combination.

If we assume that all the C=O group adopt the same orientation, we can use a delta distribution to describe such an orientation. In that case, the relation between the SFG susceptibility and hyperpolarizability was calculated. The relation for the ratio between PPP and SSP versus the orientation angle (the angle between the C=O group and the surface normal) is displayed in Figure 3-6. The SFG signal is given by equation 38.[29]

$$S(\omega) = \frac{8\pi^3 \omega^2 \sec^2 \beta}{c^3 n_1(\omega) n_1(\omega_2) n_1(\omega_3)} | \chi_{eff}^{(2)} |^2 \; I_1(\omega_1) I_2(\omega_2) A T$$
$$\chi_{ijk}^{(2)} = \chi_{NR}^{(2)} + \sum_q \frac{A_{ijk,q}}{\omega_2 - \omega_q + i\Gamma_q} \qquad \textbf{Eq. 38}$$

Since we are taking a ratio between two polarization combinations, everything except the oscillator strength will be a constant that will drop out in the ratio. Therefore, the spectra were fit to

$$S(\omega) = Offset + | NR + \frac{A}{\omega - \omega_0 + i\Gamma} |^2 \qquad \textbf{Eq. 39}$$

The Fresnel coefficients, which represent the difference in reflection and transmission between S and P polarized light, were taken into account by shifting the measured signal,

appropriately. The Fresnel coefficients contribute about a 10% difference in the intensity of the ratio.

The PPP/SSP ratio was measured to be 0.9. From the relation shown in Figure 6, it was found that under the delta distribution assumption that the C=O formed on average a 58º angle to the surface normal. The delta distribution assumption is a reasonable assumption for this system since from the STM images we know that the monolayers are extremely well oriented. The C=O stretch was chosen for this study to avoid possible spectral overlap from the phenyloctane solvent.

The SFG results on C=O group orientation for the 2D crystal are different from the structure deduced from computer modeling on STM images. The resulting structure from energy minimization calculation is presented in Figure 3-7, which shows that the C=O functional groups lie down on the surface along with the aromatic rings in the molecules.

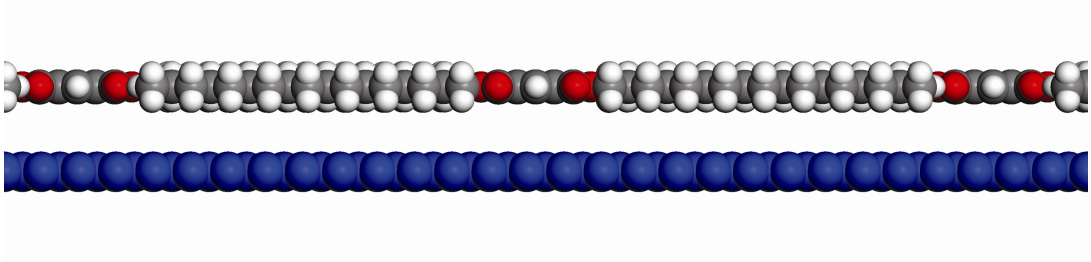

Figure 3-7 The computed model of the monolayer of 17-m-diester on HOPG. The angle of C=O is parallel to HOPG.

This picture is satisfying to ones chemical intuition of the main interaction being π stacking between the graphite surface and the aromatic rings in the 17-metadiester. However, the computer model does not include any solvent molecules. There is a favorable interaction between the phenyloctane solvent and the diester molecules since the diester molecules are soluble in the phenyloctane. It is proposed that the tilt of the C=O groups in the 2D crystals measured from the SFG experiments arises from competitive interactions between the phenyl groups in the solvent and the C=O groups in the 2D crystal, and π stacking between the graphite and the 2D crystal.

An alternative interpretation of the data is that there could be a secondary adlayer on top of the monolayer. This could be probed by a concentration dependent study.

After the SFG studies on the C=O stretching frequency region, the C-H stretching

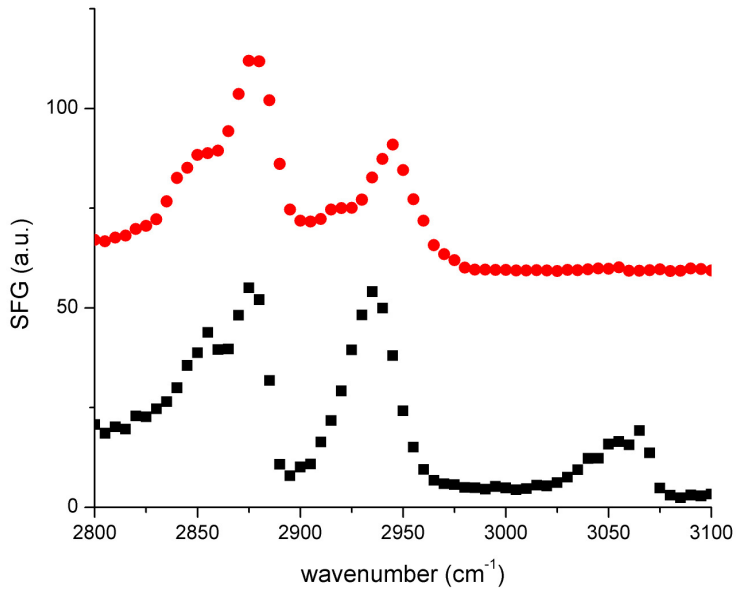

Figure 3-8 Spectra of 2D crystals of 17-metadiester (bottom) and 17-metadiester with a deuterated aromatic ring (top).

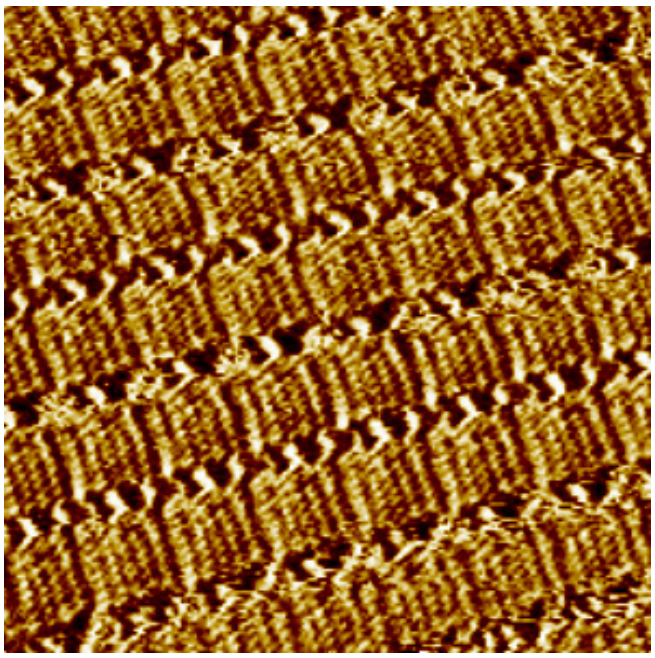

Figure 3-9 STM image of 17 metadiester with a deuterated aromatic ring.

frequency region was examined. Figure 3-8 shows the stretches from the phenyl ring and aliphatic CH_3 and CH_2 groups, indicating that these groups have some orientation orders along the surface normal at the interface. However, such SFG signals can be contributed by either the 2D crystal or the solvent molecules at the interface. In order to separate the two sources of signal, the aromatic ring of the diester molecule was then selectively deuterated. STM images of the partially deuterated diester molecules on HOPG indicate that they form an identical 2D crystal compared to their hydrogenated analogues. SFG signal was collected from such a 2D crystal formed from such partially deuterated molecules (Figure 3-8) and the SFG peak at 3060 cm^{-1} vanished. This shows that the original signal before the deuteration should be contributed by the 2-D crystals. Thus it is believed that the aromatic rings of the diester molecules in the 2-D crystal also tilt at the interface. SFG signals collected in the C-D stretching region show a weak but discernible peak at 2290 cm^{-1} (Figure 3-10), corresponding to the deuterated aromatic

stretches. This further supports the conclusion that the aromatic rings (both with and without deuteration) in the 2D crystal tilt at the interface instead of lying down. From theory, we would expect no SFG signal from an aromatic ring that is in the plane of the sample surface. The deuterated sample was tested with STM and found to form the same 2D phase. (Figure 3-9)

3.4 Ortho and Para substituted molecules

In addition the 18-meta, 18-ortho-, and 18-para - substituted phthalate diesters were also examined using SFG. The 18 meta- and 18 ortho-substituted showed similar results to the meta-substituted, that is, both C=O groups and aromatic rings tilt at the interface. For the para-substituted molecules, no SFG signal was observed, possibly due to the centrosymmetry of the molecules.

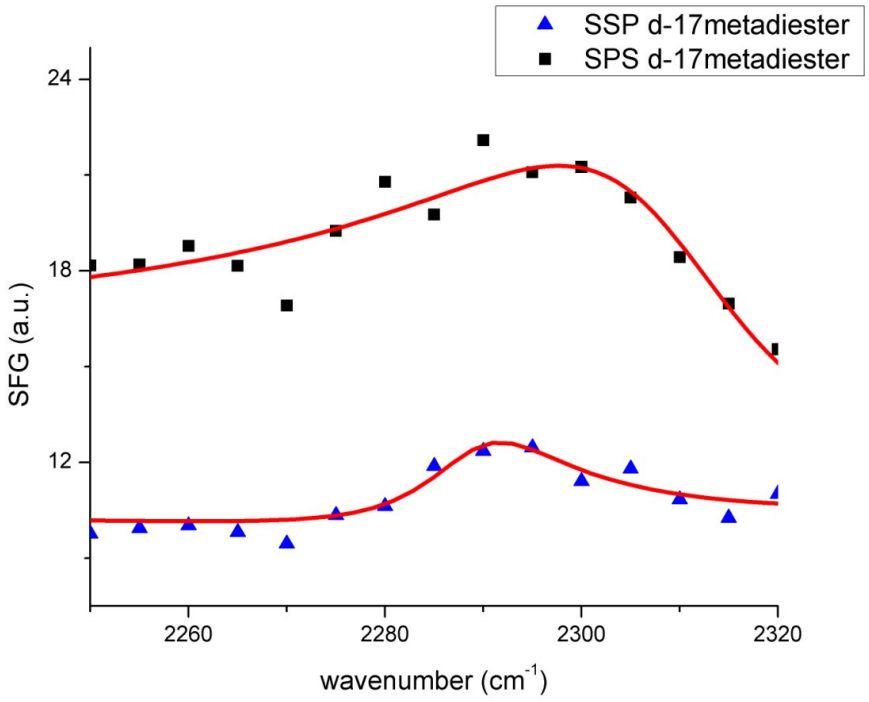

Figure 3-10 C-D Stretch of d-17 metadiester

3.5 Conclusions

It is shown here that a combination of SFG and STM techniques can be used to gain a more completed picture of a 2-D crystal on HOPG. STM and computational models can provide a detailed atomic picture and SFG can provide an average orientation angle of functional groups to better refine the computational models. The model from the STM results do not indicate that the C=O group is out of the plane of the graphite; however, this may because these techniques neglect interactions with solvent molecules. SFG results show that the C=O groups along with the aromatic rings actually twist away from the plane of the graphite, indicating the need for more sophisticated computational models that take into account interactions with the solvent.

Figure 3-11 shows a cartoon of a possible interaction that would cause a tilt such as was observed with SFG.

Another possible interpretation of the data is that there is a secondary adlayer on top of the monolayer that is tilting away from the surface. This could be tested by a concentration dependence study that will be conducted in the future.

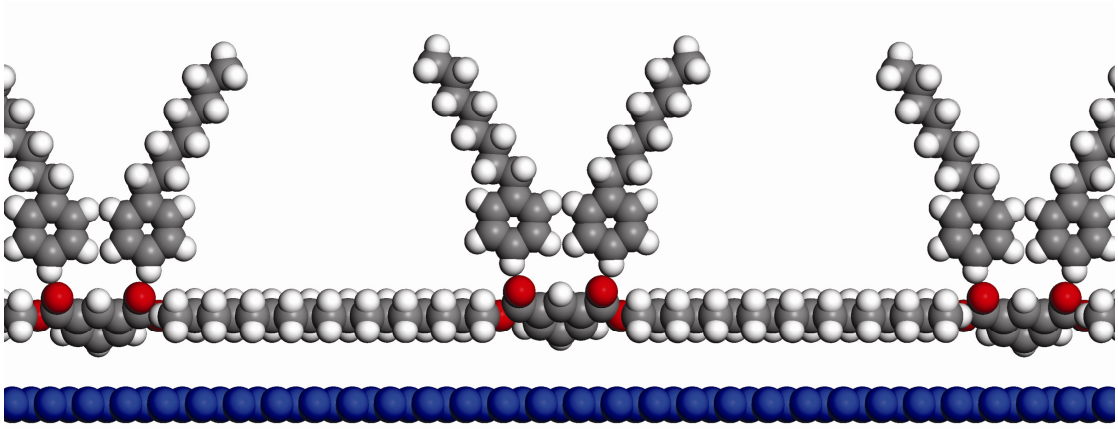

Figure 3-11 Possible interaction with phenyloctane molecules causing the tilt of the 17-metadiester molecules.

(1) Urban, G. A. *Measurement Science & Technology* **2009**, *20*.

(2) Remhof, A.; Borgschulte, A. *Chemphyschem* **2008**, *9*, 2440-2455.

(3) Srivastava, S.; Kotov, N. A. *Accounts of Chemical Research* **2008**, *41*, 1831-1841.

(4) Sun, X. Y.; Sun, Y. G. *Journal of Materials Science & Technology* **2008**, *24*, 569-577.

(5) Malinski, T.; Taha, Z. *Nature* **1992**, *358*, 676-678.

(6) Wang, D. G.; Chen, C. Z.; Ma, J.; Liu, T. H. *Applied Surface Science* **2008**, *255*, 1637-1645.

(7) Jin, Y. D.; Honig, T.; Ron, I.; Friedman, N.; Sheves, M.; Cahen, D. *Chemical Society Reviews* **2008**, *37*, 2422-2432.

(8) Hancock, J. M.; Gifford, A. P.; Champion, R. D.; Jenekhe, S. A. *Macromolecules* **2008**, *41*, 3588-3597.

(9) Kido, J.; Kimura, M.; Nagai, K. *Science* **1995**, *267*, 1332-1334.

(10) Harima, Y.; Okazaki, H.; Kunugi, Y.; Yamashita, K.; Ishii, H.; Seki, K. *Applied Physics Letters* **1996**, *69*, 1059-1061.

(11) Heimer, T. A.; Bignozzi, C. A.; Meyer, G. J. *Journal of Physical Chemistry* **1993**, *97*, 11987-11994.

(12) Oncel, N.; Bernasek, S. L. *Applied Physics Letters* **2008**, *92*.

(13) Tao, F.; Bernasek, S. L. *Surface Science* **2007**, *601*, 2284-2290.

(14) Tao, F.; Bernasek, S. L. *Langmuir* **2007**, *23*, 3513-3522.

(15) Plass, K. E.; Engle, K. M.; Matzger, A. J. *Journal of the American Chemical Society* **2007**, *129*, 15211-15217.

(16) Mullen, K.; Rabe, J. P. *Accounts of Chemical Research* **2008**, *41*, 511-520.

(17) Bonifazi, D.; Kiebele, A.; Stohr, M.; Cheng, F. Y.; Jung, T.; Diederich, F.; Spillmann, H. *Advanced Functional Materials* **2007**, *17*, 1051-1062.

(18) Mannsfeld, S. C. B.; Fritz, T. *Modern Physics Letters B* **2006**, *20*, 585-605.

(19) De Feyter, S.; De Schryver, F. C. *Journal of Physical Chemistry B* **2005**, *109*, 4290-4302.

(20) Loch, C. L.; Ahn, D.; Chen, C. Y.; Wang, J.; Chen, Z. *Langmuir* **2004**, *20*, 5467-5473.

(21) Rao, Y.; Song, D. H.; Turro, N. J.; Eisenthal, K. B. *Journal of Physical Chemistry B* **2008**, *112*, 13572-13576.

(22) Niaura, G.; Kuprionis, Z.; Ignatjev, I.; Kazemekaite, M.; Valincius, G.; Talaikyte, Z.; Razumas, V.; Svendsen, A. *Journal of Physical Chemistry B* **2008**, *112*, 4094-4101.

(23) Maeda, T.; Ishibashi, T. A. *Appl. Spectrosc.* **2007**, *61*, 459-464.

(24) Loch, C. L.; Ahn, D. C.; Chen, C. Y.; Chen, Z. *Journal of Adhesion* **2005**, *81*, 319-345.

(25) Tyrode, E.; Johnson, C. M.; Baldelli, S.; Leygraf, C.; Rutland, M. W. *Journal of Physical Chemistry B* **2005**, *109*, 329-341.

(26) Wang, J.; Even, M. A.; Chen, X. Y.; Schmaier, A. H.; Waite, J. H.; Chen, Z. *Journal of the American Chemical Society* **2003**, *125*, 9914-9915.

(27) Yokoyama, I.; Miwa, Y.; Machida, K. *Journal of Physical Chemistry* **1991**, *95*, 9740-9746.

(28) Yokoyama, I.; Miwa, Y.; Machida, K. *Journal of the American Chemical Society* **1991**, *113*, 6458-6464.

(29) Wang, J.; Paszti, Z.; Even, M. A.; Chen, Z. *Journal of the American Chemical Society* **2002**, *124*, 7016-7023.

CHAPTER 4 : SURFACE C=O ORIENTATION IN POLY-N-METHACRYLATES

4.1 Introduction

Carbonyl groups are present in many polymers, and often serve as reaction sites for chemical modification (such as corona treatment to improve adhesion)[1-4], or as sites for intermolecular interactions (such as hydrogen bonding).[5-10] Although many previous SFG studies have analyzed the orientation of other surface functional groups (such as methyl groups, phenyl rings, and methylene groups), to date very few SFG studies have been done on the orientation of carbonyl groups in general[11-13] or carbonyl groups on polymer surfaces specifically.[14-18]

Many of the commonly studied CH signals are subject to overlapping bands from multiple functional groups containing C-H bonds, complicating spectral assignment and the interpretation of molecular orientation. This is less often the case for C=O groups, enhancing the potential value and specificity of the information obtained. Furthermore, the peak center frequency of the C=O stretch is sensitive to hydrogen bonding and the local chemical environment, making it possible to study the local chemical environment of the surface by monitoring the C=O peak position with SFG. SFG can also be used to study the orientation changes of the surface C=O groups as the polymer surface interacts with other molecules. Although limitations in laser design have previously prevented

study of the C=O stretch, the development of more broadly tunable infrared sources now enables the study the carbonyl orientation using SFG.[12,18-22]

In this study, a selection of similarly structured carbonyl-containing polymers was chosen for comparison (see structures in Figure 4-1). We picked polymers that had glass transition temperatures well above, near, and well below room temperature. The surface restructuring behavior in water was monitored. The orientation of C=O groups on the polymer surfaces was deduced from SFG spectra collected using different input and output polarization combinations. In addition, the effects on the C=O group of corona treating a dPMMA surface were also briefly investigated and will be reported here

Previous work by the Chen group, which will be reviewed in section 4.1.1, has shown that varying the length and composition of methacrylate side chains lead to changes in orientation of surface functional groups based on CH signals, and it was hypothesized that a change in backbone and side chain chemistry might also affect orientation of the carbonyl groups.[23] This change in carbonyl group orientation might in turn affect surface interactions, including the accessibility of the surface functional groups of polymer to hydrogen bonding.

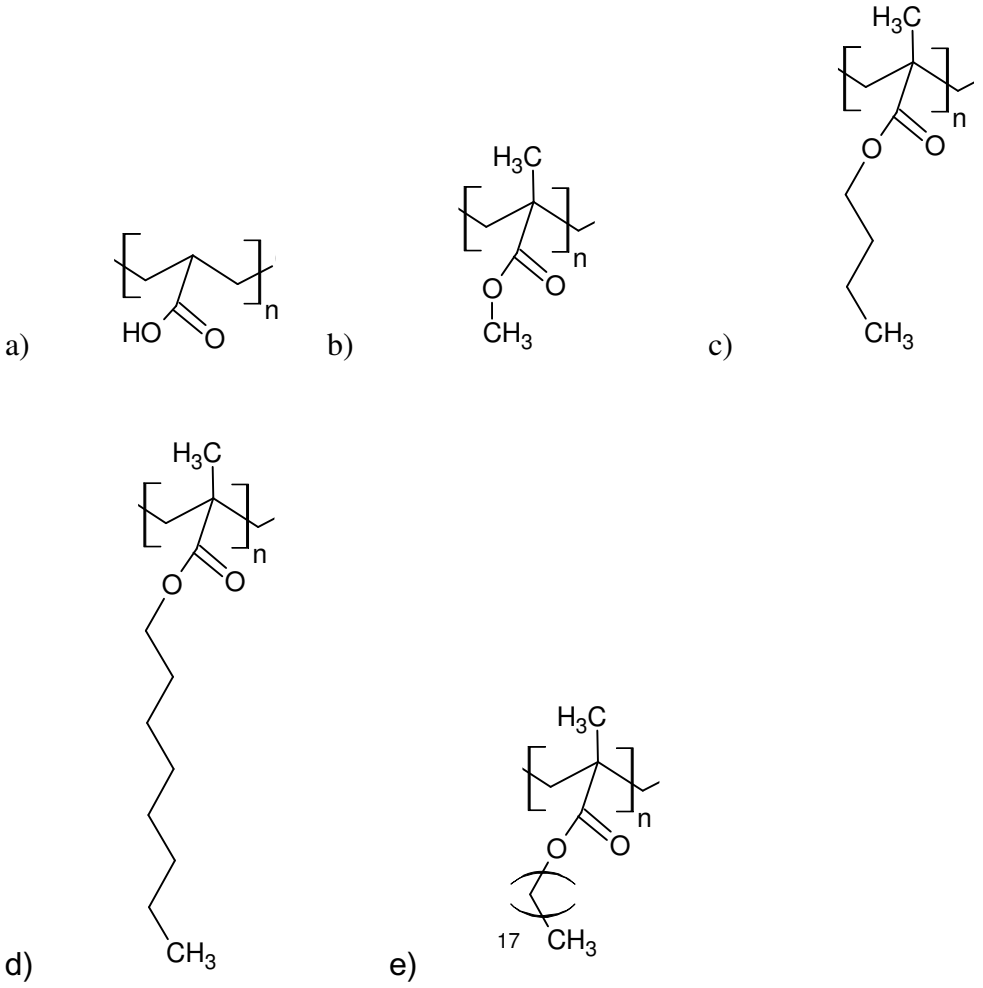

Figure 4-1 Structures of polymers a) Poly(acrylic acid), (PAA) b) Poly(methyl methacrylate) (PMMA), c) Poly(n-butyl methacrylate) (PBMA), d) Poly(n-octyl methacrylate) (POMA), e) Poly(n-octadecyl methacrylate) (PODMA),

4.1.1 Review of Previous SFG Studies of Poly-n-methacrylates

Previously the surface structures of a similar series of poly-n-methacrylates were systematically investigated in air and in water using SFG in the C-H stretching frequency region.[23] Such observations were correlated to the polymer glass transition temperatures. The glass transition temperature (T_g) is the temperature at which a polymer transforms

from a more flexible rubber like state to a more brittle glass like state.[24] The chain flexibility will have a strong effect on the glass transition temperature.[24] Even though the glass temperature describes a bulk polymer property, we believe that the flexibility of surface groups is also correlated to the glass transition temperature. For example, if the experimental temperature is above a polymer's T_g, the polymer molecules on the surface are more likely to be able to reorder when the local chemical environment is changed. Room temperature is below the T_g for bulk poly(acrylic acid) (PAA) and poly (methyl methacrylate) (PMMA), near the glass transition temperature for bulk poly (butyl methacrylate) (PBMA), and far above the T_g for bulk poly (octyl methacrylate) (POMA) and poly(octaldecyl methacrylate) PODMA. PAA and PODMA are somewhat different from the other polymers. PAA can self hydrogen bond, as is evidenced in the FTIR spectrum (Figure 4-2). The peak at 1709 cm^{-1} is due to carbonyl groups in the bulk that are hydrogen bonded to nearby OH groups. PODMA is also different because it is a semicrystalline polymer and has a melting temperature of 37º C.

Polymer	PAA	PMMA	PBMA	POMA	PODMA
T_g	102ºC[25]	108ºC[23]	20ºC[23]	-20ºC[23]	-100ºC[23]

Table 2 Glass transition temperatures for the polymers studied.

Previously, SFG spectra in the C-H stretching frequency region were collected from the PMMA surface in air using different polarization combinations of the input and output beams by our research group.[26,27] The ssp spectrum was dominated by the contribution from the symmetric stretching mode of the ester methyl group in PMMA. Both ppp and sps spectra were dominated by two asymmetric stretching modes of the

ester methyl group. It was found that the PMMA surface in air is dominated by the ester methyl groups and these groups orient normal to the surface.[23,27,28]

Our previous studies also showed no evidence of substantial surface restructuring for PMMA in water as compared to air.[23] Both ssp and sps SFG spectra of PMMA in water were dominated by the signals from ester methyl groups, similar to those of the PMMA-air interface, although they were much weaker.[23] Detailed analysis of the spectra shows that the weaker spectra were mainly due to the differences in the indices of refraction for air and water, which alters the Fresnel coefficients. The Fresnel coefficients are the terms that describe the transmission or reflection of light at an interface. They depend on the polarization of the light and the index of refraction of the materials at the interface and determine the intensity of the light that actually reaches the sample. If we normalize the spectra for the difference in Fresnel coefficients, the SFG spectra collected in water overlap with those in air quite well. This shows that the structure of C-H groups (especially ester methyl groups) on the PMMA surface remains largely unchanged when contacted with water.[23]

Both ssp and sps SFG spectra were also collected from PBMA/air and PBMA/water interfaces. In air, the ssp spectrum was dominated by the symmetric stretching (2875 cm^{-1}) and Fermi resonance (2940 cm^{-1}) of the methyl end group of the ester side chain, while the sps spectrum collected in air and both SFG spectra collected in water are dominated by the asymmetric stretching of the end methyl group at 2960 cm^{-1}. These results indicate that the PBMA surface is dominated by the end methyl groups of the side chain in both air and water. The orientation of such end methyl groups changed when the surface was exposed to water, this was manifest by different intensity ratios of

the symmetric/asymmetric peaks in the same spectrum or those of the same peak in different polarized spectra.[23,26,27] We further quantitatively examined the orientation and orientation distribution of surface functional groups on PBMA using SFG.[23] It was found that methyl groups oriented more normally towards the surface in air with a broader distribution. However in water the methyl groups tilted more towards the surface with a narrower distribution.[23] The surface change of PBMA in water was reversible, because the SFG spectra collected from the PBMA after removing the surface from water and exposing to air again are the same as those collected in air before contacting water.

SFG spectra in the C-H stretching were also previously collected from other polymethacrylates with varied side chain lengths, such as poly (ethyl methacrylate) (PEMA), poly (n-propyl methacrylate) (PPMA), poly (n-hexyl methacrylate) (PHMA), poly (n-octyl methacrylate) (POMA), poly (n-laurel methacrylate) (PLMA), and poly (n-octyldecyl methacrylate) (PODMA).[23] In addition, the surface of poly (ethyl acrylate) was also studied by SFG in the C-H stretching region.[29] It was found that the surface restructuring behaviors of PEMA, PPMA, and PHMA in water are similar to that of PBMA. They had reversible end group reorientations in water. For POMA, PLMA, and PEA, whose glass temperatures are substantially lower than the room temperature, irreversible surface changes were observed in water. For PODMA, which has a very long side chain, the surface exhibited a reversible change in water.[23]

4.2 Experimental:

The SFG laser system used in these experiments was described in detail in the previous chapters.[26,30,31] In this work, SFG spectra were collected using the near-

total internal reflection prism geometry previously discussed[13] with the ssp and ppp polarization combinations.

Polymer materials studied here were ordered from Scientific Polymer Products INC. Ontario, NY. All polymer samples were prepared by spin coating 2% weight polymer solutions onto optically clear CaF_2 prisms. The poly(n-methacrylate) (P-nMA) solutions were prepared in toluene. The poly(acrylic acid) (PAA) solution was prepared using ethanol as the solvent.

The corona treater (Model BD-20) is from Electro-Technic Products, Inc. (Chicago, IL). It generates an air plasma. It was held approximately 3 cm from the surface being treated for 10 seconds.

Fourier Transform Infrared Spectroscopy (FTIR) was performed on a Nicolet Magna IR 550 spectrometer.

4.3 Orientation of carbonyl groups

The orientation determination of C=O groups was based on the same analysis introduced in Chapter 3. In the polymer system though, the delta distribution in orientation is not a very realistic assumption. A Gaussian distribution of C=O orientations is a more realistic approximation. Unfortunately, in the current experiments SFG does not provide enough measurements to determine the orientation and orientation distribution. This problem is worked around by plotting a series of curves for the different orientation distributions and seeing which curves the measured data intersects.

Fourier Transform Infrared (FTIR) spectroscopy showed that polymethacrylates have a C=O stretch around 1730 cm^{-1}. (Figure 4-2, Table 3). Some small variations of the C=O stretching peak centers for different polymethacrylates were observed.

Deuteration of the polymers did not affect the C=O peak positions significantly. FTIR of PBMA and dPBMA are shown in Figure 4-2 for reference.

PAA is slightly different from the other polymers since the C=O can hydrogen bond with a nearby OH group. Thus the bulk C=O in PAA has a large number of hydrogen bonded C=O groups generating a peak centered at about 1710 cm^{-1} (Figure 4-2), the shoulder centered at 1738 cm^{-1} is due to the C=O groups without hydrogen bonding. The SFG spectra of the PAA show a significant signal from free C=O stretches, which will be discussed in detail below.

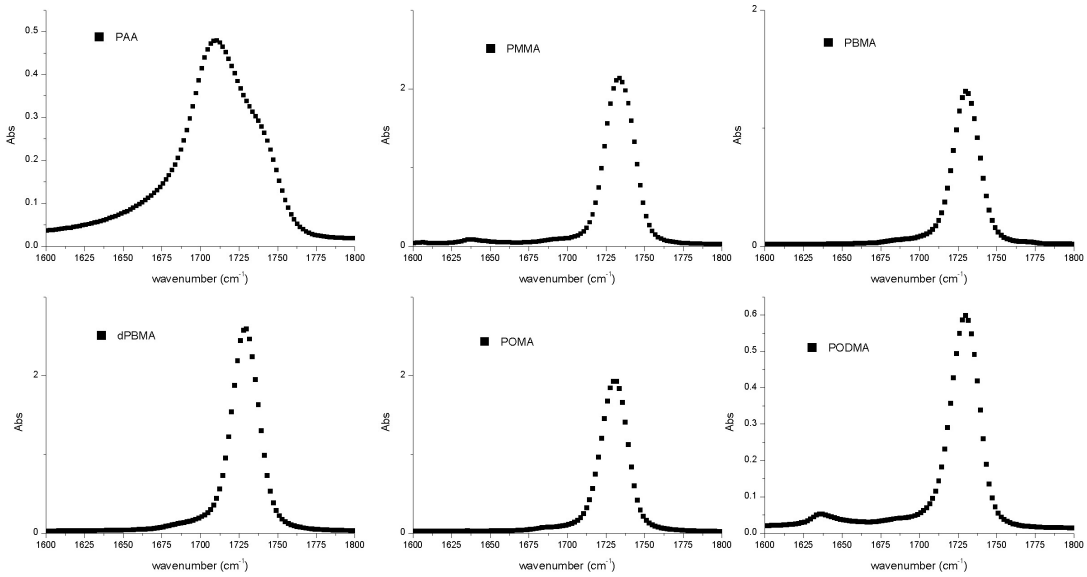

Figure 4-2 FTIR spectra showing bulk C=O stretch peak positions

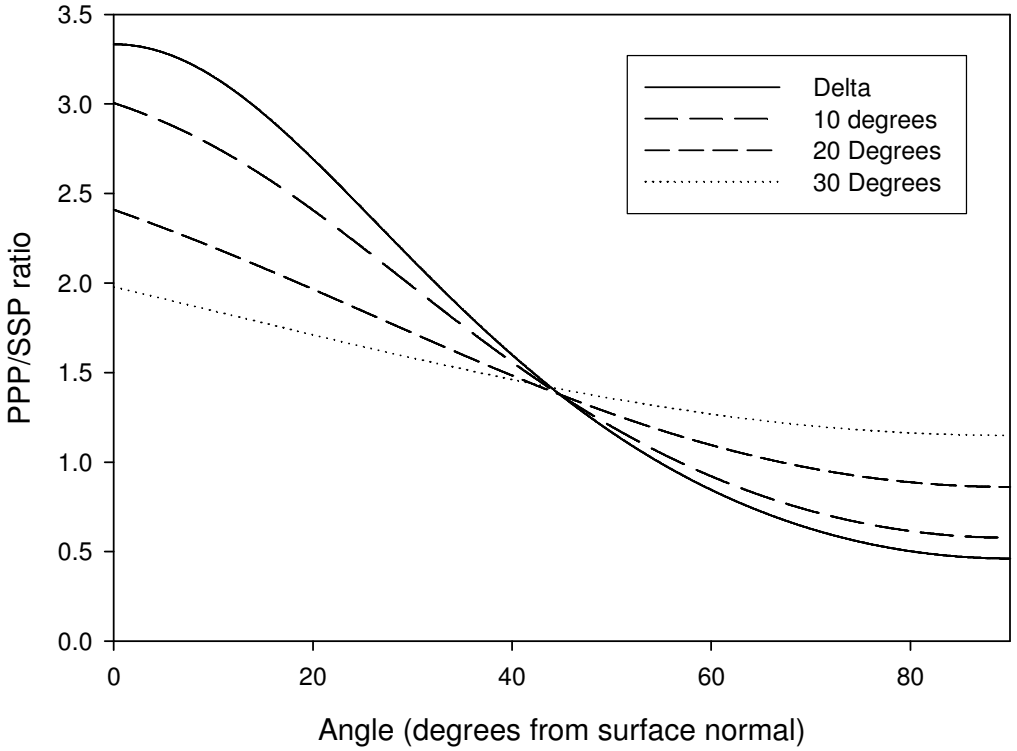

Figure 4-3 PPP/SSP ratio versus C=O orientation from surface normal

Polymer Material	Fit FTIR C=O Peak Center
PAA	1710 cm^{-1}, 1738cm^{-1}
PMMA	1734 cm^{-1}
PBMA	1730 cm^{-1}
dPBMA	1729 cm^{-1}
POMA	1730 cm^{-1}
PODMA	1729 cm^{-1}

Table 3 Bulk C=O peak positions as determined by FTIR

4.3.1 Orientation of C=O groups in air

SFG ssp and ppp spectra of C=O groups collected from polymer surfaces in air and water are shown in Figure 4-4,Figure 4-5, Figure 4-6, Figure 4-7, and Figure 4-8. All the SFG spectra were fitted as previously explained and the results for air are presented in Table 4.

In Figure 4-3 the theoretical response of the C=O groups are plotted with the fitted signal strength ratio of the ppp/ssp polarization combination versus the angle from the surface normal. However, it is unrealistic to suggest that all C=O angles in the polymer adopt the same orientation (a delta distribution). Although we do not have enough measurements to determine both the orientation angle and the distribution of orientation angles here, the theoretical responses for Gaussian distributions of various widths are also plotted for comparison purposes.

Polymer (in air)	Polarization	peak center (cm^{-1})	height	width	PPP/SSP	Assignment
PAA	SSP	1725	262	22	0.90	Free C=O
	PPP	1730	247	23		
PMMA	SSP	1725	187	21	1.53	Free C=O
	PPP	1727	241	17		
PBMA	SSP	1727	247	15	1.79	Free C=O
	PPP	1727	441	15		
POMA	SSP	1734	195	14	0.96	Free C=O
	PPP	1730	250	19		
PODMA	SSP	1733	141	20	2.51	Free C=O
	PPP	1728	283	16		

Table 4 Fits to the SFG spectrum of the poly-n-methacrylates in air

It is interesting to compare the FTIR spectrum of PAA in air with the SFG spectrum of PAA in air. The FTIR spectrum has a dominant peak at 1710 cm^{-1} which indicates that most of the bulk C=O groups in PAA form hydrogen bonds with adjacent OH groups. The shoulder at 1738cm^{-1} indicates that some bulk "free" C=O groups exist also. No SFG signal around 1710 cm^{-1} was observed in ssp or ppp signal. Even though we could not entirely exclude the possibility that some surface C=O groups may form hydrogen bonds and completely lie down on the surface (thus cannot be detected by SFG), we believe that it is very unlikely. The SFG signal observed was centered at ~1730 cm^{-1}, showing that most of the surface C=O groups detected by SFG may not form hydrogen bonds with adjacent OH groups. The peak shift from 1738 cm^{-1} to 1730 cm^{-1}may be because of some small contributions from the hydrogen bonded C=O groups which are not completely lying down, but the SFG spectra fits using two peaks have not proved to be very reliable, we thus ignore the small contribution and perform the data analysis on the one peak fit. The ppp/ssp ratios for PAA for the 1730 cm^{-1} peak which corresponds mainly to "free" C=O stretching is 0.9. Under the delta distribution assumption (Figure 4-3) this corresponds to a 58º angle from the surface normal. Using a more realistic Gaussian distribution however, the fitted intensity ratios could correspond to a wide range of possible orientations from 58º to 90º depending on the width of the Gaussian used. This comparison of the FTIR and SFG spectra emphasizes how the surface chemical environment can be very different from the bulk chemical environment.

For the PMMA samples, the peak centers for both the ssp and ppp SFG spectra were more than five wavenumbers lower than detected using FTIR. This suggests that

some of the surface C=O groups might form hydrogen bonds with water molecules in the air, but again the spectral resolution does not allow reliable 2 peak fits, so we use a one peak fit here also. For PMMA the orientation of the free C=O groups was determined to be 42º if a delta distribution is assumed. However, if a Gaussian distribution is assumed, the orientation passes through a point of ambiguity. The Gaussian width and orientation could be anything.

For PBMA, the C=O peak centers in the SFG spectra collected in air are not very different from those in FTIR spectra showing that the signal is dominated by the free C=O contribution. The free C=O orientation in air ranges from 38º with a delta distribution to 0º orientation with a 40º Gaussian distribution. The POMA free C=O orientation ranges from a 58º from the surface normal with a delta distribution to a 90º distribution with a 20º Gaussian distribution. The PODMA free C=O orientation in air ranges from a 24º degree angle with a delta distribution to a 0º with a 20º Gaussian distribution.

In summary, while there could some surface hydrogen bonding in air, we do not have the spectral resolution to reliably fit the spectrum with two peaks, so we chose to ignore the possibility of C=O groups hydrogen bonding to water vapor in the air.

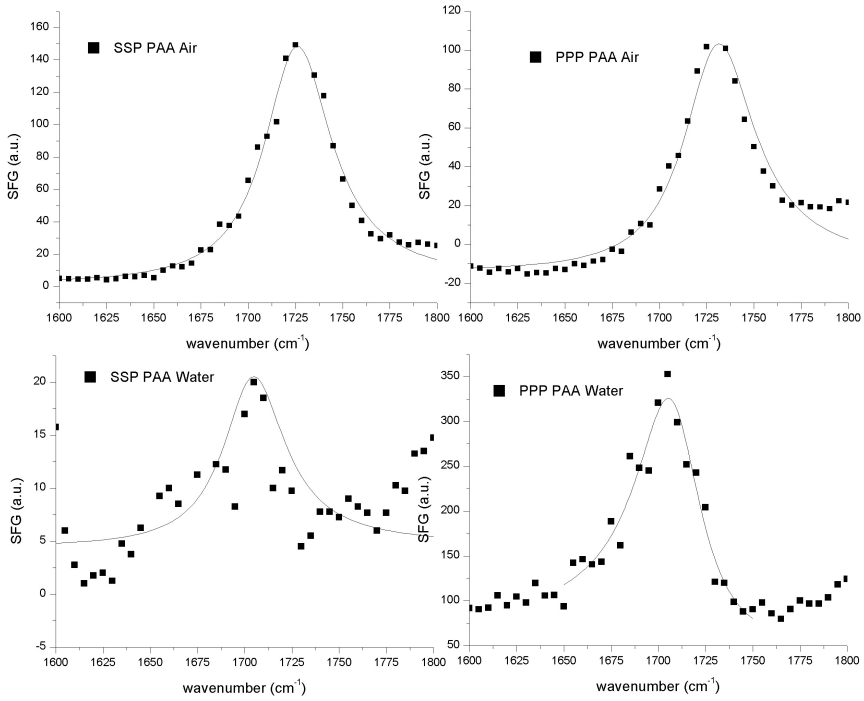

Figure 4-4 SFG spectra of PAA in air and in water

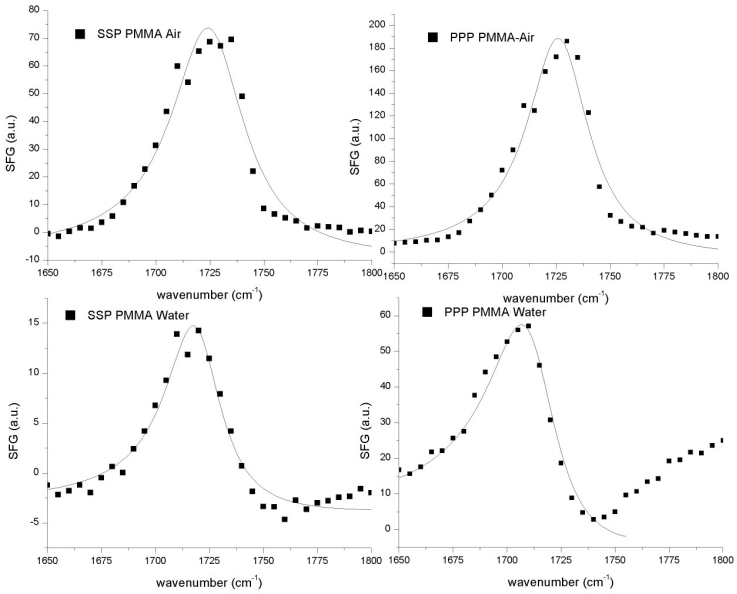

Figure 4-5 SFG spectra of PMMA film C=O stretching region in air and in water

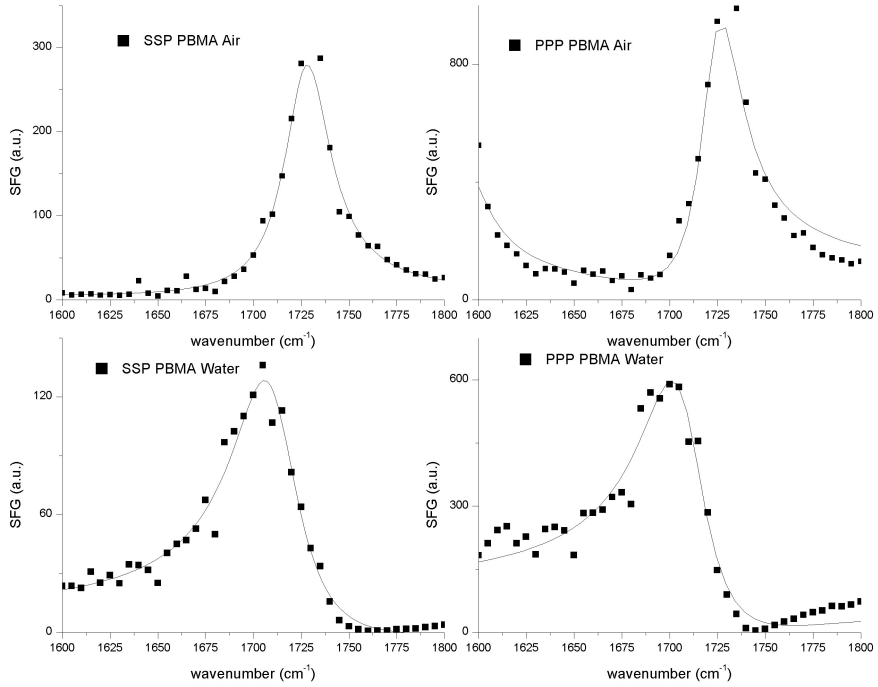

Figure 4-6 SFG spectra of PBMA film C=O stretching region in air and in water

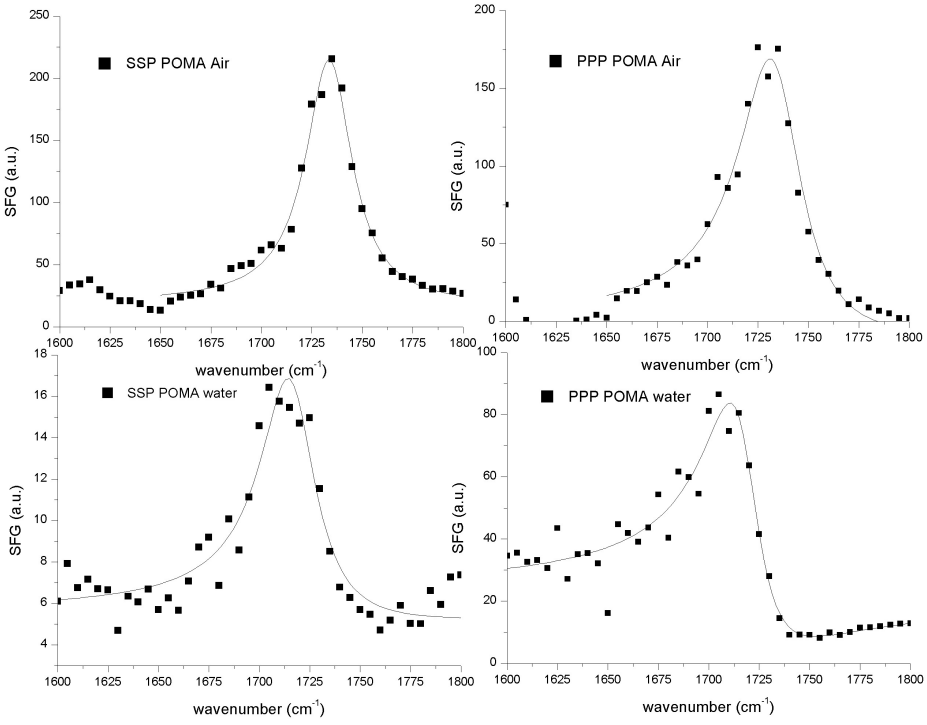

Figure 4-7 SFG spectra of POMA film C=O stretching region in air and in water

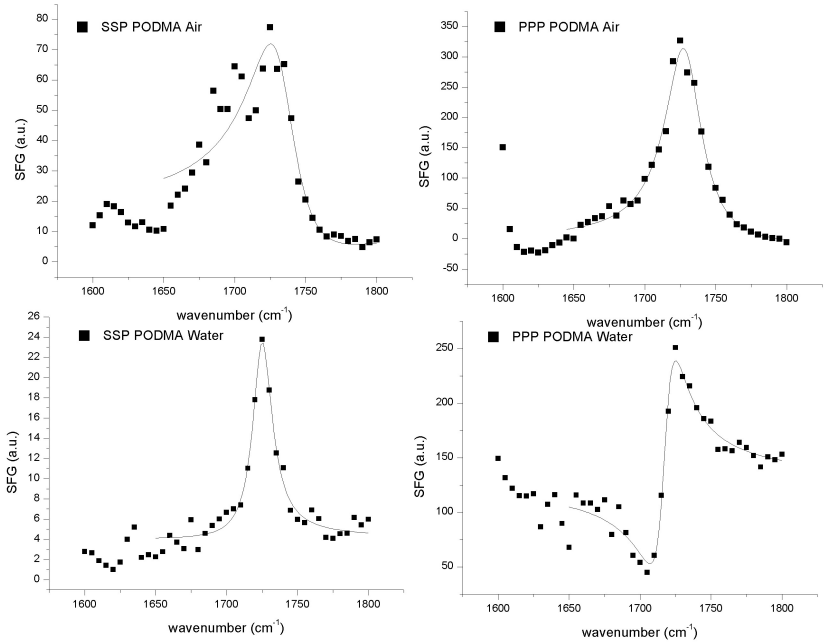

Figure 4-8 SFG spectra of PODMA film C=O stretching region in air and in water

4.3.2 Orientation of C=O groups in contact with water

The polymers were next contacted to deionized water and the SSP and PPP polarization combinations were again collected. The first point to note is that almost all the C=O groups are accessible for hydrogen bonding to water, as the peak around 1730 cm^{-1} almost completely vanished for all of the polymers examined. If only some of the surface C=O sites were accessible to hydrogen bonding with the water, then we would expect to see a double peak in the SFG spectrum. The peak shifts range from 10 to 20 cm^{-1} indicating some variation in the strength of hydrogen bonding between the water and the polymers.

The PAA SSP spectrum gave a very noisy spectrum, but it is clear that the ppp spectrum is much stronger than the ssp spectrum. This is indicative the hydrogen bonded

C=O groups standing straight up with a narrow distribution of angles. The hydrogen bonded C=O groups in the PMMA, PBMA, and POMA samples adopt roughly the same orientation ranging from a 32º angle from the surface normal with a delta distribution to a 0º angle with slightly less than a 30º Gaussian distribution. The PODMA unfortunately runs though a point of complete ambiguity. In the delta distribution assumption then the hydrogen bonded C=O groups form a 41º angle. This ratio is near the point where signal would arise from a randomly ordered surface.

Except for PAA, which has a different molecular formula, all the poly-methacrylates have a similar ppp/ssp signal stretching ratio, showing that the surface hydrogen bonded C=O groups have a similar orientation in water. In air, a much larger variation for the ppp/ssp signal strength was observed. This correlates well to the SFG C-H studies on PBMA surfaces. In air, the surface methyl groups on PBMA are more randomly oriented, while in water they are much more ordered. Here, in the air, the free C=O groups can have more varied orientations on different polymethacrylate surfaces, depending on their local environments (e.g. next to an ester methyl or a normal methyl groups, in a crystalline domain or an amorphous domain on PODMA, etc.) and flexibility of the surface groups (above, around, or below the glass transitions temperatures). In water, because of the hydrogen bonding formation between water molecules and C=O groups, the orientations of surface C=O groups on different polymethacrylates are not very different.

Polymer (in water)	Polarization	Peak center (cm^{-1})	height	Width	Peak Shift (cm^{-1})	PPP/SSP
PAA	SSP PPP	1704 1709	80 339	20 21	~21	 4.03
PMMA	SSP PPP	1719 1712	67 137	16 19	~11	1.72
PBMA	SSP PPP	1711 1711	229 349	21 18	~16	1.77
POMA	SSP PPP	1717 1718	56 112	17 16	~16	2.09
PODMA	SSP PPP	1720 1718	44 54	11 9	~12	1.50

Table 5 Fits of SFG spectra of C=O groups of poly-n-methacrylates in contact with water

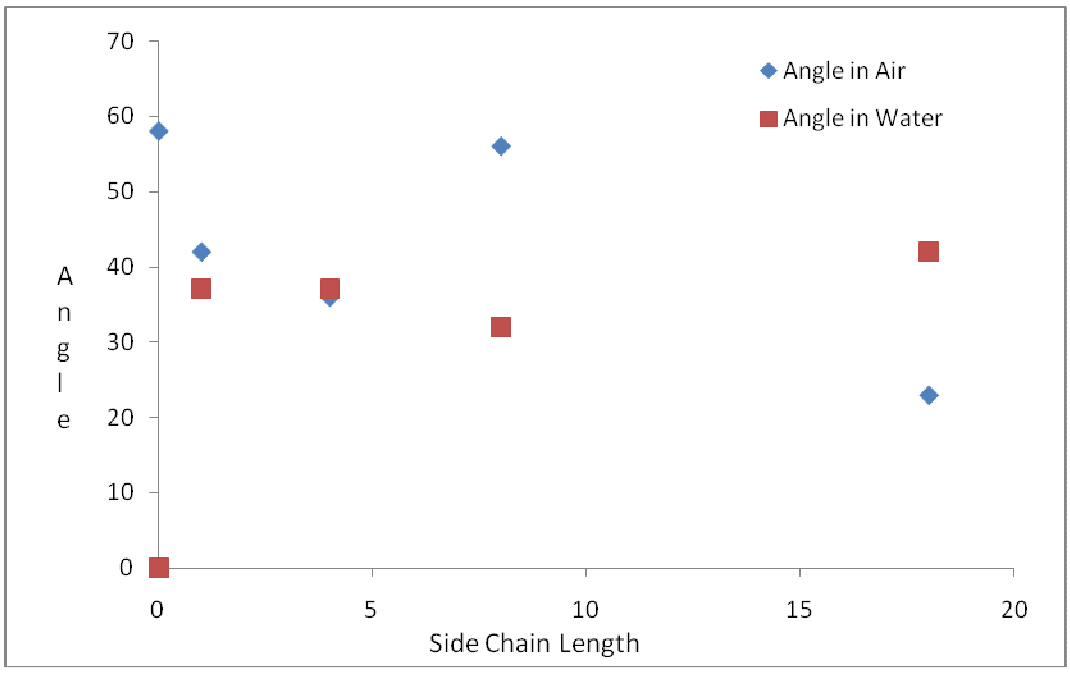

Figure 4-8 Plot of angle from the surface normal versus chain length

4.4 Effects of Corona Treatment

Corona treatment is a widely used method of surface modification for polymers,[32-40] particularly for biocompatibility and adhesion. Corona treatment is thought to increase the number of reactive C=O sites at the expense of alkyl groups.[37] The effect of corona

treatment on the C=O groups in dPMMA was briefly examined with SFG here. The fits are presented in Table 6. Deuterated PMMA was used for convenience, in order to reduce the need for changes in laser alignment, as the CD and CO spectral stretch regions are relatively close. As can clearly be seen from Figure 4-9, the corona treatment affects the deuterated methyl stretches much more strongly than the C=O stretch. This is consistent with previously reported results,[37] which used X-ray Photoelectron Spectroscopy (XPS) in order to show the loss of alkyl components and the increased number of CO groups of PMMA after corona treatment. The increased number of CO groups can have a variety of useful purposes, such as providing more reaction sites for adhesion.

Interestingly, the dPMMA sample used here shows no hydrogen bonded C=O signal prior to corona treatment, and some hydrogen bonded C=O signal after treatment. This would correlate with the theory that corona treatment makes the C=O groups more reactive. Here they become available to hydrogen bond to water in the atmosphere.

In summary, the corona treatment method destroys the CD bonds and creates C=O bonds. This can be seen by the disappearance of the CD stretches in the SFG spectrum. This is consistent with previously published XPS studies of the effects of corona treatment on PMMA. After the corona treatment, some C=O groups can form hydrogen bond to water vapor in the air. This is seen by the increase in width of the C=O peak in the SFG spectrum, which can now be fit with a free C=O peak at 1732 cm^{-1} and a hydrogen bonded C=O peak at 1717 cm^{-1}.

	dPMMA Corona Treated 10s			dPMMA Air		
	Peak center (cm^{-1})	**Height**	**Width**	**Peak center (cm^{-1})**	**Height**	**Width**
H-bonded C=O	1717	45	15	-	-	-
Free C=O	1732	81	15	1732	116	15
CD_3 Stretches	2084	14	5	2077	27	4
	2131	11	8	2118	24	7
	2161	4	11	2154	9	6
	2195	12	11	2185	27	8

Table 6 SFG fits for dPMMA in air compared to 10 second corona treatment

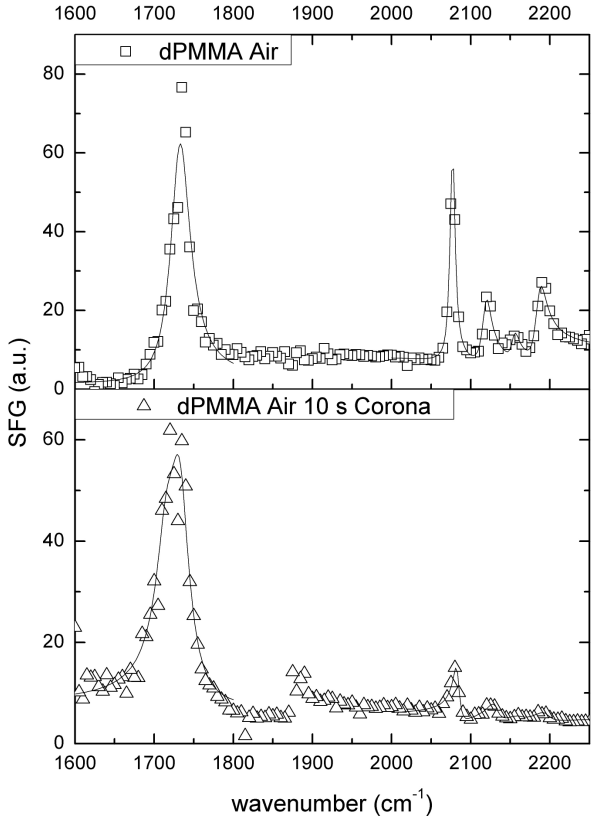

Figure 4-9 SSP SFG spectra of dPMMA before and after 10 seconds of corona treatment

4.5 Conclusions

Surface C=O groups in polymers are important interaction and reaction sites. Here the orientation of surface C=O groups were examined in several similar C=O containing polymers. In air, different, ppp/ssp signal strength ratios for C=O groups on different polymer surfaces were observed. In water, the C=O groups can hydrogen bond to water. When the polymers were contacted to water they all showed a hydrogen bond shift. In the most realistic interpretation of the data, the length of the aliphatic side chain in most of the poly-n-methacrylates seems to have very little effect on the orientation of the surface C=O groups, as they all stand up; however, it does seems to have an effect on the distribution of the orientation angles. PAA, which formula is more different from other polymer molecules, showed a very narrow distribution of the C=O orientations. The surface C=O groups in PMMA, PBMA, and POMA could be interpreted to still stand up but with a wider distributions of angles. The data from the PODMA surface C=O groups are difficult to interpret, but according to the ppp/ssp strength ratio, the C=O groups may not be very different from those on other surfaces.

The corona treatment was shown affect the alkyl groups more than the C=O groups. There also seemed to be evidence of increased reactivity of the C=O groups as evidenced by hydrogen bonding to water from the atmosphere.

(1) Novak, I.; Elyashevich, G. K.; Chodak, I.; Olifirenko, A. S.; Steviar, M.; Spirkova, M.; Saprykina, N.; Vlasova, E.; Kleinova, A. *European Polymer Journal* **2008**, *44*, 2702-2707.

(2) Zenkiewicz, M. *Polimery* **2008**, *53*, 3-13.

(3) Novak, I.; Pollak, V.; Chodak, I. *Plasma Processes and Polymers* **2006**, *3*, 355-364.

(4) Kojima, A.; Yamada, K.; Fujii, T.; Hirata, M. *Journal of Applied Polymer Science* **2006**, *101*, 2632-2638.

(5) Chen, H. In *Analytical chemistry*, 2008; Vol. 80, pp 4119-4124.

(6) Lahann, J. *Chemical Engineering Communications* **2006**, *193*, 1457-1468.

(7) Bouzouia, F.; Djadoun, S. *Journal of Applied Polymer Science* **2008**, *110*, 3574-3581.

(8) Khan, F. L. A.; Sivagurunathan, P. *Physics and Chemistry of Liquids* **2008**, *46*, 504-509.

(9) Imamura, K.; Ohyama, K.; Tani, K.; Yokoyama, T.; Maruyama, Y.; Imanaka, H.; Nakanishi, K. *Spectroscopy Letters* **2008**, *41*, 305-312.

(10) Chang, C. C.; Hou, S. S. *European Polymer Journal* **2008**, *44*, 1337-1345.

(11) Miranda, P. B.; Du, Q.; Shen, Y. R. *Chemical Physics Letters* **1998**, *286*, 1-8.

(12) Tyrode, E.; Johnson, C. M.; Baldelli, S.; Leygraf, C.; Rutland, M. W. *Journal of Physical Chemistry B* **2005**, *109*, 329-341.

(13) Wang, J.; Even, M. A.; Chen, X. Y.; Schmaier, A. H.; Waite, J. H.; Chen, Z. *Journal of the American Chemical Society* **2003**, *125*, 9914-9915.

(14) Miyamae, T.; Yamada, Y.; Uyama, H.; Nozoye, H. *Surface Science* **2001**, *493*, 314-318.

(15) Miyamae, T.; Nozoye, H. *Surface Science* **2005**, *587*, 142-149.

(16) Miyamae, T.; Yamada, Y.; Uyama, H.; Nozoye, H. *Applied Surface Science* **2001**, *180*, 126-137.

(17) Miyamae, T.; Nozoye, H. *Journal of Photochemistry and Photobiology a-Chemistry* **2001**, *145*, 93-99.

(18) Loch, C. L.; Ahn, D.; Chen, C. Y.; Wang, J.; Chen, Z. *Langmuir* **2004**, *20*, 5467-5473.

(19) Rao, Y.; Song, D. H.; Turro, N. J.; Eisenthal, K. B. *Journal of Physical Chemistry B* **2008**, *112*, 13572-13576.

(20) Niaura, G.; Kuprionis, Z.; Ignatjev, I.; Kazemekaite, M.; Valincius, G.; Talaikyte, Z.; Razumas, V.; Svendsen, A. *Journal of Physical Chemistry B* **2008**, *112*, 4094-4101.

(21) Maeda, T.; Ishibashi, T. A. *Appl. Spectrosc.* **2007**, *61*, 459-464.

(22) Loch, C. L.; Ahn, D. C.; Chen, C. Y.; Chen, Z. *Journal of Adhesion* **2005**, *81*, 319-345.

(23) Clarke, M. L.; Chen, C. Y.; Wang, J.; Chen, Z. *Langmuir* **2006**, *22*, 8800-8806.

(24) Young, R. J.; Lovell, P. A. *Introduction to Polymers*; Second ed.; Chapman and Hall: London, 1994.

(25) Chan, C. K.; Chu, I. M. *Polymer* **2001**, *42*, 6089-6093.

(26) Wang, J.; Chen, C. Y.; Buck, S. M.; Chen, Z. *Journal of Physical Chemistry B* **2001**, *105*, 12118-12125.

(27) Wang, J.; Paszti, Z.; Even, M. A.; Chen, Z. *Journal of the American Chemical Society* **2002**, *124*, 7016-7023.

(28) Wang, J.; Chen, C. Y.; Chen, Z. *Abstracts of Papers of the American Chemical Society* **2001**, *222*, 164-COLL.

(29) Chen, C. Y.; Clarke, M. L.; Wang, J.; Chen, Z. *Physical Chemistry Chemical Physics* **2005**, *7*, 2357-2363.

(30) Wang, J.; Woodcock, S. E.; Buck, S. M.; Chen, C. Y.; Chen, Z. *Journal of the American Chemical Society* **2001**, *123*, 9470-9471.

(31) Chen, C. Y.; Even, M. A.; Wang, J.; Chen, Z. *Macromolecules* **2002**, *35*, 9130-9135.

(32) Swart, M.; Mallon, P. E. *Pure and Applied Chemistry* **2009**, *81*, 495-511.

(33) Magga, Y.; Derail, C.; Guerton, F.; Ponche, A.; Soulem, N. *Surface & Coatings Technology* **2009**, *203*, 1573-1579.

(34) Chen, H.; Yuan, L.; Song, W.; Wu, Z. K.; Li, D. *Progress in Polymer Science* **2008**, *33*, 1059-1087.

(35) Kawabe, M. *Sen-I Gakkaishi* **2008**, *64*, 224-228.

(36) Mirabedini, S. M.; Arabi, H.; Salem, A.; Asiaban, S. *Progress in Organic Coatings* **2007**, *60*, 105-111.

(37) Upadhyay, D. J.; Cui, N. Y.; Anderson, C. A.; Brown, N. M. D. *Polymer Degradation and Stability* **2005**, *87*, 33-41.

(38) Denes, F. S.; Manolache, S. *Progress in Polymer Science* **2004**, *29*, 815-885.

(39) Poncin-Epaillard, F.; Legeay, G. *Journal of Biomaterials Science-Polymer Edition* **2003**, *14*, 1005-1028.

(40) Grace, J. M.; Gerenser, L. J. *Journal of Dispersion Science and Technology* **2003**, *24*, 305-341.

CHAPTER 5 : INVESTIGATION OF THE MECHANISM FOR ACETAMINOPHEN POLYMORPHISM FROM POLYMER INDUCED HETERONUCLEATION

5.1 Heteronucleation Crystallization Background

How a material crystallizes can have important effects on its physical properties. The majority of crystallization processes are what is termed heteronucleation processes, where a surface in contact with the solution acts as the nucleation site. The properties of the heteronucleation site can dramatically affect the crystallization process. The following is a thermodynamic discussion of why materials prefer to heteronucleate on a surface (as opposed to homonucleation, without the aid of a surface).

Transient structures brought about by thermal fluctuations of the liquid usually initiate the nucleation process. When a liquid is supersaturated with dissolved material, these transient structures are more likely to form. Following the discussion of homogeneous nucleation by Davey,[1] the degree of supersaturation can be defined in thermodynamic terms as the dimensionless difference in the chemical potential between a solute molecule in equilibrium, μ_{eq}, and a solute molecule in the supersaturated state, μ_{ss}.

$$\sigma = \frac{\mu_{ss} - \mu_{eq}}{kT} \qquad \textbf{Eq. 40}$$

The chemical potentials may be related, by the Gibbs-Duhem equation, to the solute activities or compositions.

$$\sigma = \ln\left(\frac{a_{ss}}{a_{eq}}\right) \qquad \textbf{Eq. 41}$$

Where "a" is the activity. For an ideal solution with a small supersaturation this can be reduced to

$$\sigma = \ln\left(\frac{x_{ss}}{x_{eq}}\right) \approx \frac{x_{ss} - x_{eq}}{x_{eq}} \qquad \textbf{Eq. 42}$$

where x is mole fraction. This supersaturation can be viewed as a driving force for nucleation.[1] This can be seen as follows: Let there be a cluster of molecules formed by random thermal fluctuations containing z molecules. Of these z molecules, z_b have properties of the bulk solid and z_s have properties of the surface. The free energy of the cluster, g_z, can be written a combination of the bulk and surface free energies, g_b and g_s.

$$g_z = z_b g_b + z_s g_s = (z_b + z_s) g_b + (g_s - g_b) z_s \qquad \textbf{Eq. 43}$$

The surface tension, γ, between the cluster and the solution can be written as follows where A is the cluster surface area.

$$\gamma = \frac{(g_s - g_b) z_s}{A} \qquad \textbf{Eq. 44}$$

Thus

$$g_z = z g_b + \gamma A \qquad \textbf{Eq. 45}$$

If we approximate the cluster as a sphere it follows that

$$A \propto z^{\frac{2}{3}} \qquad \textbf{Eq. 46}$$

Rewriting the free energy in terms of the chemical potential

$$g_z = z\mu_b + \beta\gamma z^{\frac{2}{3}} \qquad \textbf{Eq. 47}$$

Where μ_b is the chemical potential of the bulk phase, and β is a shape factor dependent on the shape of the nucleus.

The nucleation of clusters can be written as a quasi-equilibrium between monomers and clusters.

$$zA \Leftrightarrow A_z \qquad \textbf{Eq. 48}$$

Where individual molecules of substance A, are present in the bulk fluid phase at mole fraction of x_{ss}. The free energy change per mole of clusters A_z nucleated is

$$\Delta G = g_z - z\mu \qquad \textbf{Eq. 49}$$

Where μ is the chemical potential of the monomers, which can be written as

$$\mu = \mu^0 + kT \ln x_{ss} \qquad \textbf{Eq. 50}$$

Substituting this into the equation for the free energy we obtain

$$\Delta G = (z\mu_b + \beta\gamma z^{2/3}) - z(\mu^0 + kT \ln(x_{ss})) \qquad \textbf{Eq. 51}$$

For a saturated solution $x = x_{eq}$ and thus $\mu_b = \mu^0 + kT \ln(x_{ss})$, so the free energy becomes

$$\Delta G = -zkT \ln\left(\frac{x_{ss}}{x_{eq}}\right) + \beta\gamma z^{2/3} \qquad \textbf{Eq. 52}$$

Where $\ln(x_{ss}/x_{eq})$ is the degree of supersaturation. By increasing the degree of supersaturation, the energy barrier to forming a crystal nucleus can be decreased. It can also be seen that there is some critical nucleus size z_c for which ΔG is a maximum. For clusters smaller than z_c, the free energy can be reduced by dissolution. For clusters larger than z_c, the free energy can be reduced by crystal growth.

In polymorphic systems, a crystal may not nucleate in the most energetically favorable form first. In 1897 Ostwald proposed the "Law of Stages" (*Gesetz der Umwandlungsstufen*) for polymorphic systems. This generalized rule postulates that a supersaturated state does not transform directly into the equilibrium state with the current conditions, but to the next most stable state than it is currently in.[2] Whether a system can make it through all the stages to the equilibrium stage is a question of kinetics. For example, diamonds will eventually turn into graphite, but not on a human timescale.

A container wall or some other foreign substance that allows adsorption of solute molecules lowers the energy barrier ΔG to nucleation. This crystallization on a foreign

surface is known as heterogeneous nucleation.[1] The free energy cost of creating a new surface between the solution and the crystal can be partially offset by the destruction of the surface between the container wall and the solution. Consider a cluster forming in contact with a perfectly flat wall with a 'wetting angle' θ that is determined by the interfacial tensions γ_{WL}, γ_{WS}, and γ_{SL} balancing in the plane of the wall.

$$\gamma_{WL} = \gamma_{WS} + \gamma_{SL} Cos\theta \qquad \textbf{Eq. 53}$$

The formation of such a cluster will require a free energy of

$$\Delta G_{het} = -V\Delta G_v + A_{SL}\gamma_{SL} + A_{WS}\gamma_{WS} - A_{WS}\gamma_{WL} \qquad \textbf{Eq. 54}$$

Where V is the volume of the cluster and A_{SL} and A_{WS} are the areas of the solid/liquid and wall/solid interface. The first two interfacial contributions to the free energy are positive due to the creation of the interface, whereas the third one is negative due to the destruction of the wall/ liquid interface. Using the following relations:

$$A_{SL} = 2\pi r^2 (1 - Cos\theta)$$
$$A_{WS} = \pi r^2 Sin^2\theta \qquad \textbf{Eq. 55}$$
$$V = \frac{\pi r^3 (2 + Cos\theta)(1 - Cos\theta)^2}{3}$$

Where r is the radius of the cluster, the free energy barrier for *heterogeneous* nucleation can be rewritten as

$$\Delta G_{het} = \left(-\frac{4}{3}\pi r^3 \Delta G_V + 4\pi r^2 \gamma_{SL} \right) S(\theta)$$
$$where \qquad \textbf{Eq. 56}$$
$$S(\theta) = \frac{(2 + Cos\theta)(1 - Cos\theta)^2}{4}$$

This is the same form as the free energy for homogeneous nucleation except for the addition of S(θ), which is known as the shape factor. S(θ) has a numerical value ≤ 1. This is why it is energetically favorable to nucleate heterogeneously.[3] It also shows that heterogeneous nucleation is strongly dependent on the interfacial interaction between the

cluster and the surface that it is growing on. It is this interfacial interaction leading to crystallization that this research hopes to probe with sum frequency generation vibrational spectroscopy.

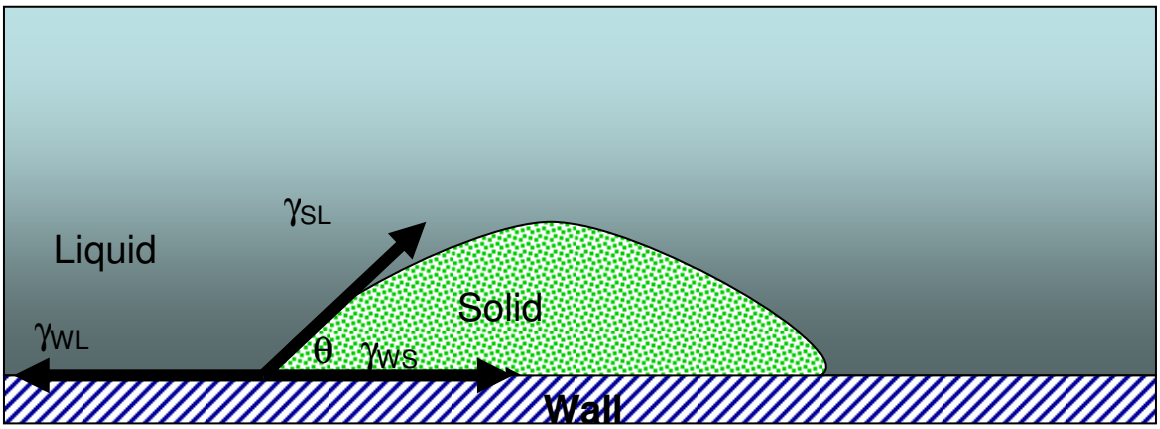

Figure 5-1 Schematic of heterogeneous nucleation

At one extreme, heterogeneous nucleation can occur by non-oriented adsorption of the solute onto a surface until it resembles a crystal. At the other extreme, a specific structural relationship between the catalyzing surface and the crystallizing solute exists, leading to what is known as epitaxial crystal growth. In the epitaxial crystal growth case, the surface structure of the catalyzing surface induces an oriented adsorption of the crystallizing solute so as to mimic its crystal structure.[1]

5.2 Acetaminophen Polymorph Introduction

Different arrangements of a molecule in a solid are termed crystal polymorphs. These polymorphs can have radically different physical properties. Graphite and diamond, two polymorphs of carbon, are the classic example. In the pharmaceutical industry, it has been widely recognized that different polymorphs have different properties of dissolution and bioavailability. Controlling the production of preferred

polymorphs would be of considerable biological and commercial value, making this an area of considerable research interest.

While the importance of polymorphism in the pharmaceutical industry is widely recognized, no good methodology for screening for new polymorphs has been developed. The Matzger Group in the chemistry department at the University of Michigan has made substantial progress in developing a methodology for polymorph screening by heteronucleating compounds of interest on a diverse polymer library. This polymer library includes both commercially available and combinatorially synthesized cross-linked polymers. This method, named Polymer Induced Heteronucleation (PIHn), has been successfully demonstrated on a wide variety of systems such as the pharmaceutical compounds acetaminophen,[4] sulfamethoxizole, carbemezapine,[5] tolfenamic acid,[6] flurbiprofen,[7] sulindac,[7] 5-methyl-2-2[(2-nitrophenyl)amino]-3-thiophenecarbonitrile (ROY),[8] as well as protein crystals,[9] platinum complexes,[10] and metal organic frameworks.[11] The mechanism for what causes the polymorphism on different polymer surfaces is still poorly understood. The research reported here attempts to probe this question.

Acetaminophen, also known as paracetamol and sold under the brand name Tylenol, is a common over-the-counter analgesic and antipyretic. The chemical structure of acetaminophen is shown in Figure 5-2. Two crystal polymorphs have been discovered for acetaminophen. The Matzger group showed that that polymer induced heteronucleation of acetaminophen forms orthorhombic crystals on all the polymers in column 1 of Table 7, monoclinic crystals on all the polymers in column 2 of Table 7, and a mix of monoclinic and orthorhombic crystals in column 3 of Table 7. It was

hypothesized that the molecular structure of the polymer surface should play a strong role in the polymorph heteronucleation process. Some important variables include functional group density, orientation, and orientation distribution. This work used sum frequency generation vibrational spectroscopy to try to understand how the molecular surface structure of the polymer interacts with the crystallizing molecule to determine the polymorph formed. This work used acetaminophen and focused on using poly(methyl methacrylate) (PMMA) surfaces and poly(n-butyl methacrylate) (PBMA) surfaces, since they heteronucleate different polymorphs despite their very similar chemical composition. The chemical structures of PMMA and PBMA are shown in Figure 5-3.

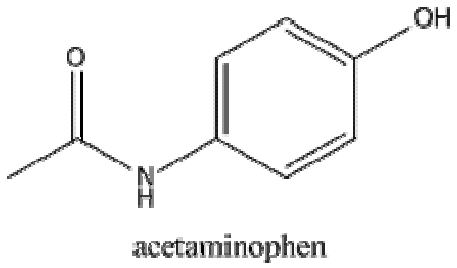

Figure 5-2 Structure of acetaminophen

An optical micrograph of orthorhombic crystals of acetaminophen heteronucleated on PMMA is shown in Figure 5-4. A crystal structure of orthorhombic acetaminophen crystal structure is shown in Figure 5-5. An optical micrograph of monoclinic acetaminophen crystals heteronucleated on PBMA is shown in Figure 5-6. The crystals structure of monoclinic acetaminophen is shown in Figure 5-7.

Orthorhombic form induced	Monoclinic form induced	Mixtures of orthorhombic and monoclinic induced
Alginic acid, sodium salt	Butyl methacrylate/isobutyl methacrylate copolymer	Acrylonitrile/butadiene/styrene resin
Nylon 6, 11, 6/6, 6/9, 6/10, 6/12, 6/T(polytrimethyl hexamethylene terephthalamide)	Cellulose acetate butyrate	Ethylene/acrylic acid copolymer
	Cellulose propionate	Ethylene/vinyl acetate (25, 28, 33, and 40% VA) copolymer
	Cellulose triacetate	Phenoxy resin
	Ethyl cellulose	Polyacrylamide, carboxyl modified (low content)
Polyacetal	Ethylene/ethyl acrylate copolymer	Poly(diallyl isophthalate) and Poly(diallyl phthalate)
1,2-Polybutadiene	Ethylene/propylene copolymer	Poly(4,4-dipropoxy-2,2-diphenyl propane fumarate)
Polycaprolactone	Ethylene/vinyl acetate (14 and 18% VA) copolymer	Poly(ethyl methacrylate)
Poly(2,6-dimethyl-*p*-phenylene oxide)	Hydroxypropyl methyl cellulose	Polyethylene, chlorinated (25% chlorine)
	Polyamide resin	Polyethylene, oxidized
Polyethylene, high density	Poly(1-butene), isotactic	Poly(ethylene terephthalate)
Polyethylene, chlorinated (36, 42, and 48% chlorine)	Poly(*n*-butyl methacrylate)	Poly(isobutyl methacrylate)
	Polycarbonate	Polyisoprene, chlorinated
Polyethylene, chlorosulfonated	Poly(2-hydroxyethyl methylate)	Poly(phenylene sulfide)
Poly(methyl methacrylate)	Poly(*α*-methylstyrene)	Polystyrene
Poly(4-methyl-1-pentene)	Poly(*p*-phenylene ether-sulphone)	Polysulfone
Polypropylene, isotactic and isotactic, chlorinated	Poly(vinyl acetate)	Poly(vinyl stearate)
	Poly(vinyl alcohol), 98 and 99.7% hydrolyzed	Poly(vinylidene fluoride)
Poly(tetrafluoroethylene)	Poly(vinyl butyral) and Poly(vinyl formal)	Styrene/acrylonitrile copolymer (75/25)
Poly(2,4,6-tribromostyrene)	Styrene/acrylonitrile copolymer (70/30)	Styrene/isoprene ABA block copolymer
Poly(vinyl chloride), and PVC 1.8% carboxylated	Styrene/allyl alcohol copolymer	Vinyl chloride/vinyl acetate (81, 88 and 90% VCl) copolymer and 1% carboxylated
Styrene/ethylene-butylene, ABA block copolymer	Styrene/butadiene, ABA block copolymer	
	Styrene/butyl methacrylate copolymer	Vinyl chloride/vinyl acetate/hydroxylpropyl acrylate terpolymer
	Styrene/maleic anhydride copolymer	
	Vinyl alcohol/vinyl butyral copolymer (20/80)	Vinyl chloride/vinyl acetate/vinyl alcohol terpolymer

Table 7 Table of acetaminophen polymer induced heteronucleated polymorphs[14]

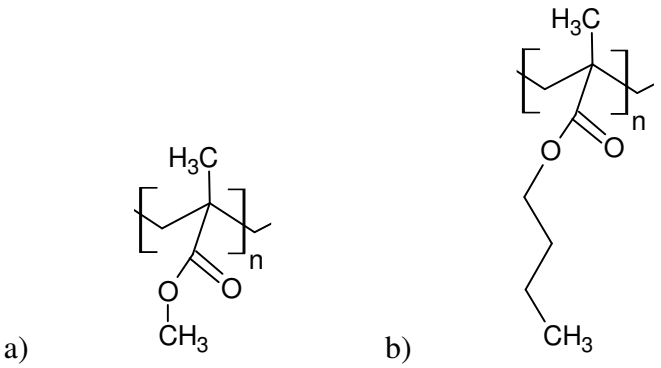

Figure 5-3a) Structure of PMMA, b) structure of PBMA

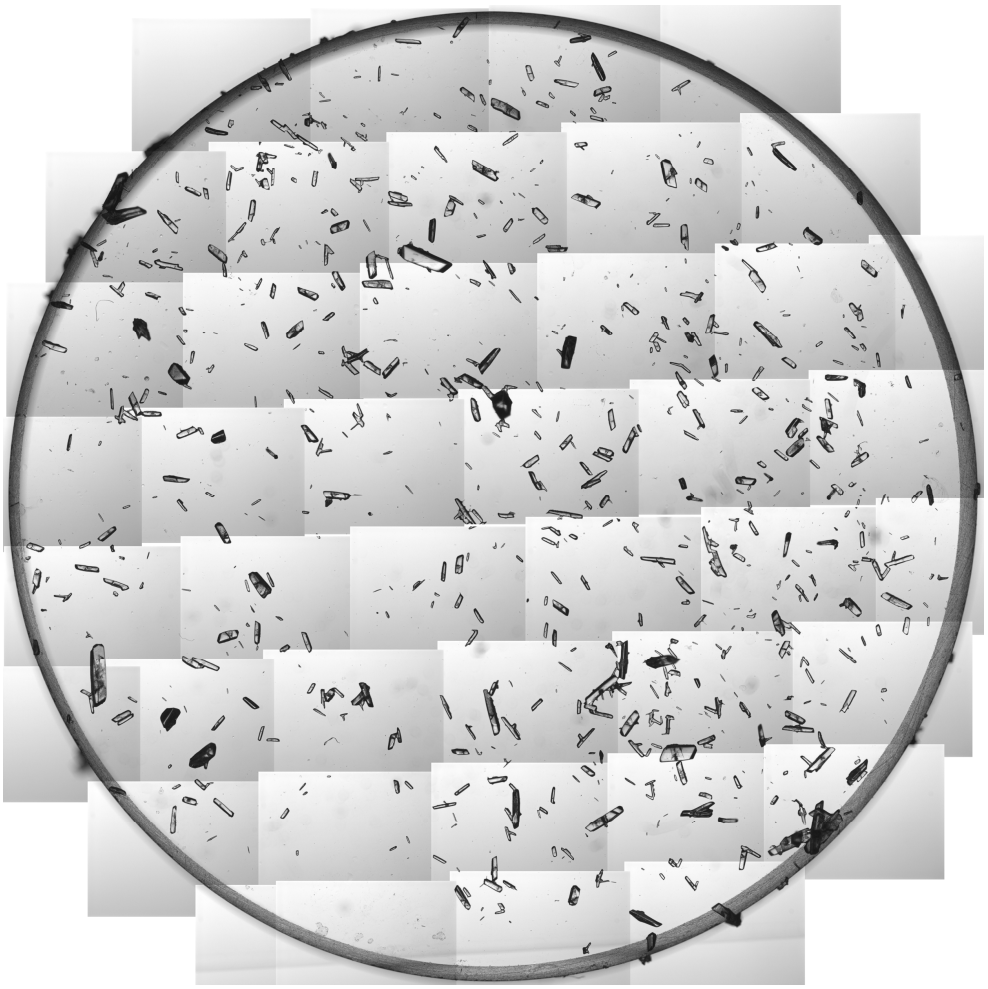

Figure 5-4 Optical micrograph of orthorhombic acetaminophen crystals grown on PMMA. The substrate is 1 inch in diameter.

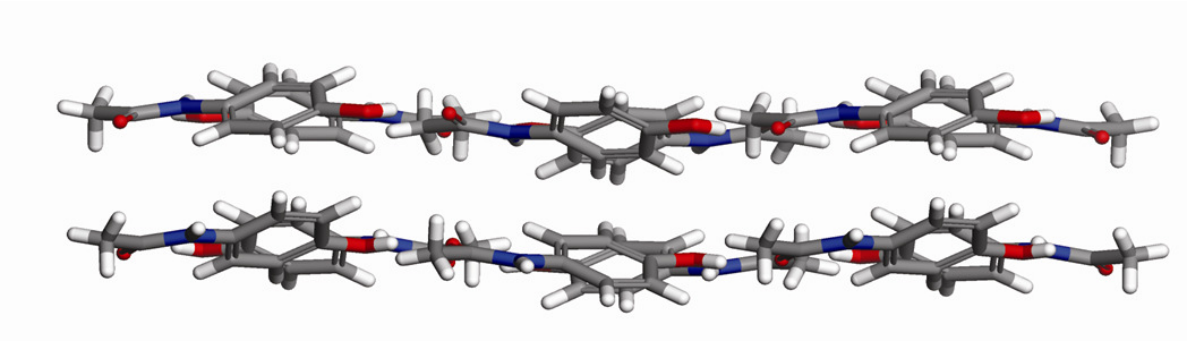

Figure 5-5 Model of orthorhombic acetaminophen crystal. The colors represent: white – hydrogen, grey carbon, blue-nitrogen, red -oxygen

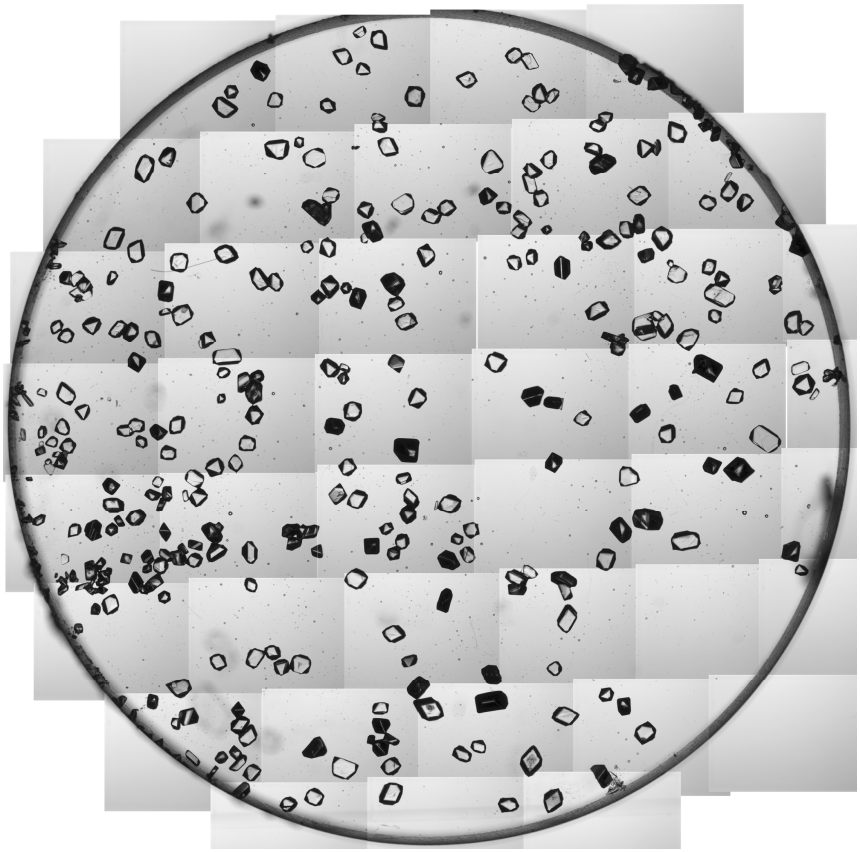

Figure 5-6 Optical micrograph of monoclinic acetaminophen crystals grown on a PBMA film. The substrate is 1 inch in diameter.

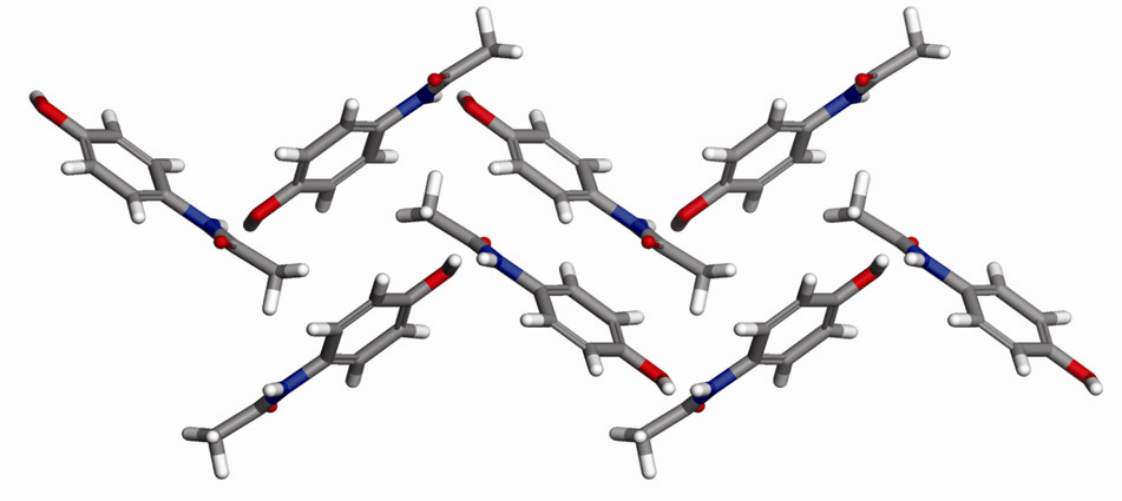

Figure 5-7 Model of a monoclinic acetaminophen crystal. The colors represent: white – hydrogen, grey carbon, blue-nitrogen, red -oxygen

5.3 Experimental Setup:

In this work, the near-total internal reflection prism geometry previously described[15] was employed. The sample geometry is shown again in Figure 5-8. This geometry has favorable Fresnel coefficients to give a stronger reflected SFG signal compared to a flat window geometry. In addition, this geometry reduces sample damage, as excess laser light is largely reflected as opposed to transmitted through the sample.

All polymer samples were prepared by spin coating 2% by weight polymer solutions onto optically clear CaF_2 prisms at 2500 rpm on a Speedline Technologies Spin Coater. The poly(methyl methacrylate) (PMMA) (Aldrich, MW 15,000), poly(n-butyl methacrylate) (nPBMA) (Scientific Polymer Products Inc.) and deuterated forms of PMMA (dPMMA, Polymer Source Inc., MW 219,000) and d-nPBMA (synthesized by Vilmali Lopez-Mejias, with deuterated side chains) were all dissolved in toluene.

Acetaminophen, phenol, methoxyacetanilide, and acetanilide were ordered from Aldrich. They were used as received. Saturated solutions were prepared with nanopure water. The acetaminophen crystals were grown by submerging the coated prism in a saturated solution for 30 minutes to several days. The samples were then dried overnight at atmospheric conditions.

The sublimated acetaminophen crystals were deposited under vacuum at 120º C for 15 minutes by Vilmali Lopez-Mejias.

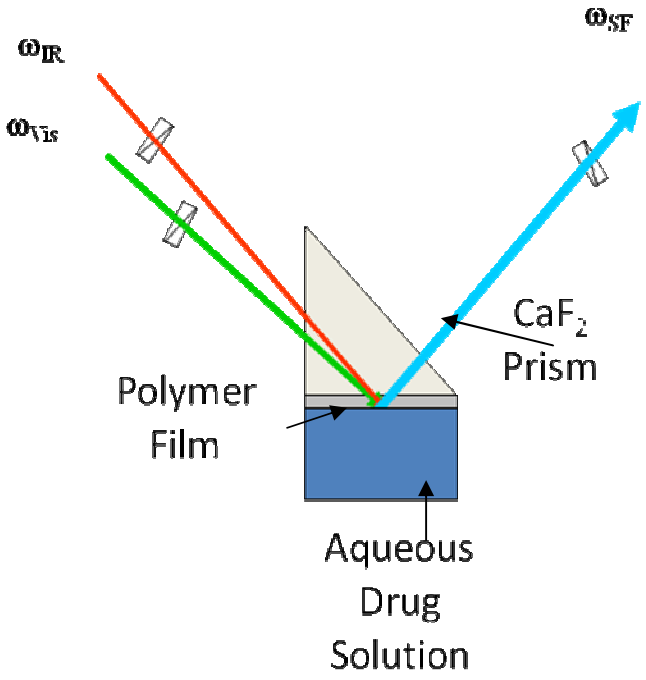

Figure 5-8 Experimental sample geometry

5.3.1 Interaction Site

We began by exploring the nature of the interaction between the polymer surface and the acetaminophen molecules. As was previously discussed in Chapter 4, PMMA and PBMA do show different restructuring behavior in water with regards to their methyl groups. Even so, it was hypothesized that the methyl groups probably did not interact strongly with the acetaminophen molecules as they crystallized. Spectroscopically, the possibility of hydrogen bonding with a methyl group ("improper" hydrogen bonding[16-22]) may be considered. This type of interaction would cause a blue shift in the vibrational frequency, due to shortening of the bonds involved. A peak shift of up to 14 cm^{-1} has been reported for the asymmetric methyl stretch due to "improper" hydrogen binding.[16] So a blue shift in the amide I stretch of the acetaminophen around 1650 cm^{-1} would be indicative of an "improper hydrogen bond" between the polymer CH_3 groups and the

C=O group of the acetaminophen. A blue shift of the polymer C=O stretch would indicate an "improper hydrogen bond" between the polymer C=O and the acetaminophen methyl group. Such a shift would be resolvable by SFG, but this was not observed.

Another possible interaction between the polymer and acetaminophen is a normal hydrogen bond between the C=O in the polymer and either the NH or OH in the acetaminophen. If there was a hydrogen bonding event, then the C=O peak position of the polymer should shift to the red (lower in frequency) in the SFG spectrum, as seen in Chapter 4 between H_2O and the polymer C=O groups.

In order to address the question of which part of the acetaminophen molecule was interacting with the polymer surface, phenol and acetanilide were used to model the two halves of the acetaminophen compound (see figure 5-9). In order to test the theory that the OH group interacts with the surface, methoxyacetanilide was also examined. In methoxyacetanilide, the OH in acetaminophen is replaced with a methyl group. Unfortunately, the spectra collected when this compound was contacted were of poor quality, and no conclusions could be drawn. The peaks were weak, broad and noisy, so no reliable fitting could be done.

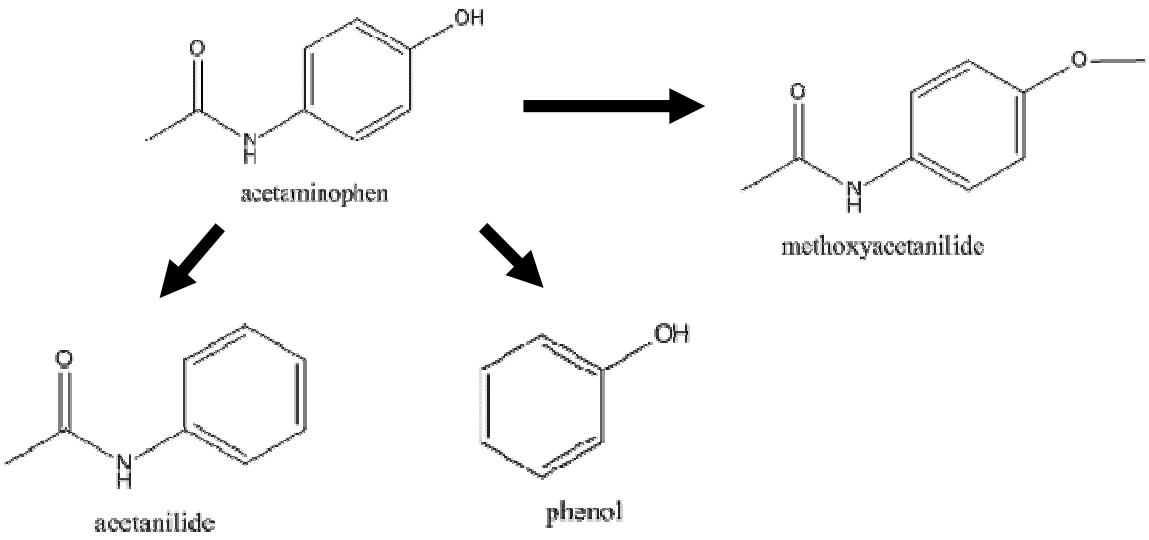

Figure 5-9 To separate the possible functional groups that were interacting with the polymer surface saturated aqueous phenol and acetanilide solutions were used to model parts of acetaminophen.

5.4 SFG data

5.4.1 Solution/Polymer Interface

As mentioned previously, one mode of interaction between the acetaminophen and the polymer could be by hydrogen bonding between either the OH or NH groups on the acetaminophen molecule and the C=O group on the polymer. If this is the case, then an attendant red shift in the polymer C=O peak position would be observed as a result.[23-27] Fitted results showing peak shifts are summarized in Table 8. The bulk polymers have C=O stretches at 1734 cm^{-1} for PMMA and 1730 cm^{-1} for PBMA as measured by absorbance FTIR. If we believe that the signal from the free C=O groups should match the FTIR peak position of 1734 cm^{-1}, then the SFG spectra with the PMMA peak centered at 1725 cm^{-1}, may be interpreted as having some contribution from C=O groups hydrogen bonded to water from the air. It is believed however that most of the signal is from the free C=O groups. When PMMA and PBMA were contacted to water and both

showed an average peak shift of around 15 cm^{-1}. The resolution of the SFG system is 5 cm^{-1}.

PMMA and PBMA films were next contacted to saturated aqueous solutions of phenol, acetanilide, acetaminophen and the SFG spectra were collected. (See Figure 5-10 and Figure 5-11) The peak shift when contacted to acetaminophen solution and acetanilide are similar around 15cm^{-1} for PMMA and PBMA if considering the peak centers in FTIR spectra as those from free C=O groups. In Table 8 we listed the C=O peak center shifts for the SFG spectra collected from different interfaces. For comparison, we use the peak centers from the SFG spectra collected in air as opposed to the FTIR peak centers. The peak shift when the samples were contacted to phenol solution was very different (around 30 cm^{-1}) from the shift for acetanilide and acetaminophen for both PMMA and PBMA. The much larger peak shift with the phenol solution definitively shows that the OH group is not the interaction site of the acetaminophen molecule with the polymer C=O groups. The similarity in peak shift for the acetanilide and acetaminophen implies that it is probably the amine group in acetaminophen and acetanilide that is hydrogen bonding to the carbonyl group in the polymer. The peak shift is not dramatically different from the peak shift that we observe when the polymers are contacted to just water, therefore it is possible that at the polymer/acetaminophen solution interface, polymer C=O groups hydrogen bond to water molecules. However, we know that the acetaminophen and acetanilide are present at the polymer surface due to the presence of amide I signals (around 1650 cm^{-1}), we believe that the SFG C=O stretching signal shift cannot be solely attributed to hydrogen bonding between polymer and water molecules. The hydrogen bonding between polymer C=O and acetaminophen groups

play important roles. Unfortunately, the amide I signals from solution were not strong and distinct enough to perform reliable orientation analysis upon when the polymers are contacted to the drug solution.

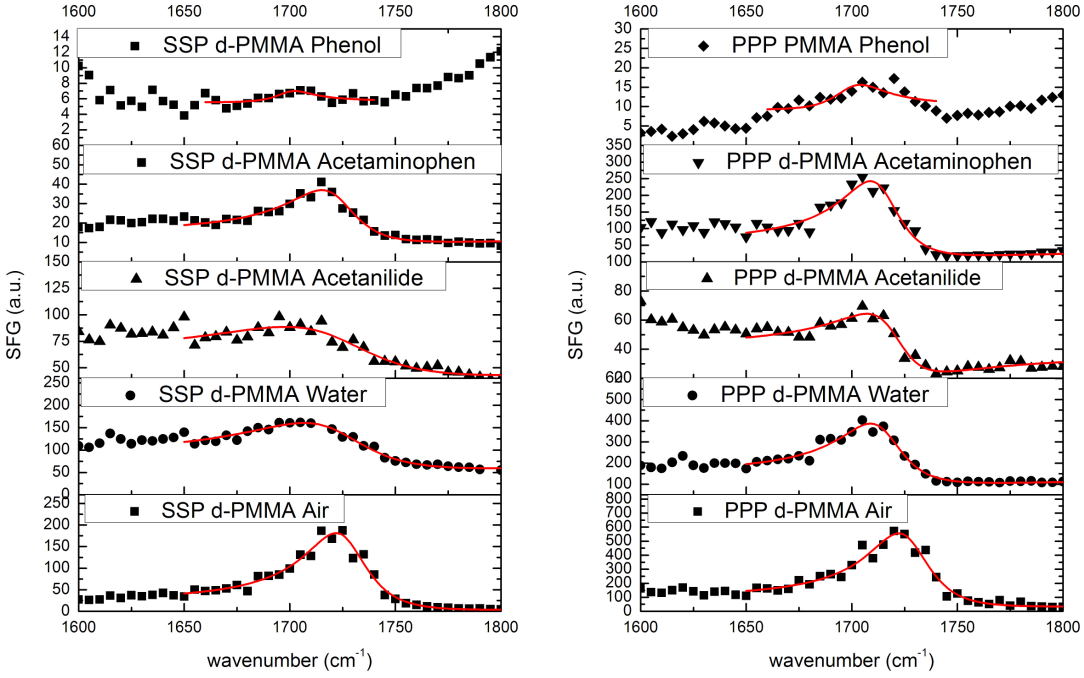

Figure 5-10 SSP and PPP polarization combination SFG spectra. Deuterated PMMA contacted to saturated aqueous solution of phenol, acetanilide, and acetaminophen. The spectra of d-PMMA in air and water are given for reference.

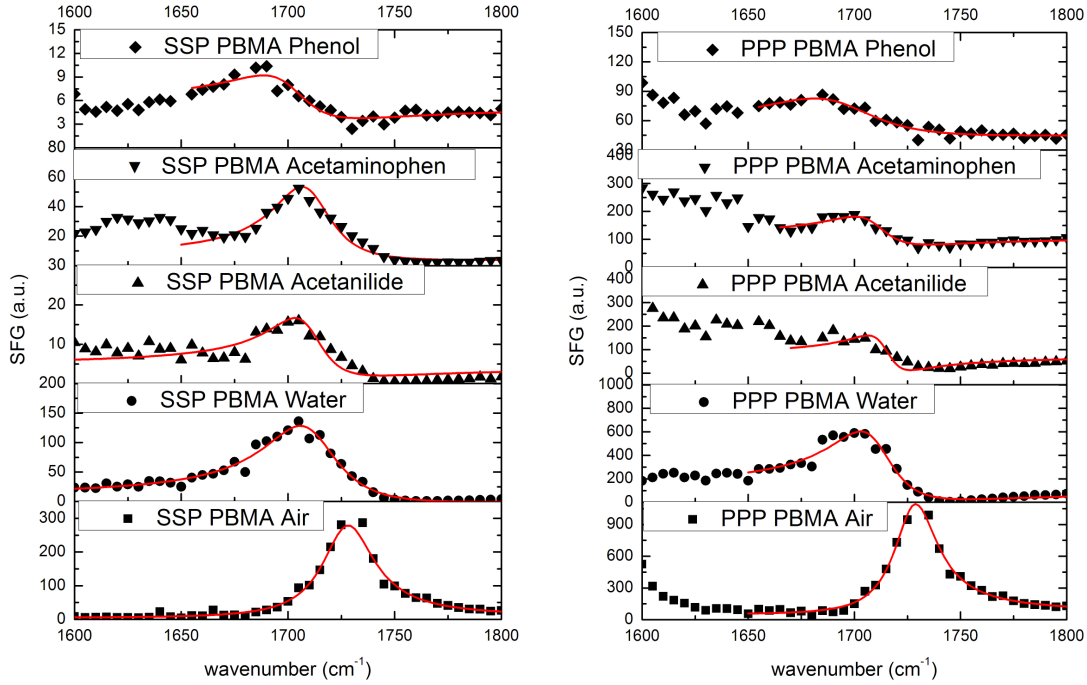

Figure 5-11 SSP and PPP SFG spectra of PBMA contacted to saturated aqueous solutions of phenol, acetanilide, and acetaminophen. The spectra of PBMA contacted to air and water are given for reference.

	SSP dPMMA Peak Center (cm^{-1})	Shift	PPP dPMMA Peak Center (cm^{-1})	Shift	SSP dPBMA Peak Center (cm^{-1})	Shift	PPP dPBMA Peak Center (cm^{-1})	Shift
Air	1725	-	1727	-	1727	-	1727	-
Water	1718	7	1712	15	1711	16	1711	16
Phenol Solution	1700	25	1700	27	1697	30	1694	33
Acetanilide Solution	1706	19	1720	7	1710	17	1715	12
Acetaminophen Solution	1716	9	1715	12	1707	20	1710	17

Table 8 Table of peak centers and peak shifts from the polymer-air peak position

Based on the above results, we conclude that the polymer C=O group and the NH in the acetaminophen form hydrogen bonds. The similarity in peak shifts between the acetanilide and acetaminophen as compared to the phenol indicates that the NH group in the acetaminophen is the hydrogen-bonding site in the acetaminophen molecule.

However, both PMMA and PBMA in theory have similar interactions functional groups present for interactions. The question remains, why are different polymorphs observed when acetaminophen is heteronucleated on these two polymer surfaces?

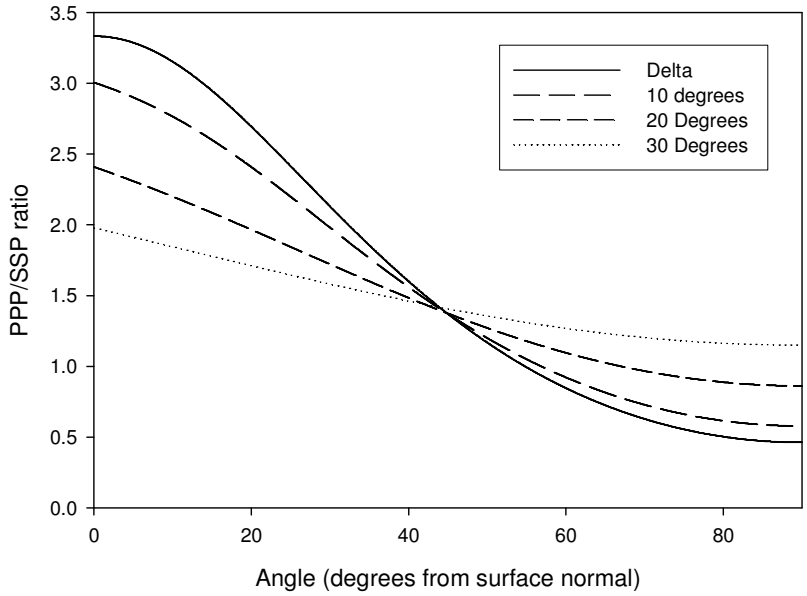

Figure 5-12 C=O orientation plot for various orientational angles and distributions

One possible explanation for the difference in polymorph heteronucleated between PMMA and PBMA is that there is a difference in the surface structure (and in particular the orientation of C=O groups on the polymer). By taking the ratio of the peak intensities in the PPP and SSP polarization combinations, the orientation of the carbonyl groups can be deduced as discussed in Chapter 3. Both PMMA and PBMA have a carbonyl stretch centered ~1730 cm^{-1}. First, SFG spectra were collected from the polymer alone in air. From these polarization combinations the orientation of the C=O group was determined. The theoretical curves were plotted (Figure 5-12), and the measured ratio was compared to the theoretical curves in order to deduce the possible orientational angles and orientational distributions.

As can be seen in Table 9 the C=O orientations of PMMA and PBMA in both air and water give very similar PPP/SSP ratios, demonstrating that such C=O groups may adopt similar orientation in air and water.

The SFG PPP/SSP signal strength ratios of C=O stretches from the polymer/acetanilide solution interface and the polymer/acetaminophen solution interface are different from the polymer/air and polymer/water interfaces for both PMMA and PBMA. This shows that the acetanilide and acetaminophen both induce very different orientations of the C=O groups on PMMA and PBMA. The difference between the polymer/acetaminophen solution interface and the polymer/water interface further indicates that the hydrogen bonds at the polymer/acetaminophen solution interface are not only contributed from those between polymer C=O groups and water molecules. The fact that there is a difference in the acetaminophen and acetanilide hydrogen bonded orientation of the polymer C=O groups could be due to the acetaminophen's ability to hydrogen bond to water with the OH group on the other end of the molecule that is absent in the acetanilide molecule. In PMMA the acetanilide induces the C=O groups to lie down, while acetaminophen causes the C=O group to form a 20° angle from the surface normal under the δ distribution assumption. In contact with PBMA, acetanilide PPP/SSP ratio passes though the "magic angle" where the orientation cannot be definitively determined. The acetaminophen induces the C=O groups in the PBMA to form a 53° angle from the surface normal under the δ distribution assumption. The difference in angles of the C=O groups in the polymers could be due to steric hindrance effects of the longer side chain of the PBMA. The difference between the orientation of the C=O

groups when hydrogen bonded to acetaminophen clearly could play an important role in the determination of the polymorph heteronucleated on the two different polymers.

	SSP		PPP			
	Peak Center (cm^{-1})	**Height**	**Peak Center (cm^{-1})**	**Height**	**Peak Assignment**	**PPP/SSP ratio normalized for peak width**
PMMA-Air	1725	187	1727	241	Free C=O	1.53
PMMA-Water	1718	67	1717	137	H-Bonded C=O	1.72
PMMA-Phenol	1700	13	1700	35	H-Bonded C=O	2.04
PMMA-Acetanilide	1706	191	1720	61	H-Bonded C=O	0.63
PMMA-Acetaminophen	1716	88	1715	205	H-Bonded C=O	2.70
PBMA-Air	1727	247	1727	441	Free C=O	1.79
PBMA-Water	1711	229	1711	349	H-Bonded C=O	1.77
PBMA-Phenol	1697	35	1694	184	H-Bonded C=O	2.66
PBMA-Acetanilide	1710	47	1715	47	H-Bonded C=O	1.51
PBMA-Acetaminophen	1707	129	1710	103	H-Bonded C=O	1.05

Table 9 Table of fits for the polymer-solution interface experiments.

5.4.2 Acetaminophen Crystal - Polymer Interface

Different crystal polymorphs of acetaminophen were successfully grown on the PMMA and PBMA surfaces. Figure 5-4 and Figure 5-6 clearly show the different polymorphic crystals on PMMA and PBMA surfaces. The two polymorphs have unique Raman signatures, unfortunately in a spectral region that is inaccessible to our SFG system.

SFG spectra were collected from the polymer/crystal interfaces using SSP, PPP, and SPS polarization combinations. The experimental geometry is shown in Figure 5-13. Since the acetaminophen crystals are millimeters thick, the input IR beam cannot penetrate the entire acetaminophen crystal to reach the acetaminophen crystal/air interface. Therefore, SFG signal would not be contributed from the acetaminophen crystal/air interface. In addition, we detected similar signals from different sized crystals, so the signal did not arise from the bulk. Both the acetaminophen monoclinic and orthorhombic crystals have inversion symmetry in the bulk. Under the electric-dipole approximation, no SFG signal will be generated from the crystal bulk. Therefore, any SFG signals detected must originate from the polymer/ acetaminophen crystal interface. The polymer C=O signal is still detectable also, lending further evidence to the polymer/crystal interface being the source of the SFG signal. At the crystal/air interface no polymer signal would be detected.

For reference, the C=O region Raman spectra from the two crystal polymorph forms are shown in Figure 5-14.

In the SFG spectra of the crystal/ polymer interface, signals from several acetaminophen stretching modes were observed, including the amide I stretch, the methyl C-H stretch, and some aromatic C-H stretches.

SFG spectra were collected from the interface of acetaminophen crystals with PMMA and PBMA; the resulting spectra were markedly different. (Figure 5-16 and Figure 5-15) These spectra do not show only the C=O group, but also the amide I mode from the acetaminophen.[28]

The amide I stretch from the acetaminophen shows up at 1650cm^{-1}, and this peak is quite strong in SFG spectra from monoclinic acetaminophen crystals on PBMA. However, the polymer C=O signal (around 1730 cm^{-1}) is relatively weak. This shows that at the PBMA/acetaminophen crystal interface, the orientation of PBMA C=O groups can be quite random, or lie down at the interface.

In contrast, the SFG spectrum from the PMMA/acetaminophen orthorhombic crystal interface showed very weak amide I signal. It is interesting that no SFG signal from the amide I stretch was observed, as a peak is clearly present in the Raman spectrum, Figure 5-14. SFG is sensitive to molecular orientation, and thus certain orientations will generate no detectable signal, even when molecules are present. Unfortunately, there are a number of possible orientations that would lead to no SFG signal, and so we were unable to quantify this in more detail.

The SFG spectrum obtained from the orthorhombic crystal/PMMA interface showed predominately the C=O stretching signals on the PMMA surface, centered around 1715 and 1732 cm^{-1}, respectively.(Figure 5-16) As we discussed above, the 1715 cm^{-1} peak can be assigned to the stretching mode of the C=O groups hydrogen bonded to

–NH-groups, while 1735 cm^{-1} peak should be the "free" C=O groups. This observation indicates that at the PMMA/acetaminophen crystal interface, the majority of the PMMA C=O groups form hydrogen bonds with –NH- groups on acetaminophen, as was observed at the PMMA/acetaminophen solution interface. Clearly, hydrogen bonding between PMMA C=O groups and the acetaminophen NH groups are related to the heteronucleation of the orthorhombic acetaminophen crystals on PMMA.

The observation of a shoulder at 1735 cm^{-1} indicates that at the PMMA/acetaminophen crystal interface, some PMMA C=O groups do not form hydrogen bonding. This signal might be contributed to the C=O groups near the PMMA/acetaminophen crystal interface where inversion symmetry for C=O groups is already broken. Another possibility is that some C=O groups at the PMMA/ acetaminophen interface may interact with hydrophobic groups on acetaminophen, such as end methyl groups, therefore they do not form hydrogen bonds and their frequency is at 1735 cm^{-1}. Our results demonstrate that hydrogen bonding to the PMMA C=O groups do occur at the acetaminophen orthorhombic crystal/PMMA interface.

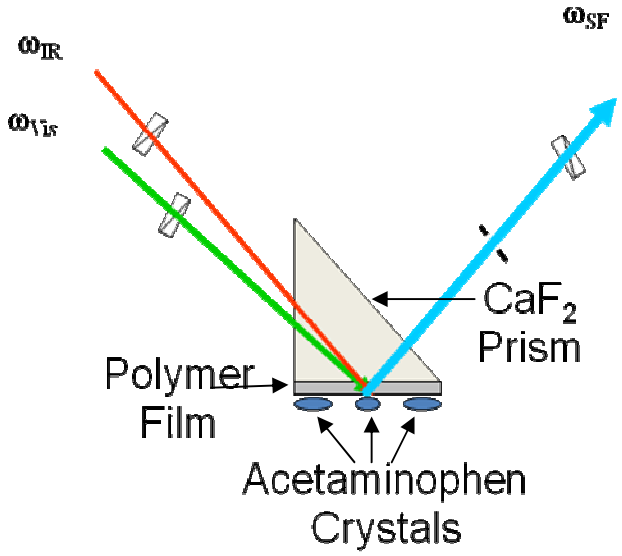

Figure 5-13 Sample geometry used for the crystal polymer interface experiments.

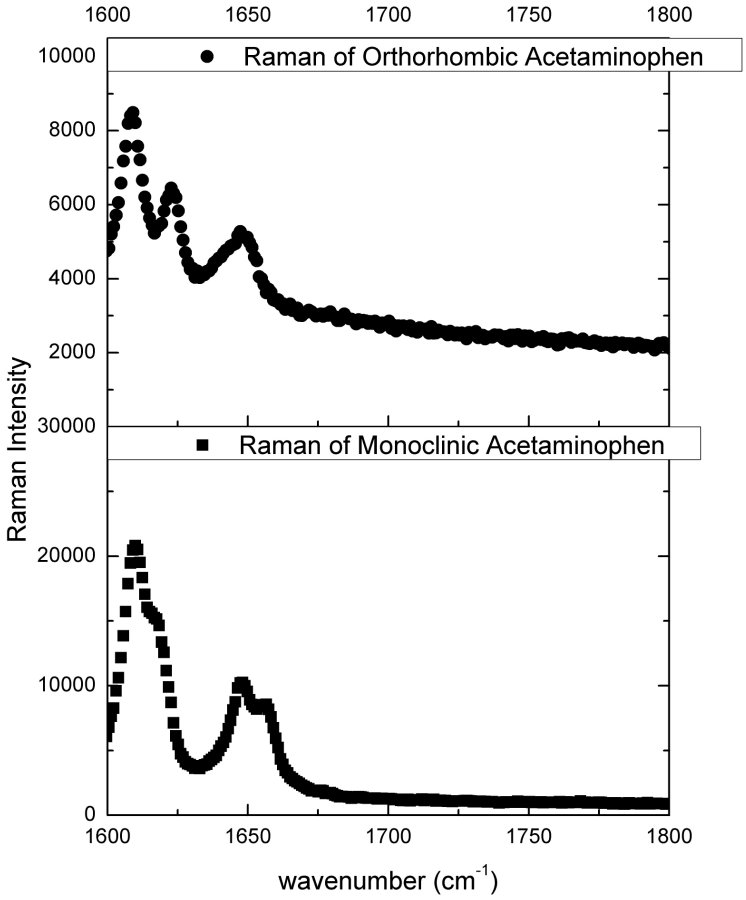

Figure 5-14 Raman spectra of orthorhombic and monoclinic acetaminophen crystals in the C=O stretching region.

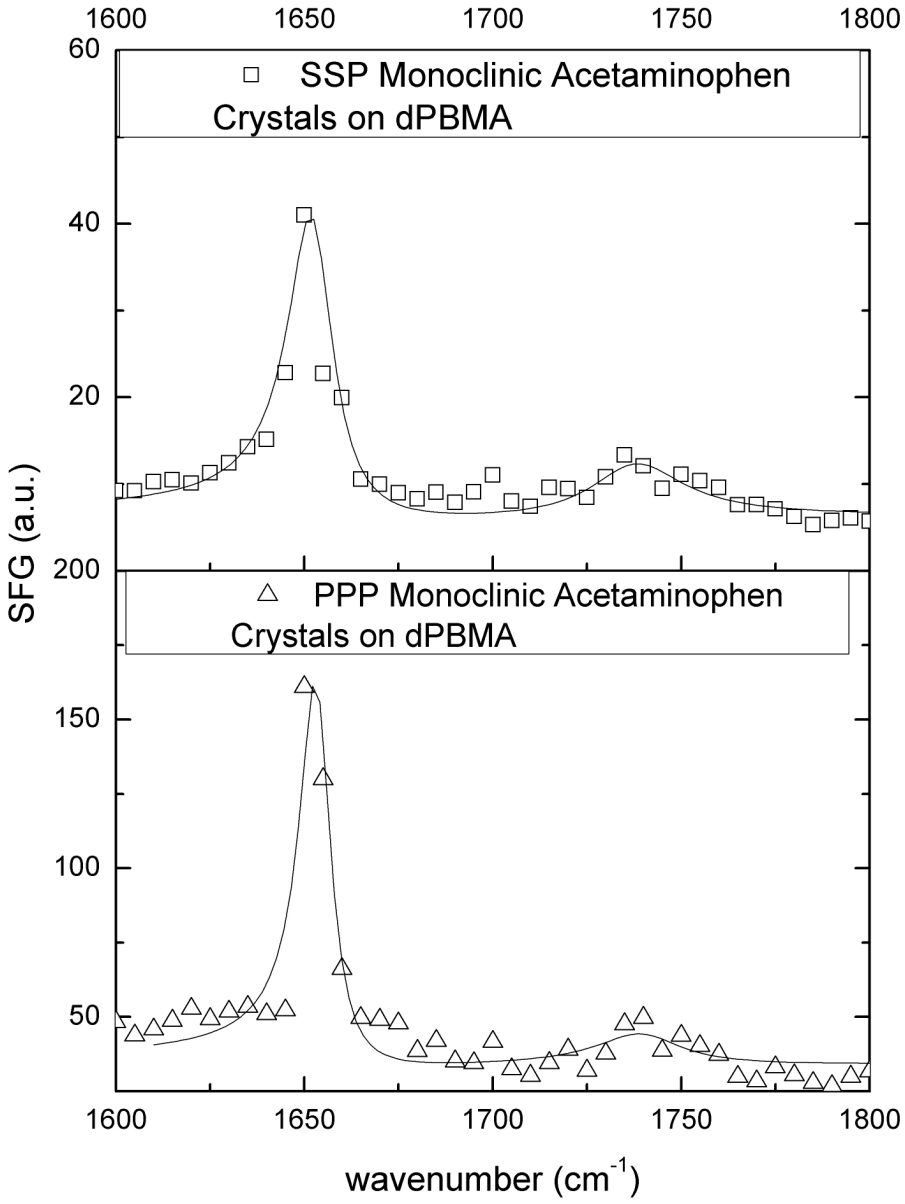

Figure 5-15 SFG spectra of monoclinic acetaminophen crystals on dPBMA in the SSP and PPP polarization combinations in the C=O stretching region.

	Peak Center (cm^{-1})	Height	Width
SSP Monoclinic	1652	42	7
	1737	36	15
PPP Monoclinic	1654	56	5
	1740	43	14

Table 10 SFG fit values for the monoclinic acetaminophen dPBMA interface

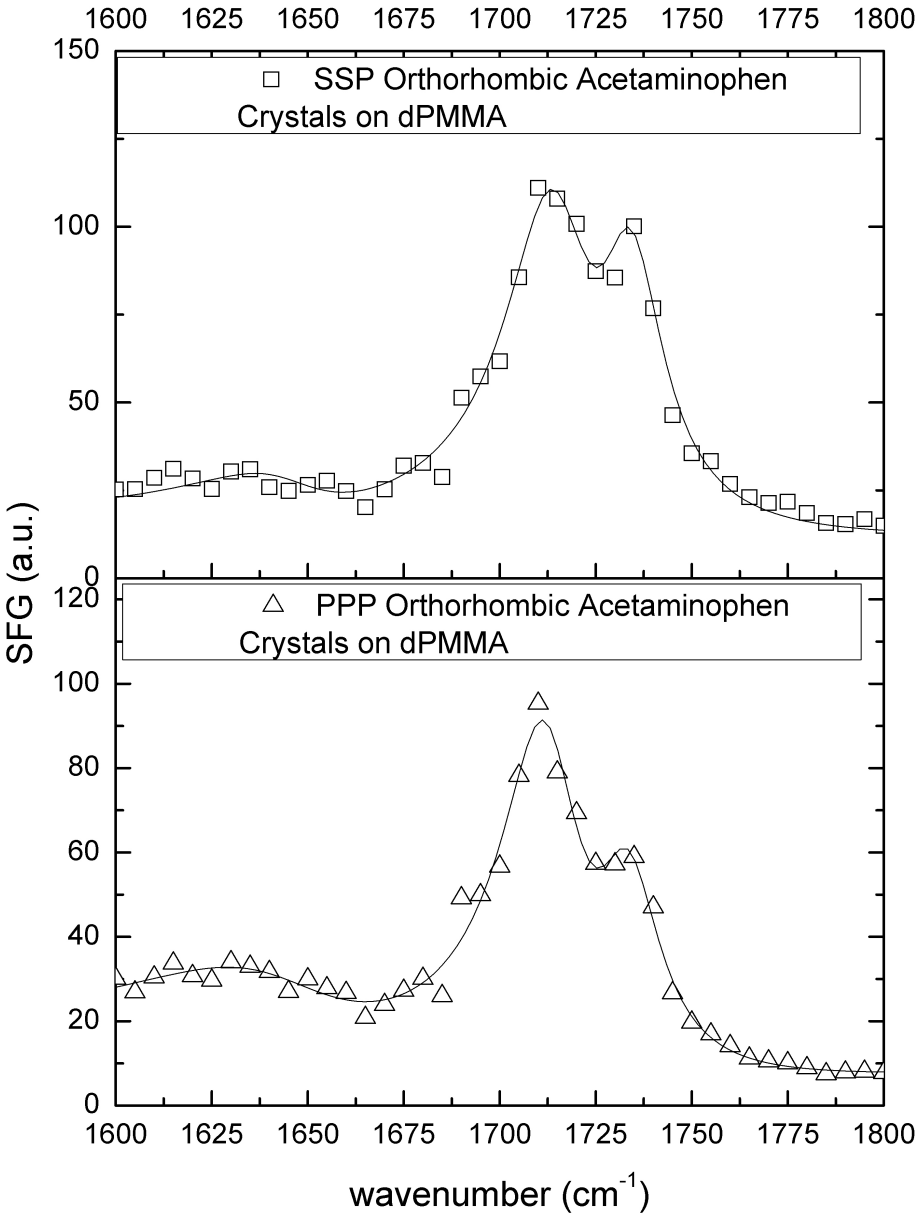

Figure 5-16 SFG spectra from the dPMMA/orthorhombic acetaminophen crystal interface

	Peak Center (cm^{-1})	Height	Width
SSP Orthorhombic	1734	60	10
	1715	109	14
	1645	34	20
PPP Orthorhombic	1733	47	10
	1713	90	13
	1644	84	34

Table 11 SFG fit values for the orthorhombic acetaminophen dPMMA interface

5.4.3 Amide I Orientation

In the case of the monoclinic acetaminophen/PBMA interface, the orientation analysis can be performed similar to the manner in which the free C=O orientation was performed. The main difference is that for the amide I vibration, the Raman depolarization ratio r=0.13, and the vibrational mode lies 22° from the C=O bond axis.[28] The rest of the equations are the same as explained in Chapter 3. The amide I orientation as determined by SFG in proteins has been previously reported.[15] The PPP/SSP ratio of the amide I tensor for the monoclinic acetaminophen crystals was found to be 0.9 on average. This corresponds to an amide I tensor orientation of around 56° from the surface normal under the delta distribution assumption, which should be a reasonable assumption for a crystal.

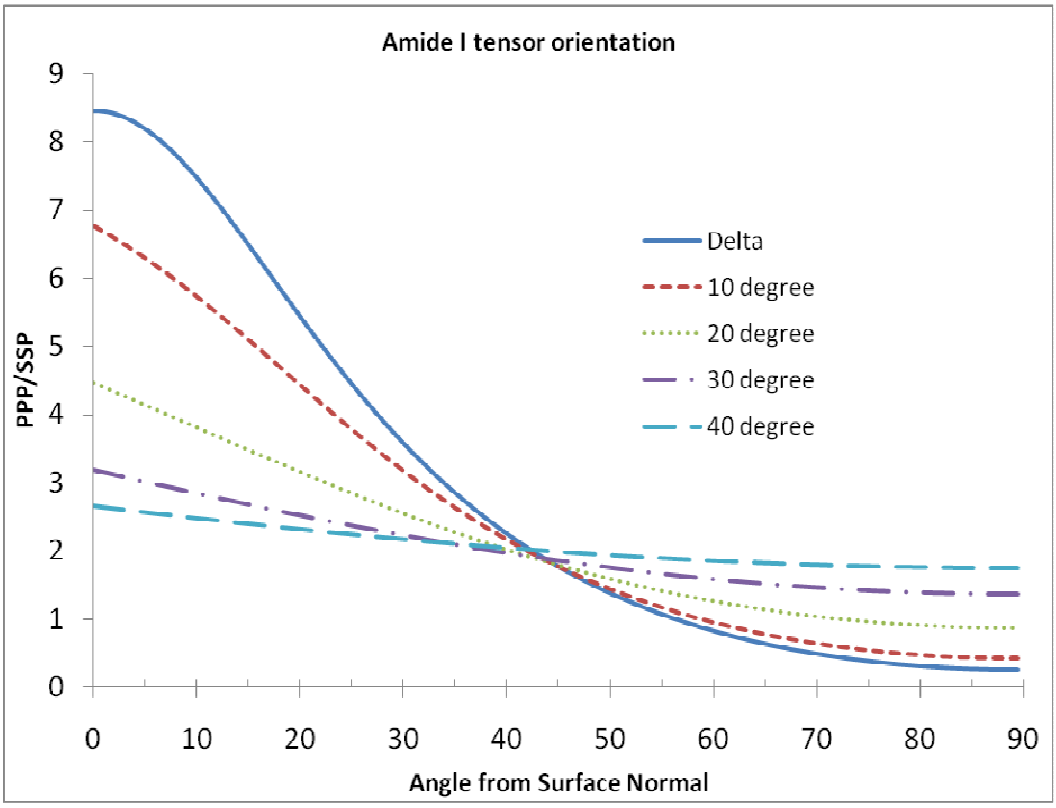

Figure 5-17 Orientation curves of the Amide I stretch.

However, this is close to the "magic angle", in which case the ratio obtained for a very narrow distribution at the magic angle would be the same as for an extremely broad distribution; our results are insufficient to distinguish between the two cases.

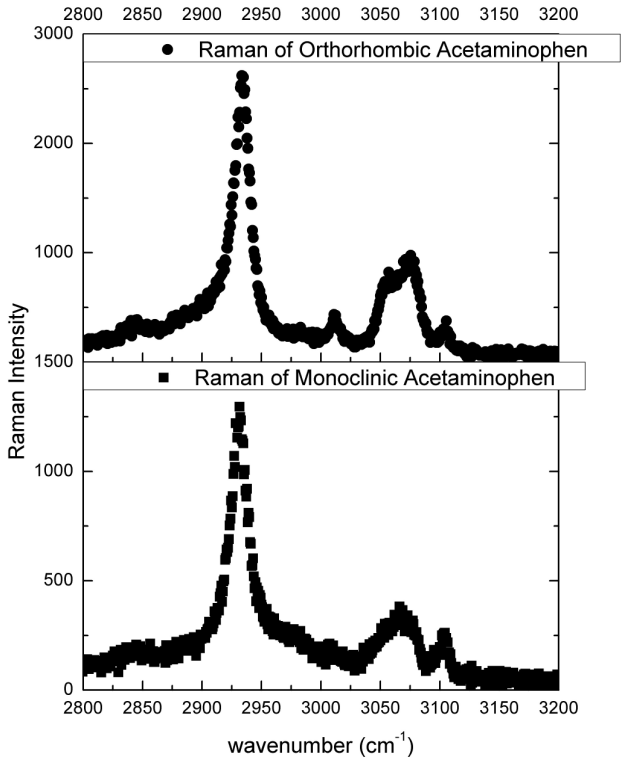

Figure 5-18 Raman spectra of monoclinic and orthorhombic acetaminophen crystals in the CH stretching region.

5.4.4 CH stretching region

The Raman spectrum for the CH stretching region is given in Figure 5-18 for reference. We do observe CH stretches at the polymer/crystal interface. This implies that there is also strong orientation of the methyl groups at the interface.

As mentioned previously the CH stretching region can be hard to interpret due to overlapping and interfering bands. In theory, there should be only a symmetric CH_3 and antisymmetric CH_3 stretch in the spectral region between 2800 and 3000 cm^{-1}. From SFG spectra, Figure 5-19 and Figure 5-20, there are clearly more than two peaks present.

Further work needs to be done to make reliable peak assignments before orientation analysis can be done.

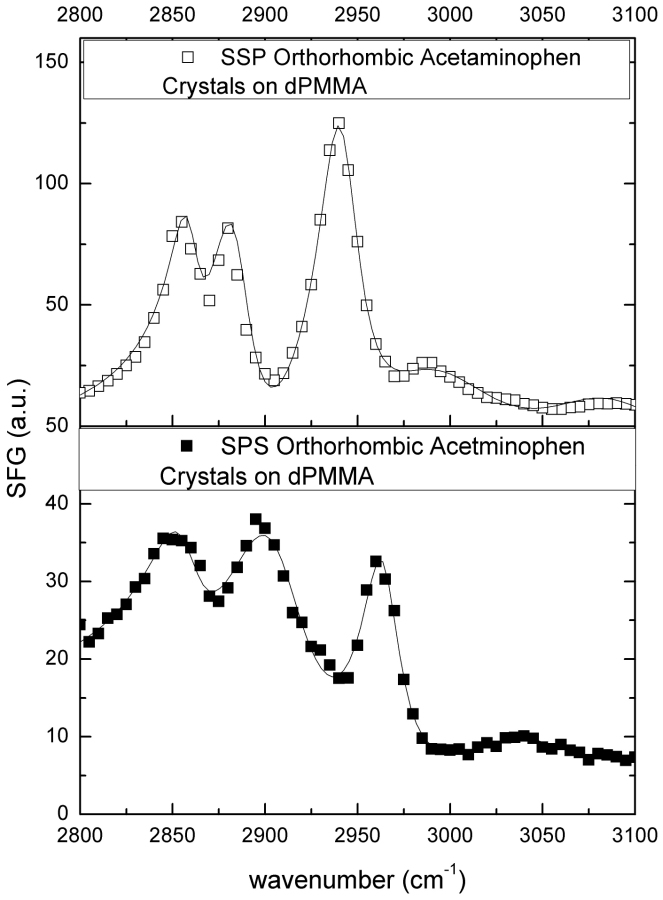

Figure 5-19 SFG spectra of orthorhombic acetaminophen on dPMMA

	Peak Center (cm^{-1})	Height	Width
SSP	2860	33	9
	2885	90	14
	2942	114	14
	2992	244	50
	3080	192	50
SPS	2858	29	17
	2909	112	29
	2964	50	13
	3045	44	34

Table 12 SFG fits for CH region for orthorhombic acetaminophen crystals on dPMMA

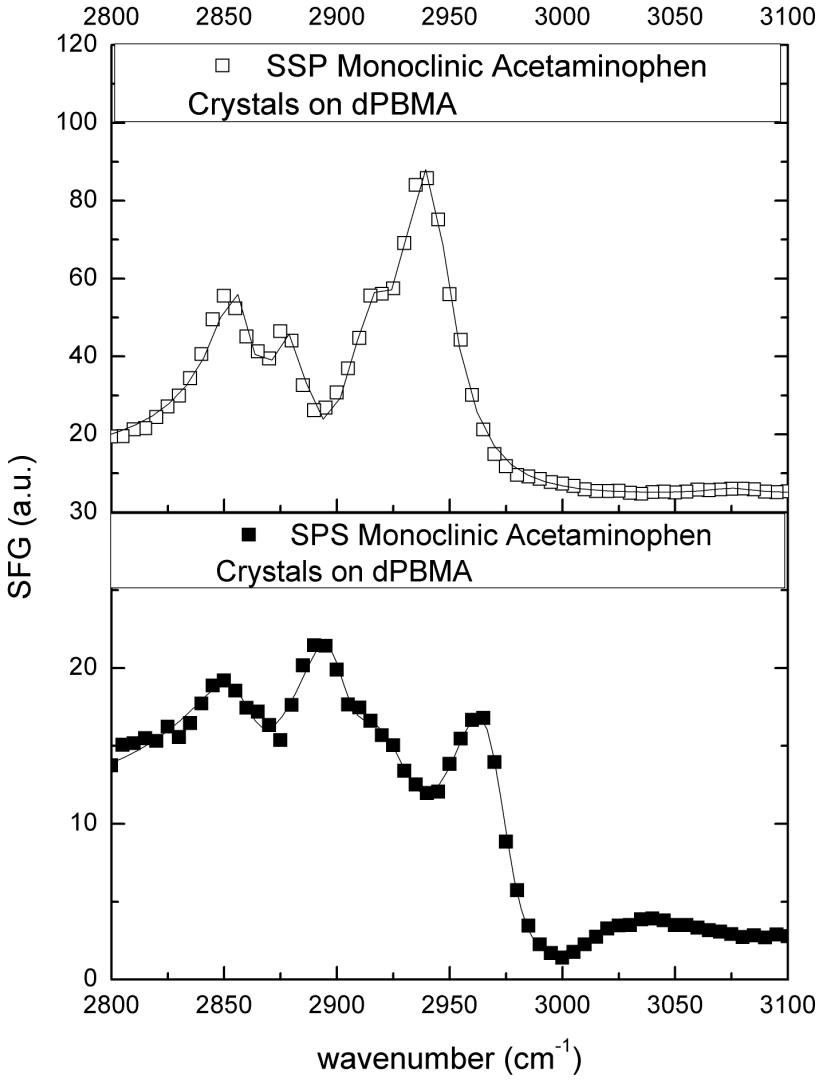

Figure 5-20 SFG spectra of monoclinic acetaminophen in the SSP and SPS polarization combinations in the CH stretching region.

	Peak Center (cm^{-1})	Height	Width
SSP	2863	6	12
	2947	26	12
	2982	18	29
SPS	2859	12	16
	2900	12	13
	2970	44	16
	2926	31	21
	3054	22	36

Table 13 SFG fit results of monoclinic acetaminophen crystals on dPBMA

5.5 Acetaminophen Samples Formed by Sublimation

Our collaborator (Vilmali Lopez-Mejias) observed that acetaminophen crystals prepared by sublimation onto the PMMA and PBMA surfaces resulted in different preferred crystal orientations, using powder x-ray diffraction (PXRD). No polymorphism was observed in the sublimated samples. The sublimated acetaminophen on a PMMA film showed strong preferential ordering of the crystals along the (001) plane. (Figure 5-21) In contrast, PXRD of sublimated acetaminophen on a PBMA film showed preferential ordering along the (021) plane but the degree of preference was not nearly as strongly as on the PMMA film.(Figure 5-23) Our SFG results correlate well with these observations, showing that the PMMA surface has a more ordered distribution of C=O groups than PBMA film.

When crystals were grown via sublimation, all the crystals grew in the monoclinic form regardless of the polymer surface. Clearly, the kinetics of crystal growth from vapor vs. from saturated solution are quite different. Further, the molecular surface structures of the PMMA and PBMA surfaces are very different in air than in solution (water), as was discussed in Chapter 4. We examined whether SFG could provide some insight into the differences in the interactions between acetaminophen vapor and a polymer surface, as compared to the growth of crystals in solution.

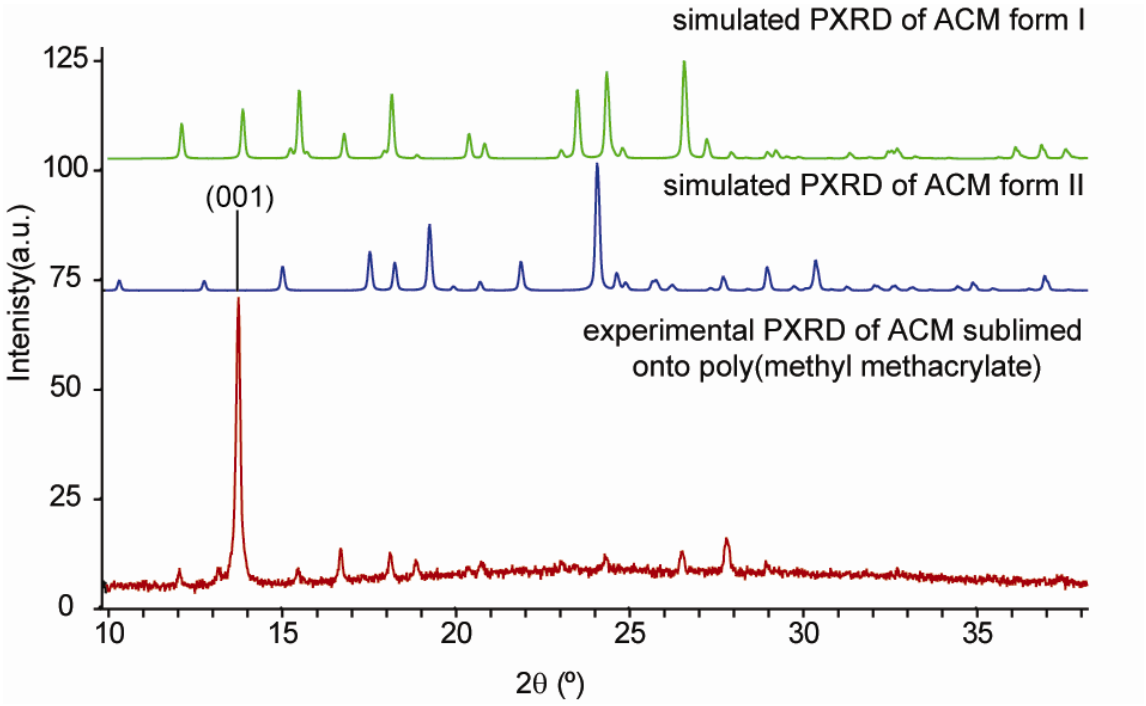

Figure 5-21 Powder X-Ray Diffraction of acetaminophen sublimated onto PMMA

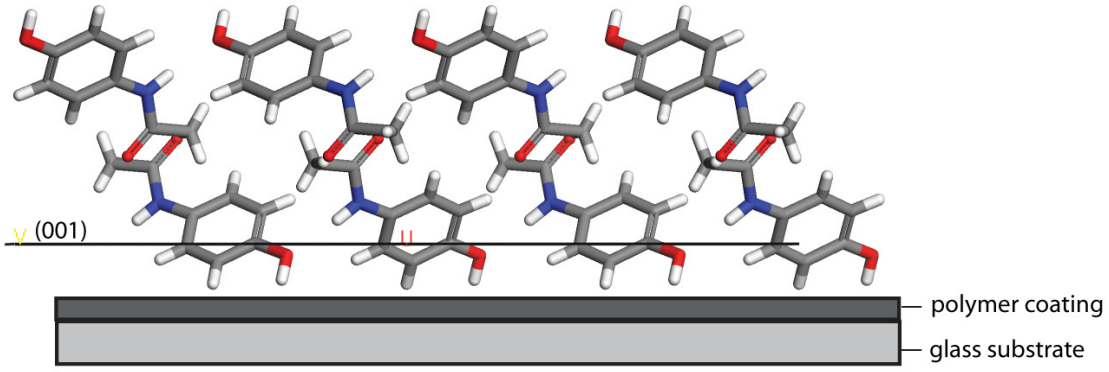

Figure 5-22 Model of the (001) plane of acetaminophen

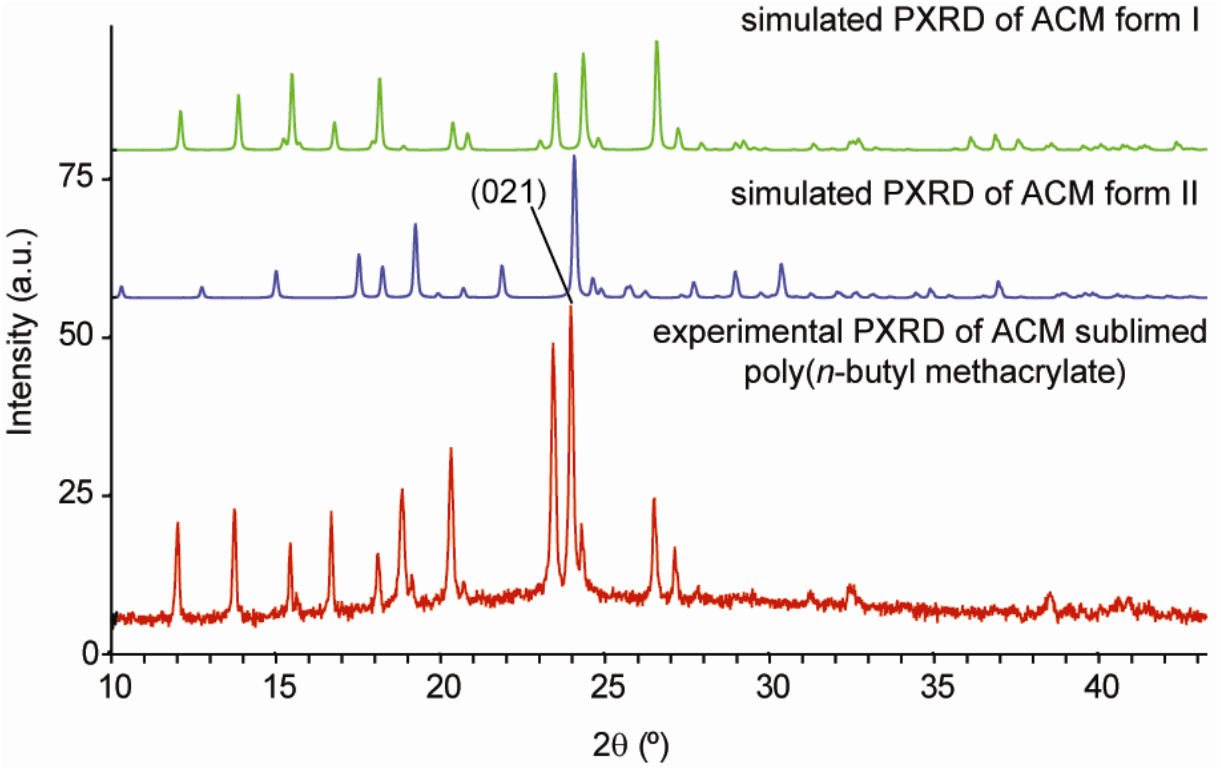

Figure 5-23 Powder X-Ray diffraction of sublimated acetaminophen on PBMA

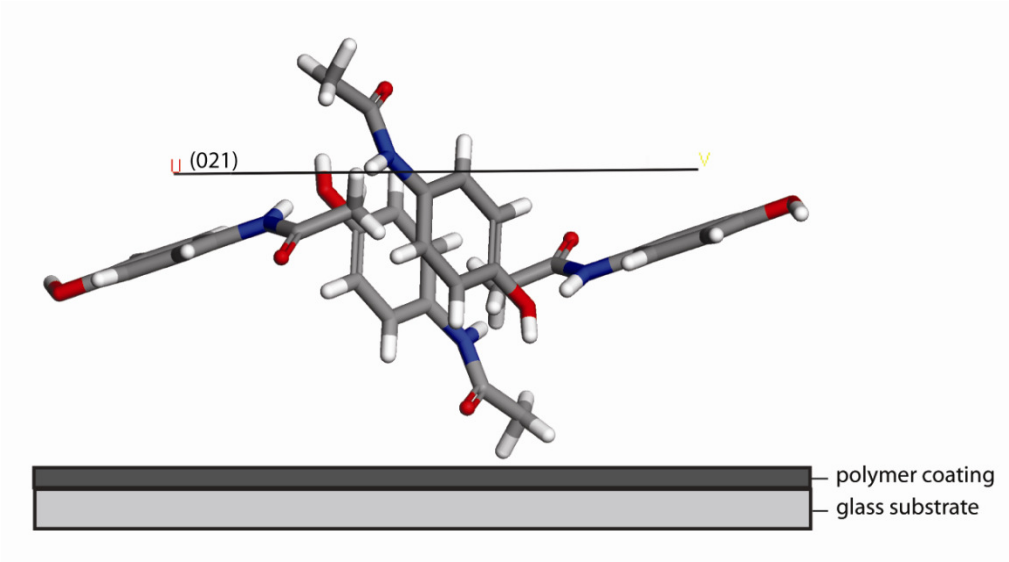

Figure 5-24 Model of the (021) plane of an acetaminophen crystal

The CH region sps polarization combination SFG spectra of the samples made by sublimation, Figure 5-25 and Figure 5-26, are clearly quite different from the samples made from solution. This implies that there is very different surface orientation, probably due to the difference in the kinetics of deposition. Again, reliable peak assignments need to be made before more analysis can reasonably be done on the CH region spectra.

As can be seen in Figure 5-27 there is no evidence of a hydrogen bonding induced peak position shift for the PMMA C=O as was observed in the solution grown samples. This would imply that hydrogen bonding plays a less important role in the samples made by sublimation. It could be interpreted that hydrogen bonding between the acetaminophen and PMMA is important in generating the orthorhombic form, since in the sublimated samples the monoclinic polymorph is formed and there is no evidence of hydrogen bonding.

In Figure 5-28 the PBMA C=O signal is much stronger compared to the acetaminophen amide I signal than in the solution grown crystal samples.

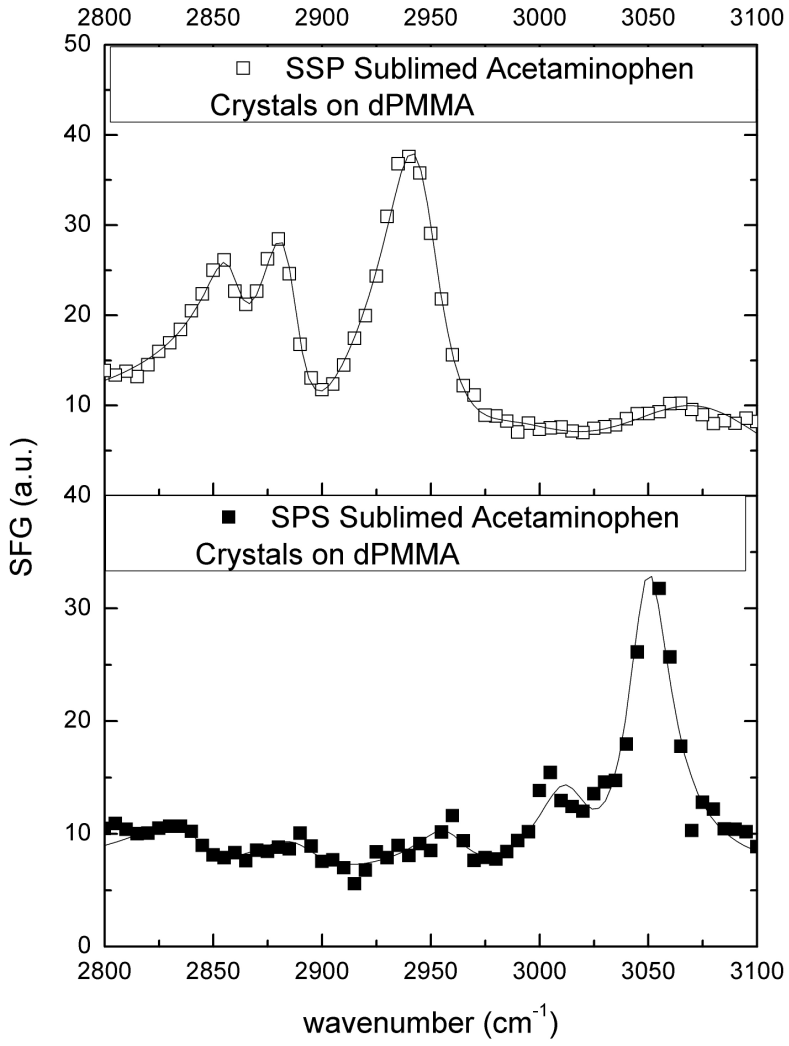

Figure 5-25 SFG spectra of sublimated acetaminophen crystals on dPMMA

	Peak Center ($cm^{-1)}$	Height	Width
SSP	**2859**	**12**	**10**
	2885	**29**	**11**
	2946	**71**	**17**
	2991	**52**	**42**
	3079	**130**	**50**
SPS	**2837**	**22**	**16**
	2959	**18**	**14**
	2889	**21**	**18**
	3013	**29**	**15**
	3049	**58**	**12**

Table 14 SFG fit of sublimated acetaminophen on dPMMA

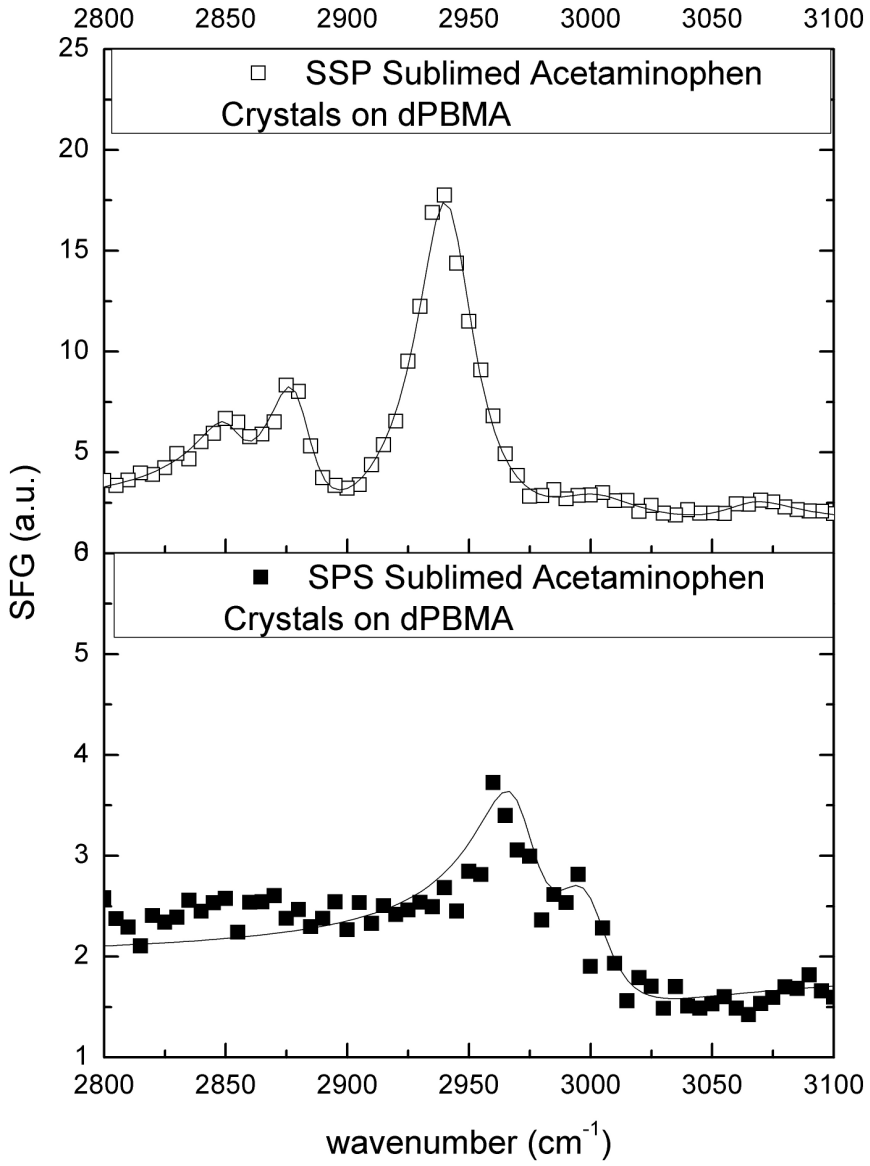

Figure 5-26 SFG spectra of sublimated acetaminophen crystals on dPBMA

	Peak Center (cm^{-1})	Height	Width
SSP	2852	9	11
	2880	21	12
	2941	56	15
	2999	16	22
	3065	12	18
SPS	2972	12	15
	3000	12	15

Table 15 SFG fit of CH region of sublimated acetaminophen on dPBMA

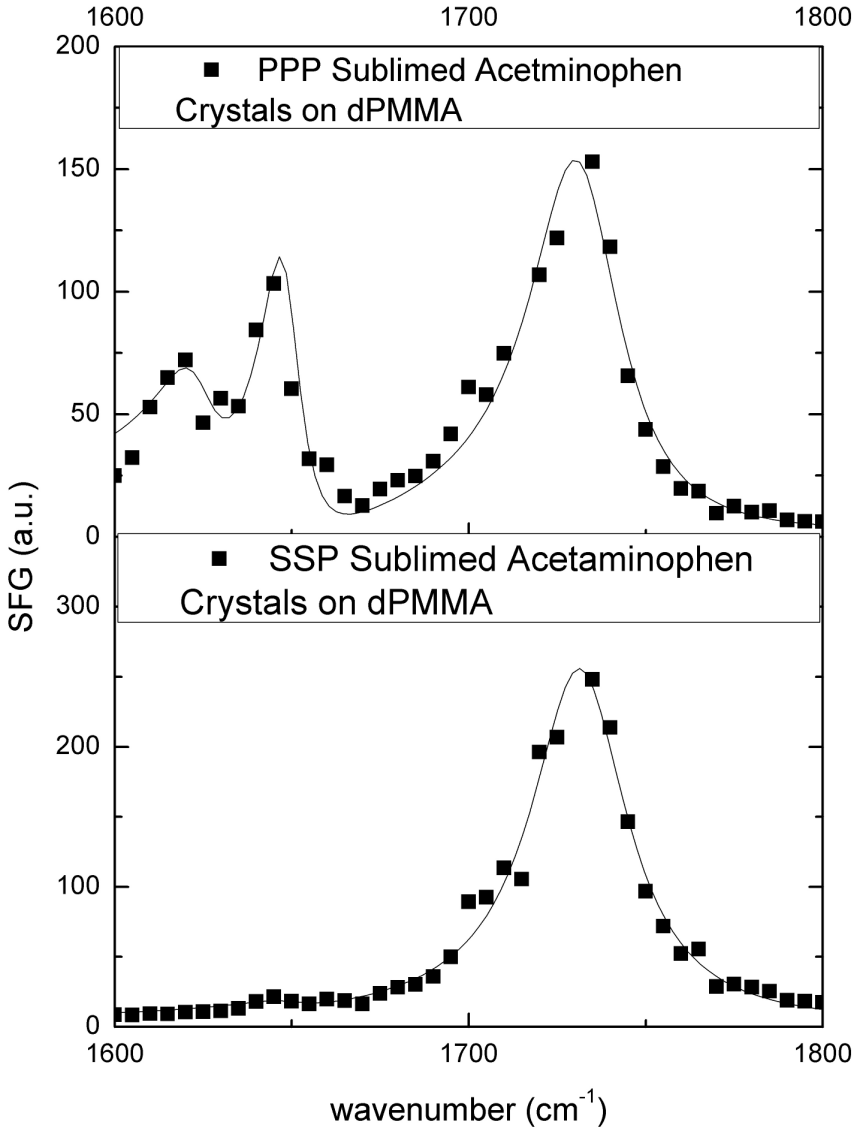

Figure 5-27 Sublimated Acetaminophen crystals on dPMMA C=O stretch region

	Peak Center (cm^{-1})	Height	Width
SSP	1732	263	17
	1650	10	12
PPP	1732	191	16
	1649	60	7
	1624	35	10

Table 16 SFG fit of C=O stretching region of sublimated acetaminophen on dPMMA

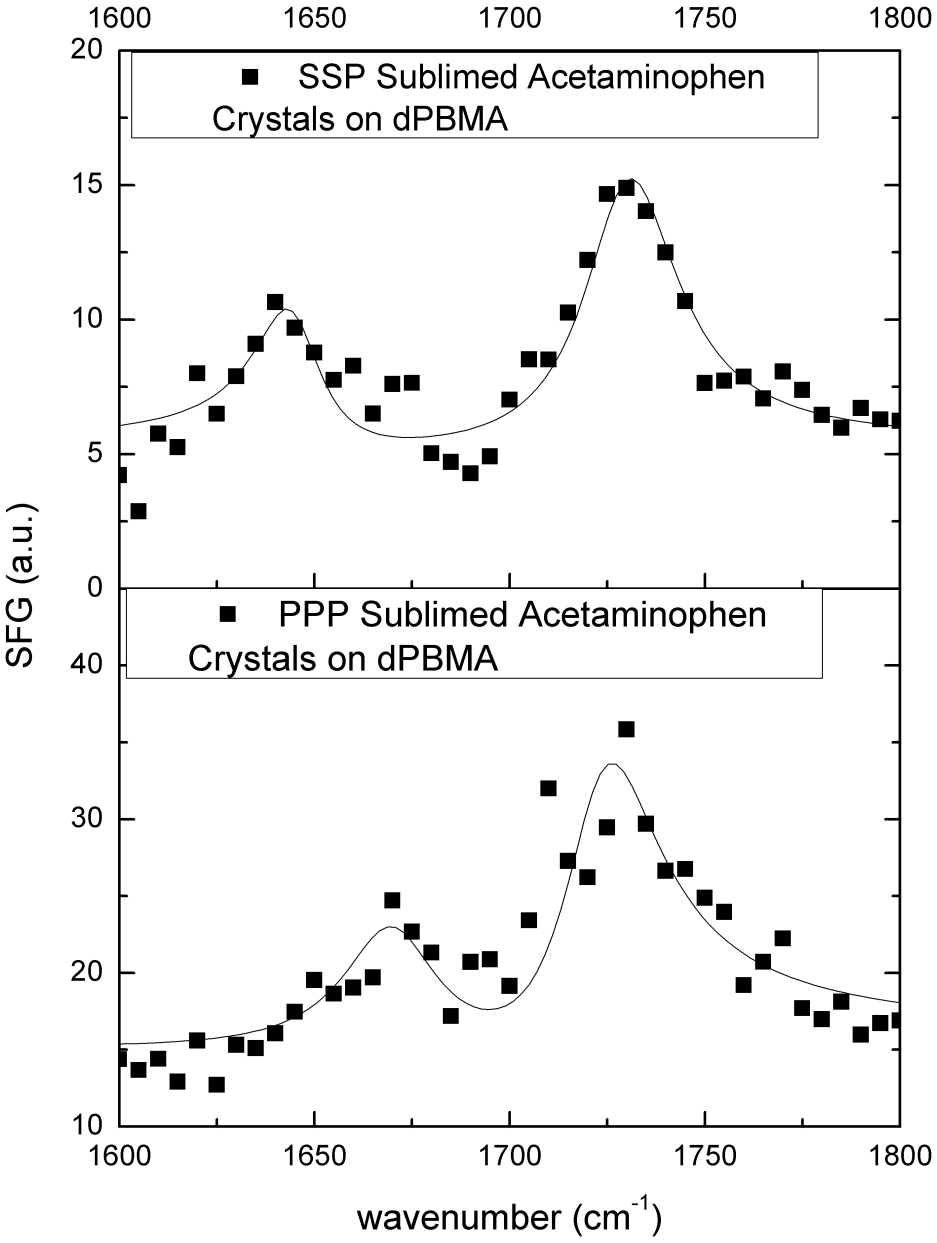

Figure 5-28 SFG spectra of sublimated acetaminophen crystals on dPBMA C=O stretching region

	Peak Center (cm^{-1})	Height	Width
SSP	1729	49	19
	1643	71	29
PPP	1728	69	15
	1680	45	15

Table 17 SFG fit of C=O stretching region of sublimated acetaminophen on dPBMA

5.7 Summary and Conclusions

In conclusion, the mechanism of polymer induced heteronucleation was examined with the nonlinear optical technique sum frequency generation vibrational spectroscopy. Acetaminophen was used as the model polymorphic system. The PMMA and PBMA surfaces were studied specifically as heteronuclei, since they heteronucleate different polymorphs of acetaminophen, despite having similar chemical composition.

In a series of experiments that looked at the saturated solution/ polymer interface, a red shift was observed in the polymer C=O peak position. The red shift was indicative of hydrogen bonding interactions between the acetaminophen and the polymer. By comparing the peak shifts when the polymers were contacted to saturated solutions of acetaminophen, acetanilide, and phenol, it was determined that the polymer C=O group was hydrogen bonding with the NH in the acetaminophen.

SFG peak intensities in the SSP and PPP polarization combinations were then used to determine that the C=O groups of PMMA and PBMA adopt different orientations when hydrogen bonded to acetaminophen molecules. Acetaminophen hydrogen bonding to the C=O groups in PMMA cause the C=O groups to form a 20° angle from the surface normal under the δ distribution assumption. Acetaminophen hydrogen bonding to the C=O groups in PBMA cause the C=O groups to form a 53° angle from the surface normal the δ distribution assumption. The steric hindrances of the longer aliphatic side chain in the PBMA could contribute to the differences in orientation. The differences in the hydrophobicity between ester methyl groups in PMMA and regular methyl groups in PBMA could also play a role. The differences in orientation probably play an important role in the determination of the acetaminophen polymorph that is heteronucleated.

The acetaminophen crystal-polymer interface was also studied by SFG. The amide I, methyl, and aromatic stretches were observed from the acetaminophen . The orientation of the amide I stretches were deduced for the monoclinic polymorph. The orthorhombic/PMMA interface shows clear hydrogen bonding shift of the PMMA C=O groups. The monoclinic/PBMA interface shows very weak PBMA C=O signal indicating either a disordered PBMA interface or that the PBMA C=O groups lie down when the full acetaminophen crystal forms.

Finally, samples prepared by sublimation were examined. There was no evidence of hydrogen bonding between the sublimated acetaminophen and PMMA. Since only monoclinic crystals formed by subliming, it is thought that the hydrogen bonding to the C=O in the PMMA plays an important role in the formation of the orthorhombic polymorph.

(1) Davey, R., J. Garside *From Molecules to Crystallizers, An Introduction to Crystallization*; Oxford University Press: Oxford, 2000.

(2) Zettlemoyer, A. C., Ed. *Nucleation*; Marcel Dekker, Inc.: New York, 1969.

(3) Porter, D. A., K. E. Easterling *Phase Transformation in Metals and Alloys*; 2nd ed.; Stanley Thornes Ltd: Cheltenham, 1992.

(4) Price, C. P.; Grzesiak, A. L.; Matzger, A. J. *Journal of the American Chemical Society* **2005**, *127*, 5512-5517.

(5) Porter, W. W.; Elie, S. C.; Matzger, A. J. *Crystal Growth & Design* **2008**, *8*, 14-16.

(6) Lopez-Mejias, V. K., J.; Matzger, A.J. *Journal of the American Chemical Society* **2009**, *accepted*.

(7) Grzesiak, A. L.; Matzger, A. J. *Journal of Pharmaceutical Sciences* **2007**, *96*, 2978-2986.

(8) Lutker, K. M.; Tolstyka, Z. P.; Matzger, A. J. *Crystal Growth & Design* **2008**, *8*, 136-139.

(9) Grzesiak, A. L.; Matzger, A. J. *Crystal Growth & Design* **2008**, *8*, 347-350.

(10) Grzesiak, A. L.; Matzger, A. J. *Inorganic Chemistry* **2007**, *46*, 453-457.

(11) Caskey, S. R.; Wong-Foy, A. G.; Matzger, A. J. *Inorganic Chemistry* **2008**, *47*, 7751-7756.

(12) Clarke, M. L.; Chen, C. Y.; Wang, J.; Chen, Z. *Langmuir* **2006**, *22*, 8800-8806.

(13) Wang, J.; Chen, C. Y.; Buck, S. M.; Chen, Z. *Journal of Physical Chemistry B* **2001**, *105*, 12118-12125.

(14) Lang, M. D.; Grzesiak, A. L.; Matzger, A. J. *Journal of the American Chemical Society* **2002**, *124*, 14834-14835.

(15) Wang, J.; Even, M. A.; Chen, X. Y.; Schmaier, A. H.; Waite, J. H.; Chen, Z. *Journal of the American Chemical Society* **2003**, *125*, 9914-9915.

(16) Keefe, C. D.; Gillis, E. A. L.; MacDonald, L. *Journal of Physical Chemistry A* **2009**, *113*, 2544-2550.

(17) Mucha, M.; Mielke, Z. *Journal of Physical Chemistry A* **2007**, *111*, 2398-2406.

(18) Kryachko, E. S.; Karpfen, A. *Chemical Physics* **2006**, *329*, 313-328.

(19) Whitfield, T. W.; Martyna, G. J.; Allison, S.; Bates, S. P.; Vass, H.; Crain, J. *Journal of Physical Chemistry B* **2006**, *110*, 3624-3637.

(20) John, U.; Nair, K. P. R. *Spectrochimica Acta Part a-Molecular and Biomolecular Spectroscopy* **2006**, *63*, 169-173.

(21) Whitfield, T. W.; Martyna, G. J.; Allison, S.; Bates, S. P.; Crain, J. *Chemical Physics Letters* **2005**, *414*, 210-214.

(22) Vijayakumar, S.; Kolandaivel, P. *Journal of Molecular Structure* **2005**, *734*, 157-169.

(23) Bouzouia, F.; Djadoun, S. *Journal of Applied Polymer Science* **2008**, *110*, 3574-3581.

(24) Khan, F. L. A.; Sivagurunathan, P. *Physics and Chemistry of Liquids* **2008**, *46*, 504-509.

(25) Imamura, K.; Ohyama, K.; Tani, K.; Yokoyama, T.; Maruyama, Y.; Imanaka, H.; Nakanishi, K. *Spectroscopy Letters* **2008**, *41*, 305-312.

(26) Chang, C. C.; Hou, S. S. *European Polymer Journal* **2008**, *44*, 1337-1345.

(27) Li, G.; Ye, S.; Morita, S.; Nishida, T.; Osawa, M. *Journal of the American Chemical Society* **2004**, *126*, 12198-12199.

(28) Marsh, D.; Muller, M.; Schmitt, F. J. *Biophysical Journal* **2000**, *78*, 2499-2510.

(29) Hirose, C.; Watanabe, N.; Kondo, J. N.; Wada, A.; Domen, K. *Laser Techniques for Surface Science Ii* **1995**, *2547*, 12-20.

(30) Hirose, C.; Yamamoto, H.; Akamatsu, N.; Domen, K. *Journal of Physical Chemistry* **1993**, *97*, 10064-10069.

(31) Wang, J.; Chen, C. Y.; Chen, Z. *Abstracts of Papers of the American Chemical Society* **2001**, *222*, 164-COLL.

CHAPTER 6 : SFG IMAGING

6.1 Introduction

With the improvement of technology such as light sources and detector hardware most spectroscopic techniques are moving towards imaging. Examples include CARS imaging[1-11], IR imaging[12-17], and Raman imaging etc. Spectroscopic imaging is especially important in non-homogenous systems such as biological samples,[4] polymer blends,[17] copolymers, or micro-patterned samples.[18-22] Research has been performed to develop SFG imaging. The spatial resolution of the SFG images of course will not be any better than a regular optical microscope in the far-field experiment; however, the ability to map the molecular surface structure such as surface functional group coverage and orientation of the sample could provide answers to many very important questions. Other comparable techniques such as CARS or IR imaging are not surface specific and have comparable or worse spatial resolution.

- Polymer blends are of great interest to the polymer science community. Determining if the polymers blend homogeneously or phase segregate into domains is an important and tricky question. AFM and IR imaging of polymer blends[12-15,17] are two common approaches to this question. However, AFM does not provide any chemical information, and IR lacks the surface specificity needed to understand how proteins, etc. will interact with the polymer blend for example.

- As was pointed out in Chapter 4 with PAA, the bulk vibrational spectrum can be very different from the surface vibrational spectrum.
- Cells are extremely inhomogeneous systems, and local differences in structure and chemistry are essential to health, function, and growth. Being able to map the chemical distribution in cells has helped unravel some questions about how a cell functions. CARS imaging of cells[4] has proved to be quite powerful, but it is not surface sensitive and is currently limited to the CH region. The CH region is of less use in biological systems due to the large number of sources for signal.
- As devices continue to shrink, micro-patterned adhesives[18-22] will become increasingly valuable. Understanding the surface chemistry of the micro-patterned surface will help in better designs of such materials.

  The increased surface specificity of SFG imaging could have widespread applications in these and other areas.

To this end, we have designed and built an SFG imaging system.

6.2 Design

The goal of SFG imaging is to have chemical and spatial information about nonhomogeneous sample surfaces. Several groups have previously built SFG imaging systems [23-29] using a direct imaging mode, where the SFG signal is directed into a CCD camera, but the grazing angle geometry used will lead to image distortion. The approach we took was with a collinear beam geometry, a 90° incident angle, a reflective microscope objective, and a scanning stage (see Figure 6-1). It was thought that this approach would provide better images and require less post processing. The hot mirror

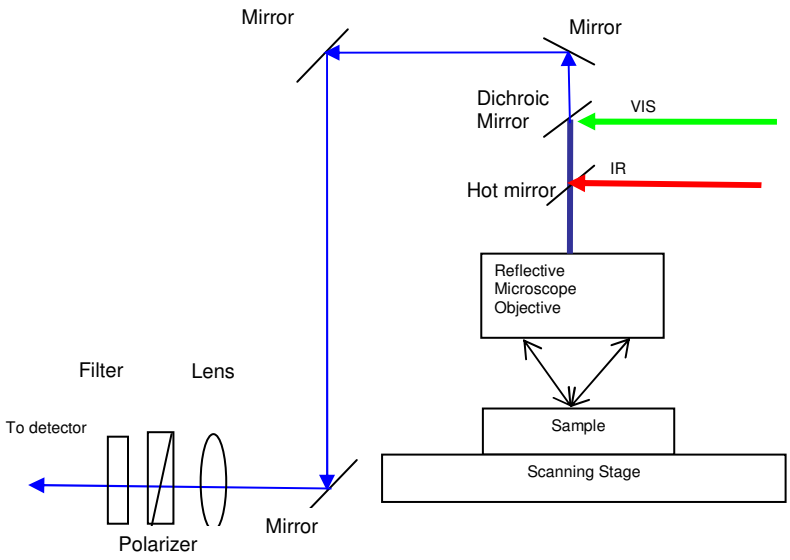

Figure 6-1 Schematic of optical setup for colinear SFG imaging system

was purchased from Reynard Corporation. An all-reflective 15x cassegrain microscope objective purchased from Ealing Catalog, was used to focus the visible and infrared laser beams. The all reflective objective was used to circumvent chromatic aberration issues.

The optical setup is sketched out in Figure 6-1. The visible input beam was reflected from the dichroic mirror. It then passed through the hot mirror and entered into the microscope objective. The IR beam was reflected from the hot mirror into the microscope objective. The signal was then collected in the back reflection direction, which was transmitted through the microscope objective, the hot mirror, and the dichroic mirror, filtered by a monochromator, and detected with a photo multiplier tube. The plan was eventually to modify the system to use a CCD camera directly above the dichroic mirror for the signal collection.

6.3 Results

As a proof of concept, a PMMA sample was microcontact printed with a PDMS stamp on a glass substrate by Dr. Jay Guo's group at the Department of Electrical Engineering and Computer Science of the University of Michigan; the patterning method has been described previously.[30-33] The IR frequency was fixed at 2955 cm^{-1} which corresponds to the ester methyl symmetric stretch in the PMMA. The sample was scanned and the sum frequency signal was collected. The patterned PMMA showed up clearly in the resulting image. See Figure 6-2. The inhomogeneities within the PMMA areas are actually due to incomplete transfer of the PMMA during the printing. The theoretical diffraction limited resolution for the image is on the order of 0.25 µm, far better than the 5µm step size the image was collected with. The stage that we used had step sizes as small as 1 µm. A better stage could of course take even smaller steps. It should be noticed that this SFG image is an image of the surface chemistry of the sample.

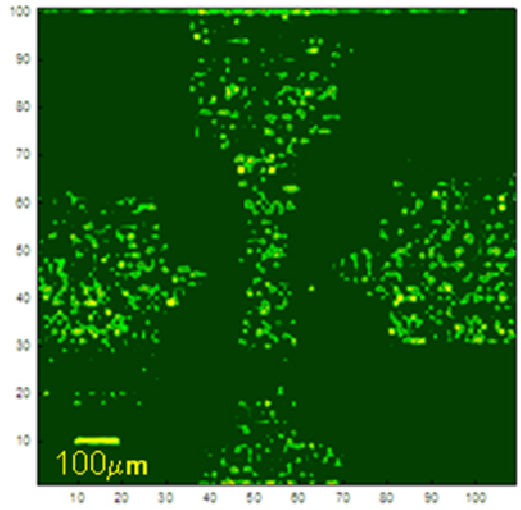

Figure 6-2 SFG image collected at 2955 cm^{-1} of PMMA microcontact printed on a glass substrate

6.4 Summary and Conclusions

SFG imaging has great potential for chemically mapping inhomogeneous samples. Studying the surface domains of polymer blends and co-polymers will help in designing these materials for various applications. For example, it has been shown that polymers with micro domains on the surface can better resist marine biofouling. Here, an SFG imaging system was designed and built. The system was successfully demonstrated with a resolution of better than 5µm with a micro-contact printed PMMA sample.

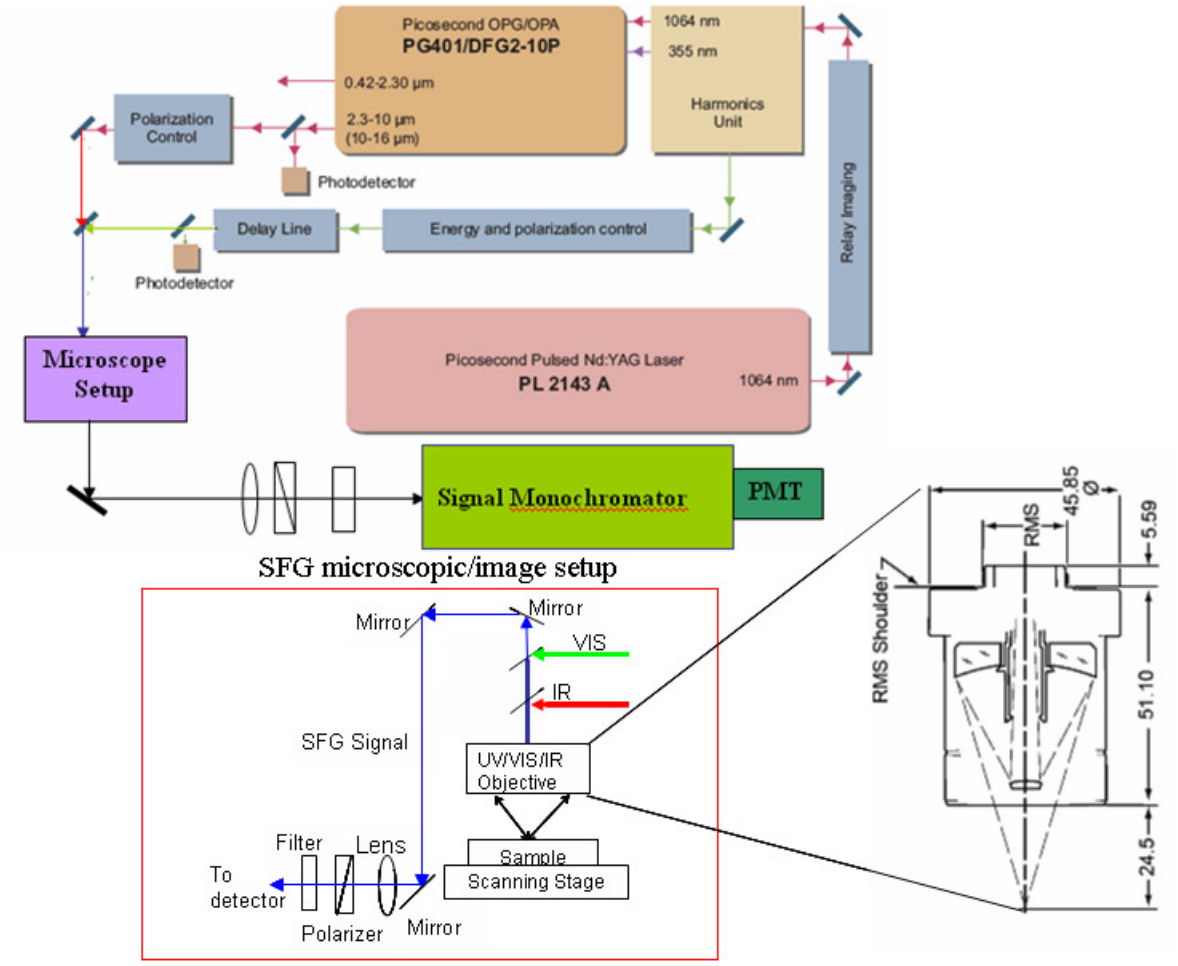

Figure 6-3 Schematic of the incorporation of the SFG microscope into the current laser system

(1) Evans, C. L.; Potma, E. O.; Puoris'haag, M.; Cote, D.; Lin, C. P.; Xie, X. S. *Proceedings of the National Academy of Sciences of the United States of America* **2005**, *102*, 16807-16812.

(2) Potma, E. O.; Xie, X. S.; Muntean, L.; Preusser, J.; Jones, D.; Ye, J.; Leone, S. R.; Hinsberg, W. D.; Schade, W. *Journal of Physical Chemistry B* **2004**, *108*, 1296-1301.

(3) Cheng, J. X.; Xie, X. S. *Journal of Physical Chemistry B* **2004**, *108*, 827-840.

(4) Cheng, J. X.; Jia, Y. K.; Zheng, G. F.; Xie, X. S. *Biophysical Journal* **2002**, *83*, 502-509.

(5) Freudiger, C. W.; Min, W.; Saar, B. G.; Lu, S.; Holtom, G. R.; He, C. W.; Tsai, J. C.; Kang, J. X.; Xie, X. S. *Science* **2008**, *322*, 1857-1861.

(6) Wright, A. J.; Poland, S. P.; Girkin, J. M.; Freudiger, C. W.; Evans, C. L.; Xie, X. S. *Optics Express* **2007**, *15*, 18209-18219.

(7) Saar, B. G.; Park, H. S.; Xie, X. S.; Lavrentovich, O. D. *Optics Express* **2007**, *15*, 13585-13596.

(8) Evans, C. L.; Xu, X. Y.; Kesari, S.; Xie, X. S.; Wong, S. T. C.; Young, G. S. *Optics Express* **2007**, *15*, 12076-12087.

(9) Ganikhanov, F.; Evans, C. L.; Saar, B. G.; Xie, X. S. *Optics Letters* **2006**, *31*, 1872-1874.

(10) Ganikhanov, F.; Carrasco, S.; Xie, X. S.; Katz, M.; Seitz, W.; Kopf, D. *Optics Letters* **2006**, *31*, 1292-1294.

(11) Potma, E. O.; Evans, C. L.; Xie, X. S. *Optics Letters* **2006**, *31*, 241-243.

(12) Fleming, O. S.; Chan, K. L. A.; Kazarian, S. G. *Polymer* **2006**, *47*, 4649-4658.

(13) Gupper, A.; Wilhelm, P.; Kothleitner, G.; Eichhorn, K. J.; Pompe, G. *Macromolecular Symposia* **2004**, *205*, 171-180.

(14) Kazarian, S. G.; Chan, K. L. A. *Macromolecules* **2004**, *37*, 579-584.

(15) Vogel, C.; Wessel, E.; Siesler, H. W. *Biomacromolecules* **2008**, *9*, 523-527.

(16) Bhargava, R.; Levin, I. W. *Appl. Spectrosc.* **2003**, *57*, 357-366.

(17) Oh, S. J.; Do, J. S.; Ok, J. H. *Appl. Spectrosc.* **2003**, *57*, 1058-1062.

(18) Karagozler, M. E.; Cheung, E.; Kwon, J.; Sitti, M. *2006 1st IEEE RAS-EMBS International Conference on Biomedical Robotics and Biomechatronics, Vols 1-3* **2006**, 866-872.

(19) Kim, H. J.; Paik, K. W. *EPTC 2006: 8th Electronic Packaging Technology Conference, Vols 1 and 2* **2006**, 143-149.

(20) Tsai, Y. C.; Shih, P. J.; Lin, T. H.; Shih, W. P. *2006 1st IEEE International Conference on Nano/Micro Engineered and Molecular Systems, Vols 1-3* **2006**, 1388-1391.

(21) Kwon, J.; Cheung, E.; Park, S.; Sitti, M. *Biomedical Materials* **2006**, *1*, 216-220.

(22) Greiner, C.; del Campo, A.; Arzt, E. *Langmuir* **2007**, *23*, 3495-3502.

(23) Baldelli, S. *Chemphyschem* **2008**, *9*, 2291-2298.

(24) Cimatu, K.; Baldelli, S. *Journal of Physical Chemistry B* **2006**, *110*, 1807-1813.

(25) Cimatu, K.; Baldelli, S. *Journal of Physical Chemistry C* **2007**, *111*, 7137-7143.

(26) Cimatu, K.; Moore, H. J.; Barriet, D.; Chinwangso, P.; Lee, T. R.; Baldelli, S. *Journal of Physical Chemistry C* **2008**, *112*, 14529-14537.

(27) Cimatu, K.; Moore, H. J.; Lee, T. R.; Baldelli, S. *Journal of Physical Chemistry C* **2007**, *111*, 11751-11755.

(28) Florsheimer, M.; Brillert, C.; Fuchs, H. *Langmuir* **1999**, *15*, 5437-5439.

(29) Florsheimer, M.; Brillert, C.; Fuchs, H. *Materials Science & Engineering C-Biomimetic and Supramolecular Systems* **1999**, *8-9*, 335-341.

(30) Li, D. W.; Guo, L. J. *Applied Physics Letters* **2006**, *88*.

(31) Cheng, X.; Guo, L. J.; Fu, P. F. *Advanced Materials* **2005**, *17*, 1419-+.

(32) Hoff, J. D.; Cheng, L. J.; Meyhofer, E.; Guo, L. J.; Hunt, A. J. *Nano Letters* **2004**, *4*, 853-857.

(33) Cheng, X.; Guo, L. J. *Microelectronic Engineering* **2004**, *71*, 277-282.

CHAPTER 7 : SUMMARY AND CONCLUSIONS

Sum frequency generation vibrational spectroscopy (SFG) is a second order nonlinear optical technique that was used to probe several different buried interfaces. It can provide the identity and orientation of surface functional groups at interfaces. Previously, a lack of appropriate analytical tools has made it hard to probe buried interfaces. Here a variety of buried interfaces were studied, to further develop SFG into a powerful *in situ,* nondestructive, analytical technique able to elucidate molecular level structures of buried interfaces. SFG can provide a unique probe of interfacial dynamics and interactions.

The first buried interface that was investigated was the interface between two functionalized poly-p-xylylene surfaces. The Lahann group in the Chemical Engineering dept at the University of Michigan developed a Solventless Adhesive Bonding (SAB) technique. In this technique an amine functionalized surface and an aldehyde functionalized surface were placed in contact and heated. After heating extremely strong adhesion occurred between the two layers. SFG allowed us to examine the behavior of the surface functional groups at the buried interface. The mechanism for the SAB technique was determined to be a chemical reaction between the amine and aldehyde groups. Other functionalized PPX surfaces were also examined. All the functionalized groups did go to the air interface as desired. There was evidence of surface restructuring when contacted to water of some of the polymer surfaces. This has implications towards

the use of these polymers for biomedical implant devices. In summary this study used SFG to reveal the surface restructuring of the functionalized PPX polymer in water. The effect of polymer exposure to an aqueous environment which was further explored in chapters 4 and 5. This study also correlates interfacial interactions to elucidate the mechanism for a new technique of polymer adhesion.

The next buried interface that was examined was a monolayer of 17 metadiester phthalates on graphite under a phenyloctane solution. The Matzger group in the chemistry department at the University of Michigan has studied this system previously with Scanning Tunneling Microscopy (STM). From the STM images, it was difficult to determine the exact orientation of the17 metadiester molecules. It was determined that the C=O groups were tilting ~30º away from the surface. This implies that there are two competing interactions, one between the monolayer and the phenyloctane solvent and one between the monolayer and the graphite surface. The solvent monolayer interaction makes some sense, since the 17 metadiester molecule is soluble in phenyl octane. To summarize this study SFG was extended to the investigation of organic liquid/solid interface. This study also shows that a combination of analytical techniques including SFG can provide a more complete picture of an interfacial interaction.

C=O groups are important surface interaction sites for many polymethacrylate polymers. A selection of C=O containing polymers were examined with SFG. The peak position of the C=O stretch is sensitive to whether the groups is hydrogen bonded or not. When the polymers were contacted to water essentially all the C=O groups formed hydrogen bonds with the water. The orientation for the C=O groups in air and in water were determined for the various polymers. This study systematically investigated the

chain length effect on polymethacryalte surface structures in air and their changes in water. It has been shown that the interfacial hydrogen bonding can be monitored with SFG.

The mechanism of polymer induced heteronucleation of acetaminophen was also examined. The Matzger group at the University of Michigan found that poly-methyl-methacrylate and poly-n-butyl-methacrylate heteronucleate different polymorphs of acetaminophen. The PMMA and PBMA surfaces were studied specifically as heteronuclei, since they heteronucleate different polymorphs of acetaminophen, despite having a very similar chemical composition.

In a series of experiments that looked at the saturated solution/ polymer interface, a red shift was observed in the polymer C=O peak position. The red shift was indicative of hydrogen bonding interactions between the acetaminophen and the polymer. By comparing the peak shifts when the polymers were contacted to saturated solutions of acetaminophen, acetanilide, and phenol, it was determined that the polymer C=O groups were hydrogen bonding with the NH in the acetaminophen.

SFG peak intensities in the SSP and PPP polarization combinations were then used to determine that the C=O groups of PMMA and PBMA adopt different orientations when hydrogen bonded to acetaminophen molecules. Acetaminophen hydrogen bonding to the C=O groups in PMMA cause the C=O groups to form a 20° angle from the surface normal under the δ distribution assumption. Acetaminophen hydrogen bonding to the C=O groups in PBMA cause the C=O groups to form a 53° angle from the surface normal the δ distribution assumption. The steric hindrances of the longer aliphatic side chain in the PBMA could contribute to the differences in orientation. The differences in

the hydrophobicity between ester methyl groups in PMMA and regular methyl groups in PBMA could also play a role. The differences in orientation probably play an important role in the determination of the acetaminophen polymorph that is heteronucleated. The acetaminophen crystal-polymer interface was also studied by SFG. The amide I, methyl, and aromatic stretches were observed from the acetaminophen . The orientation of the amide I stretches were deduced for the monoclinic polymorph. The orthorhombic/PMMA interface shows clear hydrogen bonding shift of the PMMA C=O groups. The monoclinic/PBMA interface shows very weak PBMA C=O signal indicating either a disordered PBMA interface or that the PBMA C=O groups lie down when the full acetaminophen crystal forms.

Samples prepared by subliming were also examined. There was no evidence of hydrogen bonding between the sublimated acetaminophen and PMMA. Since only monoclinic crystals formed by subliming, it is thought that the hydrogen bonding to the C=O in the PMMA plays an important role in the formation of the orthorhombic polymorph in the solution crystals.

In summary, the study of polymer/solution and polymer/drug crystal interfaces by SFG led to the beginning of understanding the interfacial molecular interactions that are important in the polymer induced heteronucleation. SFG is an ideal tool to study such molecular interactions at buried interfaces.

In the previous chapters, SFG spectra were collected from an area approximately 500 μm in diameter, making SFG basically a macroscopic probe incapable of differentiating different surface inhomogenetities. SFG imaging has great potential for chemically mapping inhomogeneous samples. Studying the surface domains of polymer

blends and co-polymers will help in designing these materials for various applications. An SFG imaging system was designed and demonstrated using a micropatterned polymer sample with better than 5μm resolution. In summary, this new SFG imaging tool will greatly enhance the spatial resolution of SFG, opening the door to studies of micro-patterned and imhomogeneous samples. The research presented in this thesis applied SFG to the study of a variety of buried interfaces, leveraging the abilities of SFG to provide *in situ* surface specific information. The results provide an understanding of many important problems and area such as polymer surface restructuring in water, surface hydrogen bonding, polymer adhesion, two-dimensional organic crystals, and polymer induced heteronucleation of pharmaceutical polymorphs.